Journal of Medicinal Chemistry

Article

A Unique Approach to Design Potent and Selective Cyclic Adenosine Monophosphate Response Element Binding Protein, Binding Protein (CBP) Inhibitors

Sarah M. Bronner, Jeremy M. Murray, F. Anthony Romero, Kwong Wah Lai, Vickie Tsui, Patrick Cyr, Maureen H. Beresini, Gladys de Leon Boenig, Zhongguo Chen, Edna F. Choo, Kevin R. Clark, Terry D. Crawford, Hariharan Jayaram, Susan Kaufman, Ruina Li, Yingjie Li, Jiangpeng Liao, Xiaorong Liang, Wenfeng Liu, Justin Q. Ly, Jonathan Maher, John S. Wai, Fei Wang, Aijun Zheng, Xiaoyu Zhu, and Steven R. Magnuson

J. Med. Chem., **Just Accepted Manuscript** • DOI: 10.1021/acs.jmedchem.7b01372 • Publication Date (Web): 20 Nov 2017

ACS Publications

Journal of Medicinal Chemistry is published by the American Chemical Society. 1155 Sixteenth Street N.W., Washington, DC 20036

A Unique Approach to Design Potent and Selective Cyclic Adenosine Monophosphate Response Element Binding Protein, Binding Protein (CBP) Inhibitors

Sarah M. Bronner,[†] Jeremy Murray,[†] F. Anthony Romero,[†] Kwong Wah Lai,[‡] Vickie Tsui,[†] Patrick Cyr,[†] Maureen H. Beresini,[†] Gladys de leon Boenig,[†] Zhongguo Chen,[‡] Edna F. Choo,[†] Kevin R. Clark,[†] Terry D. Crawford,[†] Hariharan Jayaram,[§] Susan Kaufman,[†] Ruina Li,[†] Yingjie Li,[‡] Jiangpeng Liao,[‡] Xiaorong Liang,[†] Wenfeng Liu,[‡] Justin Ly,[†] Jonathan Maher,[†] John Wai,[‡] Fei Wang,[‡] Aijun Zheng,[‡] Xiaoyu Zhu,[‡] Steven Magnuson[†]*

[†]Genentech, Inc. 1 DNA Way, South San Francisco, California 94080, United States

[‡]Wuxi Apptec Co., Ltd., 288 Fute Zhong Road, Waigaoqiao Free Trade Zone, Shanghai 200131, People's Republic of China

[§]Editas Medicine, Inc., 11 Hurley Street, Cambridge, Massachusetts 02141, United States

Abstract

The epigenetic regulator CBP/P300 presents a novel therapeutic target for oncology. Previously, we reported the development of potent and selective CBP bromodomain inhibitors by first identifying pharmacophores that bind the KAc region, and then building into the LPF shelf. Herein we report the "hybridization" of a variety of KAc-binding fragments with a tetrahydroquinoline scaffold that makes optimal interactions with the LPF shelf, imparting enhanced potency and selectivity to the hybridized ligand. To demonstrate the utility of our

hybridization approach, two analogues containing unique Asn binders and the optimized tetrahydroquinoline moiety were rapidly optimized to yield single-digit nanomolar inhibitors of CBP with exquisite selectivity over BRD4(1) and the broader bromodomain family.

Keywords: Epigenetics, CBP, CREBBP, P300, bromodomain, bromodomain inhibitor

Introduction

Epigenetics is an exciting field of research with unharnessed therapeutic potential.[1,2] Applications to human health offered by the ability to modify gene expression include cancer, aging, neuropsychiatric disease, and obesity.[3–9] While prospective therapies that result in permanent and potentially inheritable modification of chemical marks on DNA[10] are associated with greater risk,[11] epigenetic mechanisms that modify histones and alter rates of transcription represent attractive therapeutic targets.[12]

Acetylation of lysine residues on histones is a reversible post-translational modification (PTM) that loosens the DNA-histone interaction, thus altering the chromatin structure and allowing for upregulation of transcription.[13–15] Proteins that recognize PTMs such as acetylated lysine marks are collectively referred to as readers, and are involved in the recruitment of additional proteins to form large transcriptional complexes.[16–18] Bromodomains (BrDs) are arguably the most well studied class of epigenetic readers, and have recently received considerable attention as promising therapeutic targets.[19–23] Cyclic adenosine monophosphate response element binding protein, binding protein (CBP, CREBBP, or CREB-binding protein) and adenoviral E1A binding protein of 300 kDa (P300 or EP300), two closely related multi-domain transcription activating proteins containing a histone acetyltransferase (HAT) as well as

a bromodomain, have an important role in histone acetylation.[24–26] The CBP/P300 coactivator family (hereafter together referred to as "CBP") has been implicated in various cancers including leukemia and prostate cancer.[27–32] Furthermore, CBP has been found to regulate expression of *MYC*,[33,34] a transcription factor that is upregulated in many human cancers, and also has relevance to cancer immunotherapy,[35,36] thus contributing towards a rapidly growing interest in finding suitable CBP inhibitors. Despite the therapeutic opportunities offered by CBP, few potent and selective CBP BrD inhibitors have been reported.[37–52]

Recently, Genentech (GNE) identified CBP bromodomain inhibitor GNE-781 (**3**, Figure 1), which has unparalleled potency and selectivity over other bromodomains.[53] Screening hit **1** provided a starting point for the development of the pyrazolopiperidine series of CBP inhibitors, and additional potency and stability optimization led to identification of in vivo tool compound GNE-272 (**2**).[54] Ultimately, cell potency and selectivity over the bromodomain 1 of the bromodomain-containing protein 4 [BRD4(1)] were further improved via modification/rigidification of the aniline, exploration of the pyrazole substituent, and by utilizing a methyl urea in place of the *N*-acetyl group (**2** → **3**).

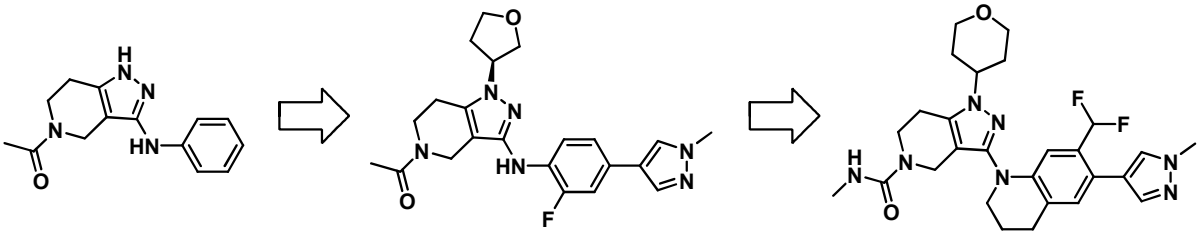

1
CBP IC_{50} = 620 nM
BRD4(1) IC_{50} = 60,000 nM
BRD4(1) IC_{50} / CBP IC_{50}= 97

GNE-272 (2)
CBP IC_{50} = 20 nM
BRD4(1) IC_{50} = 13,000 nM
BRD4(1) IC_{50} / CBP IC_{50} = 650

GNE-781 (3)
CBP IC_{50} = 0.94 nM
BRD4(1) IC_{50} = 5,100 nM
BRD4(1) IC_{50} / CBP IC_{50} = 5,400

Figure 1. Discovery and optimization of pyrazolopiperidine CBP inhibitors.

We previously reported a co-crystal structure of CBP BrD-bound **3**, which is illustrative of the interactions that govern potency and selectivity.[53] The interaction between Asn1168 and the urea moiety mimics the endogenous ligands, which are acetylated lysine residues. The selectivity over other bromodomains is attributed in part to the half-chair conformation of the piperidine ring in the tetrahydroquinoline (THQ) and the THQ sharing shape complementarity with the base of the LPF shelf (Leu1109, Pro1110, and Phe1111). In BRD4(1), the WPF shelf contains a more sterically demanding Trp81 compared to the Leu1109 residue of CBP, and this difference provides an opportunity for selectivity.[20] Additionally, a favorable interaction between the negatively polarized fluorine atoms in the difluoromethyl and the guanidinium group of Arg1173 is observed.[55] This interaction is likely to contribute to both CBP potency and improved selectivity over BRD4 since the equivalent residue to Arg1173 is Asp145 and Glu438 in BRD4(1) and BRD4(2), respectively.

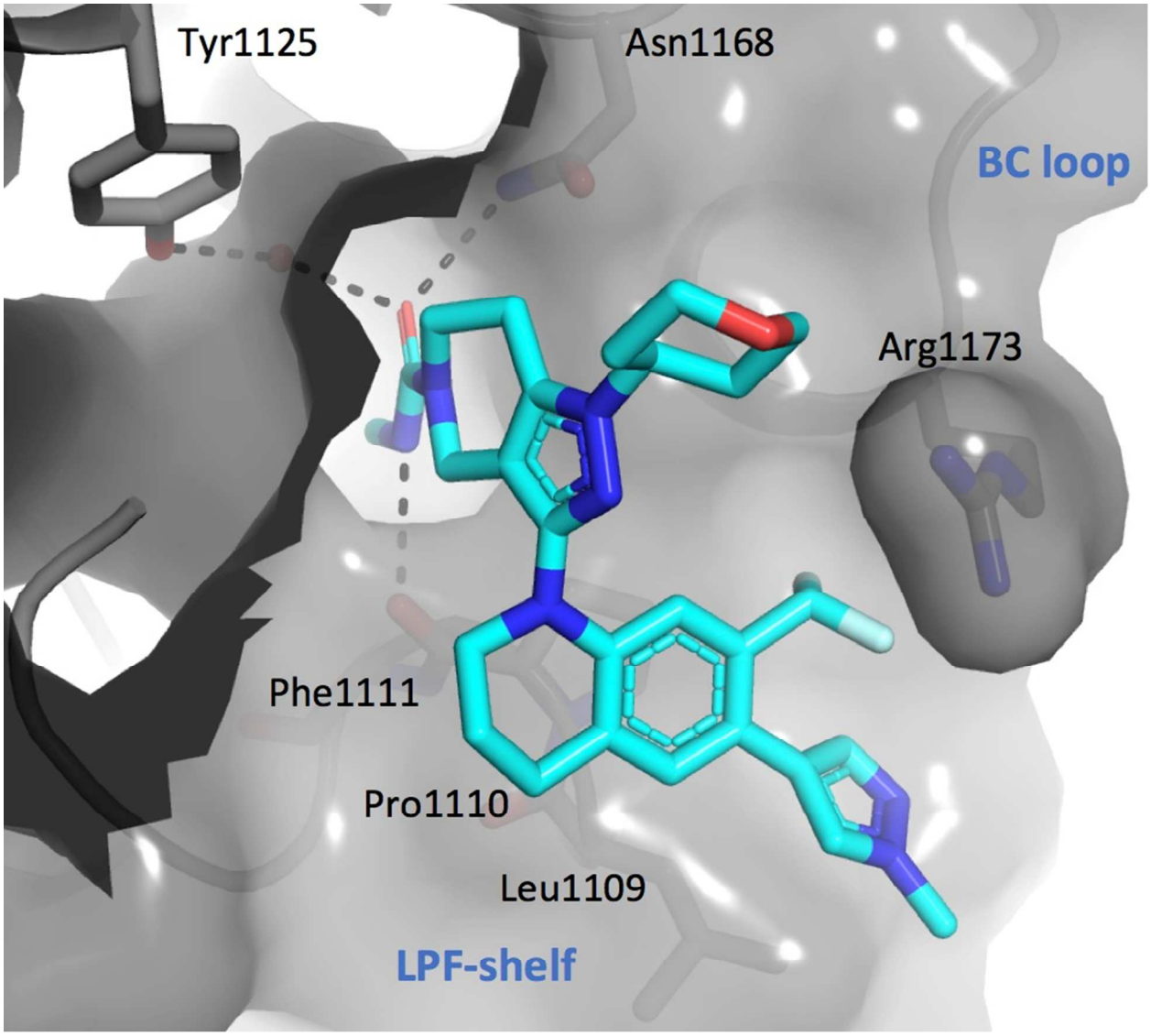

Figure 2. Co-crystal structure of CBP BrD-bound **3** (PDB-ID 5W0E).

Results and Discussion

During the course of development of **3**, we sought to develop a structurally unique second chemical series with comparable potency and selectivity to that of our lead in order to minimize risk of bringing only one series forward. Intrigued with the possibility of introducing

diversity in the Asn-binding pharmacophore, we decided to reexamine the benzodiazepinone core of CBP inhibitor **4**, which was previously developed during our program (Figure 3).[48] The benzodiazepinone scaffold had a clear vector for the THQ-CF_2H-pyrazole, and exchanging the indazole in **4** with the optimized LPF binder led to "THQ hybrid" **5**. This modification resulted in a ~9-fold increase in CBP biochemical potency as measured by the time-resolved fluorescence energy transfer (TR-FRET) assay, and an increase in selectivity over all other bromodomains assayed including bromodomain-containing protein 9 (BRD9) and cat eye syndrome critical protein 2 (CECR2). Furthermore, this result demonstrated that attaching the THQ moiety onto an Asn-binding pharmacophore, in this case the benzodiazepinone, is an effective strategy to improve selectivity and potency.

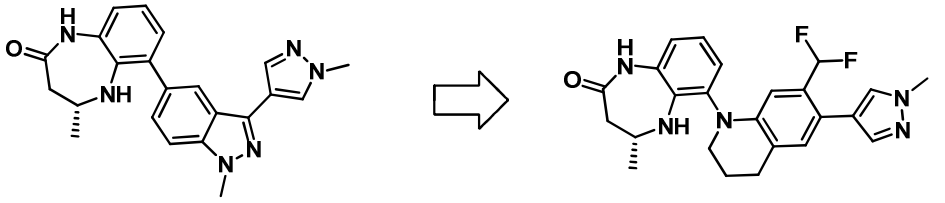

4
CBP IC_{50} = 30 nM
BRD4(1) IC_{50} = 11,000 nM
BRD4(1)/CBP Selectivity = 370
BRD9 IC_{50} = 730 nM
CECR2 IC_{50} = 7,700 nM

5
CBP IC_{50} = 3.4 nM
BRD4(1) IC_{50} = 4,500 nM
BRD4(1)/CBP Selectivity = 1,300
BRD9 IC_{50} = >20,000 nM
CECR2 IC_{50} = >20,000 nM

Figure 3. Effect of hybridization of benzodiazepinone core of **4** with THQ-CF_2H-pyrazole on CBP potency and selectivity.

As part of our screening efforts we executed a high throughput screen (HTS) targeting alternative Asn-binding cores. Cores with high ligand efficiency (LE) were selected as possible analogues for hybridization. In each case, the co-crystal structure of the CBP-bound ligand was overlaid with the co-crystal structure of **3** to evaluate whether the core had an appropriate vector

for the THQ functionality. When co-crystal structures were not available, computational docking was utilized to approximate the binding orientation of the HTS hit within the CBP bromodomain.[56] Targets were selected based on synthetic ease and whether the THQ fragment was predicted to have a similar spatial orientation in the receptor to that of lead molecule **3**. For example, a crystal structure of ligand efficient HTS hit **6** when compared to lead compound **3** indicated that appendage of the THQ onto C5 of the Asn-binding indole core might lead to a hybrid with the desired geometry (Figure 4a). Thiazolone **7** was identified as a hit in the primary HTS (Figure 4b). Although this fragment had a CBP IC_{50} >100 μM in the reconfirmation screen, **7** was nonetheless a core of interest because it was a frequently appearing motif in the HTS and also because similar scaffolds are known inhibitors of the bromodomains of tripartite motif-containing 24 protein (TRIM24) and bromodomain and PHD finger-containing protein (BRPF).[57] Docking of thiazolone **7** suggested two possible binding orientations and two potential vectors for the THQ moiety. To our delight, THQ hybrids **16** and **17** led to increases in potency from 99,000 nM to 9.5 nM in the case of the indole, and >100,000 nM to 69 nM with the thiazolone (Figure 5) relative to the parent HTS hit.

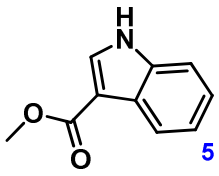

6

CBP IC_{50} = 99,000 nM

BRD4(1) IC_{50} = >100,000 nM

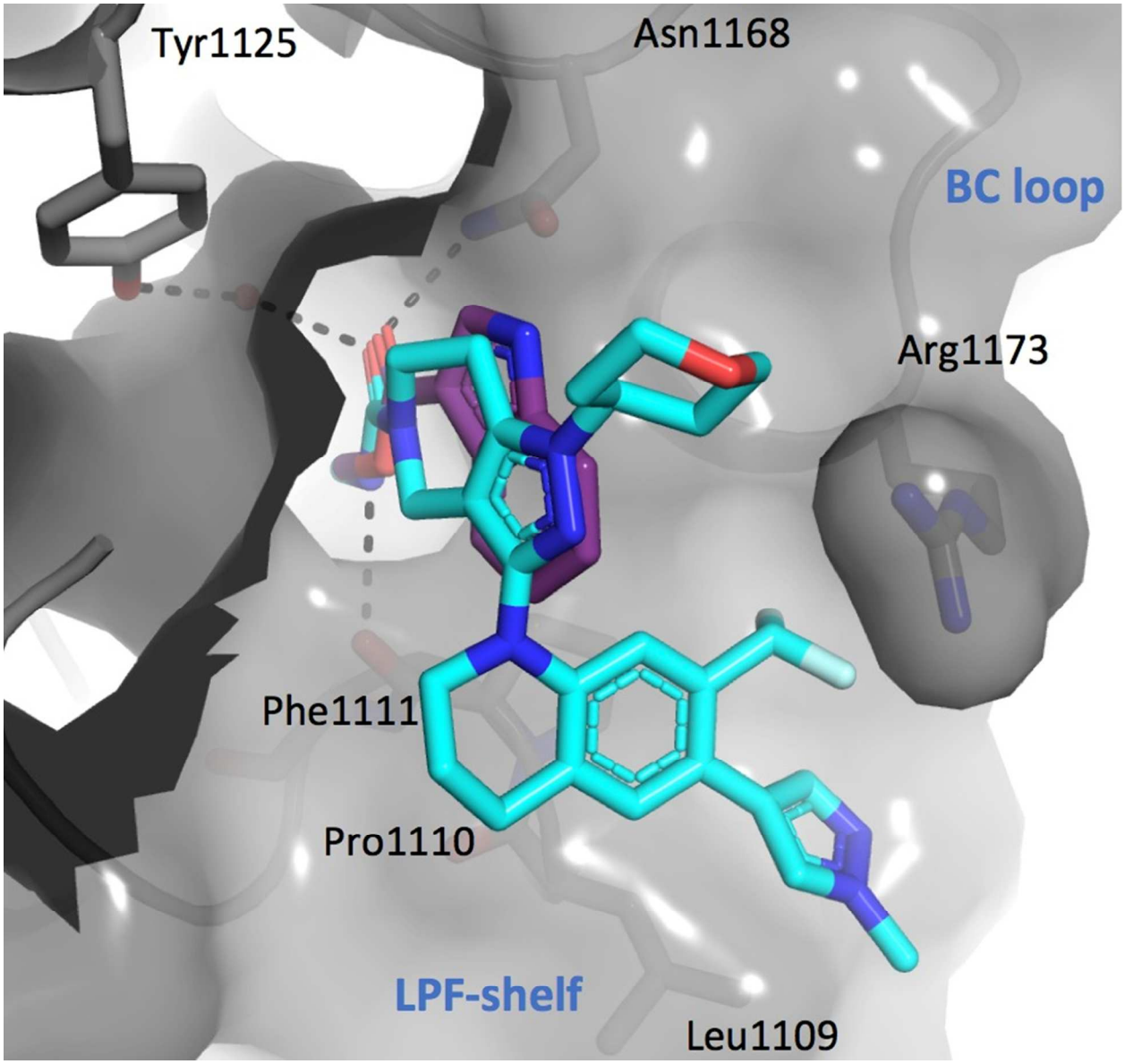

Figure 4a. Overlay of co-crystal structures of CBP BrD-bound HTS hit **6** (purple; PDB-ID 6AXQ) and **3** (cyan; PDB-ID 5W0E).

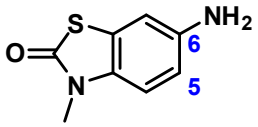

7

CBP IC_{50} = >100,000 nM
BRD4(1) IC_{50} = >100,000 nM

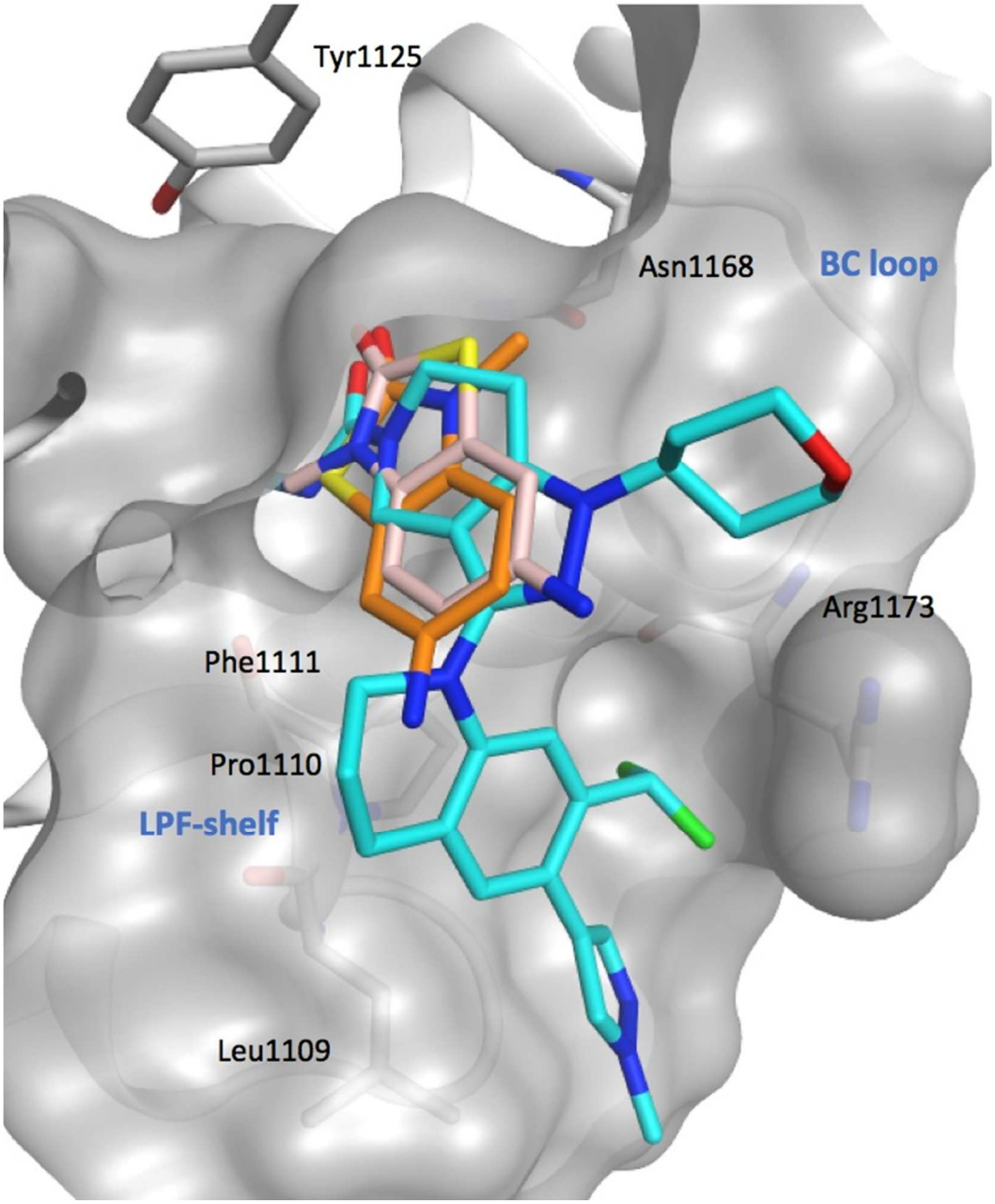

Figure 4b. Docked structures of HTS hit **7** (orange and pink) overlaid with co-crystal structure of CBP BrD-bound **3** (cyan; PDB-ID 5W0E).

In a similar fashion, HTS hits **8–13** were combined with the THQ moiety to create hybrids containing their original Asn-binging cores (Figure 5). In some cases, the Asn-binding moiety present in the core was slightly modified to provide improved potency utilizing our prior structure activity relationship (SAR) learnings.[53] The resulting THQ hybrids **18–25** demonstrated varying magnitudes of potency and selectivity increases, but nonetheless led to improved CBP inhibitors. Hybridization even rescued scaffolds that originally displayed selectivity for BRD4(1); hit **10**, which showed a 4.4-fold preference for BRD4(1)-inhibition, was transformed into a 530-fold selective CBP inhibitor via hybridization. Interestingly, the pharmacophore of **23**, although derived from the HTS hit **13**, also closely resembles that of early weak CBP inhibitor MS2126, reported by Zhou.[37] The same design exercise was performed with published CBP inhibitors with an equally fruitful outcome; hybridization of **14**[43] increased the CBP potency by 9.5-fold, while modification of **15**[41] resulted in a 34-fold improvement.[58]

X-ray co-crystal structures of CBP-bound hybrids **16** and **17** were obtained, and are depicted in Figure 6 overlaid with lead **3**. The comparison of the crystal structures with different Asn-binding motifs indicates that the binding pocket of the CBP bromodomain can accommodate some flexibility in the location of the Asn-binding core, but the THQ-CF_2H-pyrazole substituents have very similar orientations (Figure 6). This suggests that complementarity between THQ and the sub-pocket on CBP enhances both activity and selectivity in most cases. This structural comparison illustrates the crucial effect of the LPF shelf on selectivity and potency of bromodomain inhibitors and exemplifies the reduced importance of

the KAc-binding region. While the latter is necessary and is the anchor of the inhibitor, this binding region only procures modest selectivity and potency.[59]

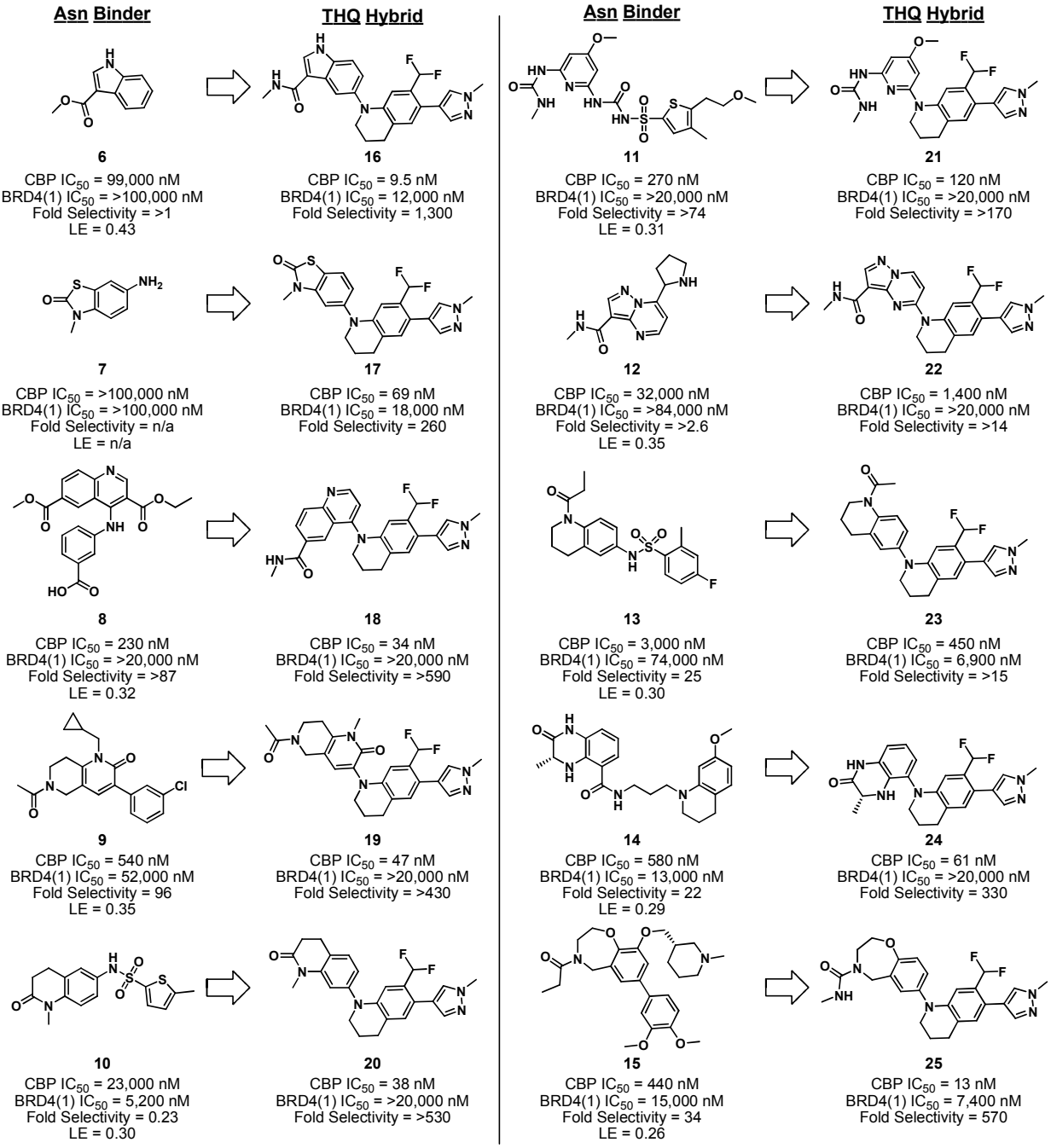

Figure 5. Hybridization of HTS hits and known CBP inhibitors with THQ LPF binder.

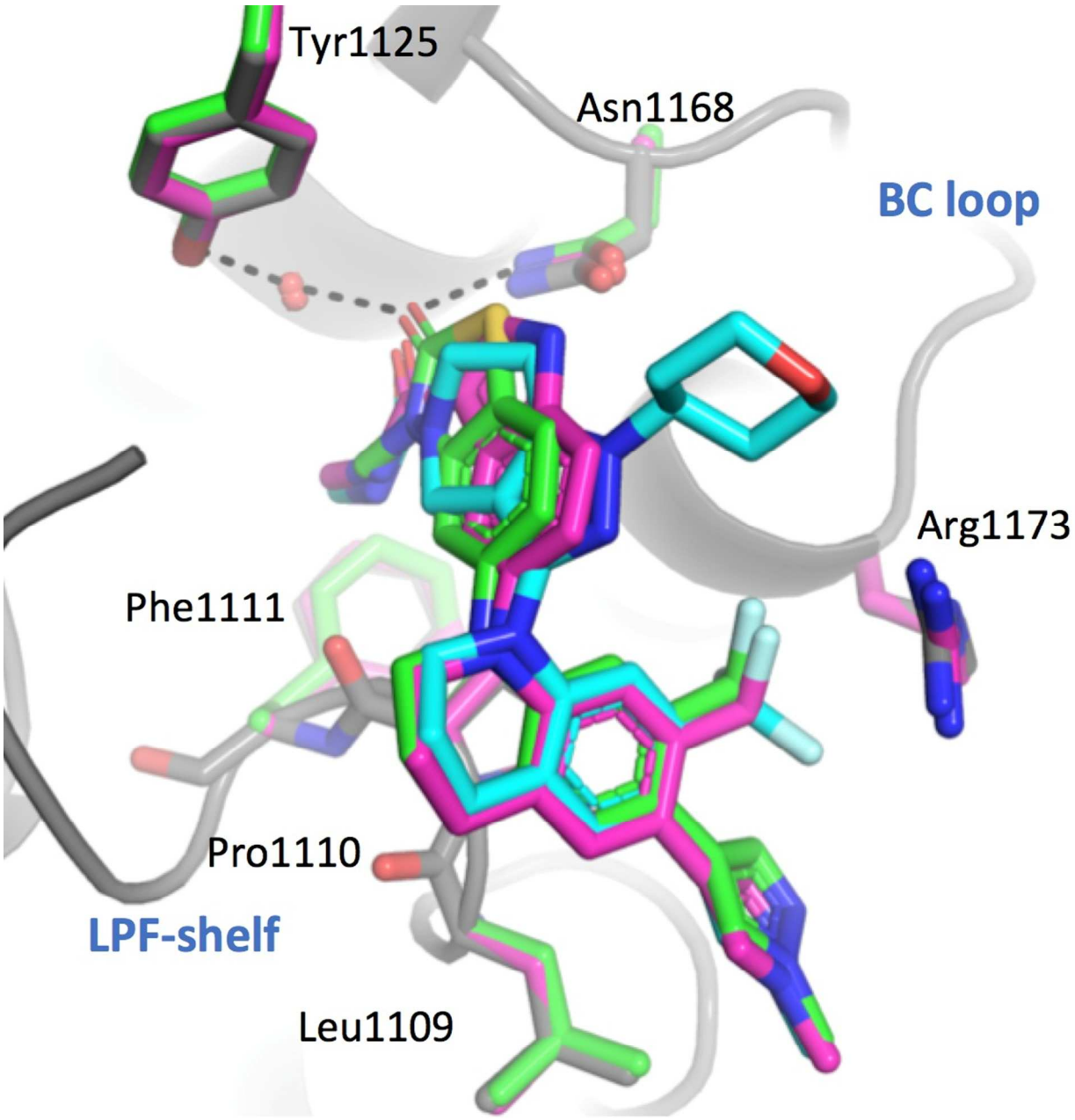

Figure 6. Overlay of co-crystal structures of CBP BrD-bound hybrids **16** (magenta; PDB-ID 6AY3), **17** (green; PDB-ID 6AY5) and **3** (cyan; PDB-ID 5W0E).

The hybridization studies described above provided a good starting point for rapid development of structurally unique and potent CBP inhibitors. Hybridization of the indole and thiazolone cores (**6** → **16** and **7** → **17**) resulted in two of the most dramatic increases in CBP

biochemical potency (10,400-fold and >1,450-fold, respectively), while also imparting exquisite selectivity over BRD4(1) (1,300-fold and 260-fold, respectively). It was anticipated that additional SAR could easily render inhibitors with similar potency to that of our lead molecule **3**. X-ray co-crystal structures also suggested that both hybrids had available vectors to grow into the loop connecting helices B and C (BC loop), which previously had been found to be a productive technique to improve potency (Figure 7a/b).[53] This further supported the decision to pursue the indole and thiazolone series.

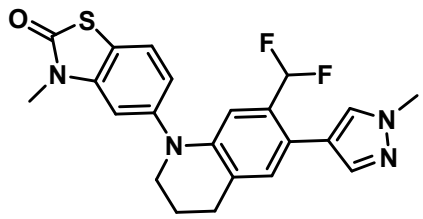

17

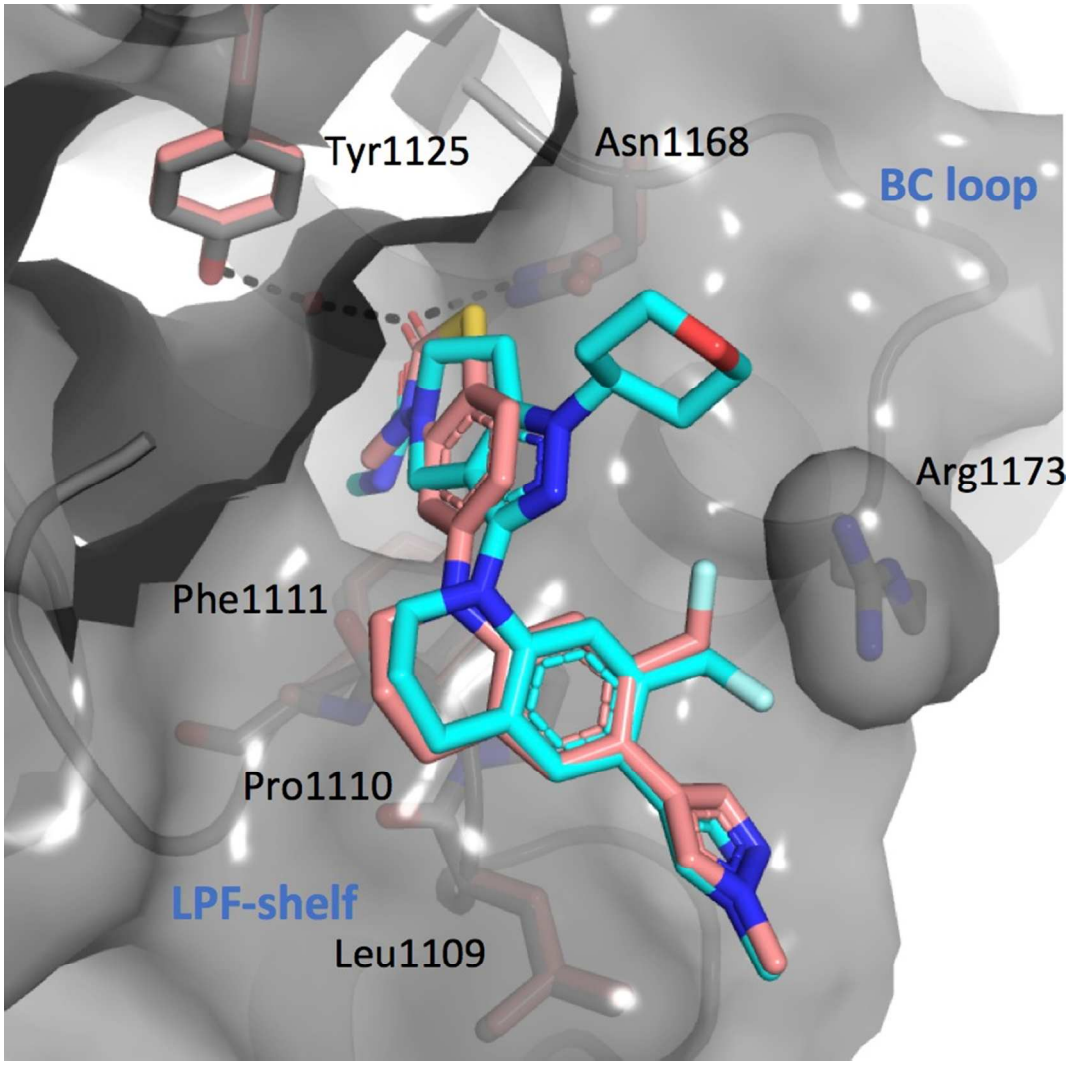

Figure 7a. Overlay of co-crystal structures of CBP BrD-bound thiazolone hybrid **17** (pink; PDB-ID 6AY5) and **3** (cyan; PDB-ID 5W0E).

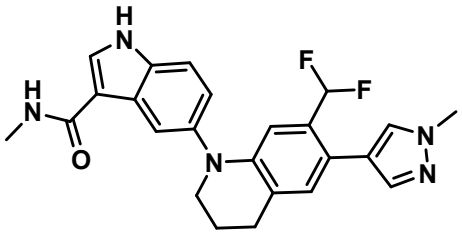

16

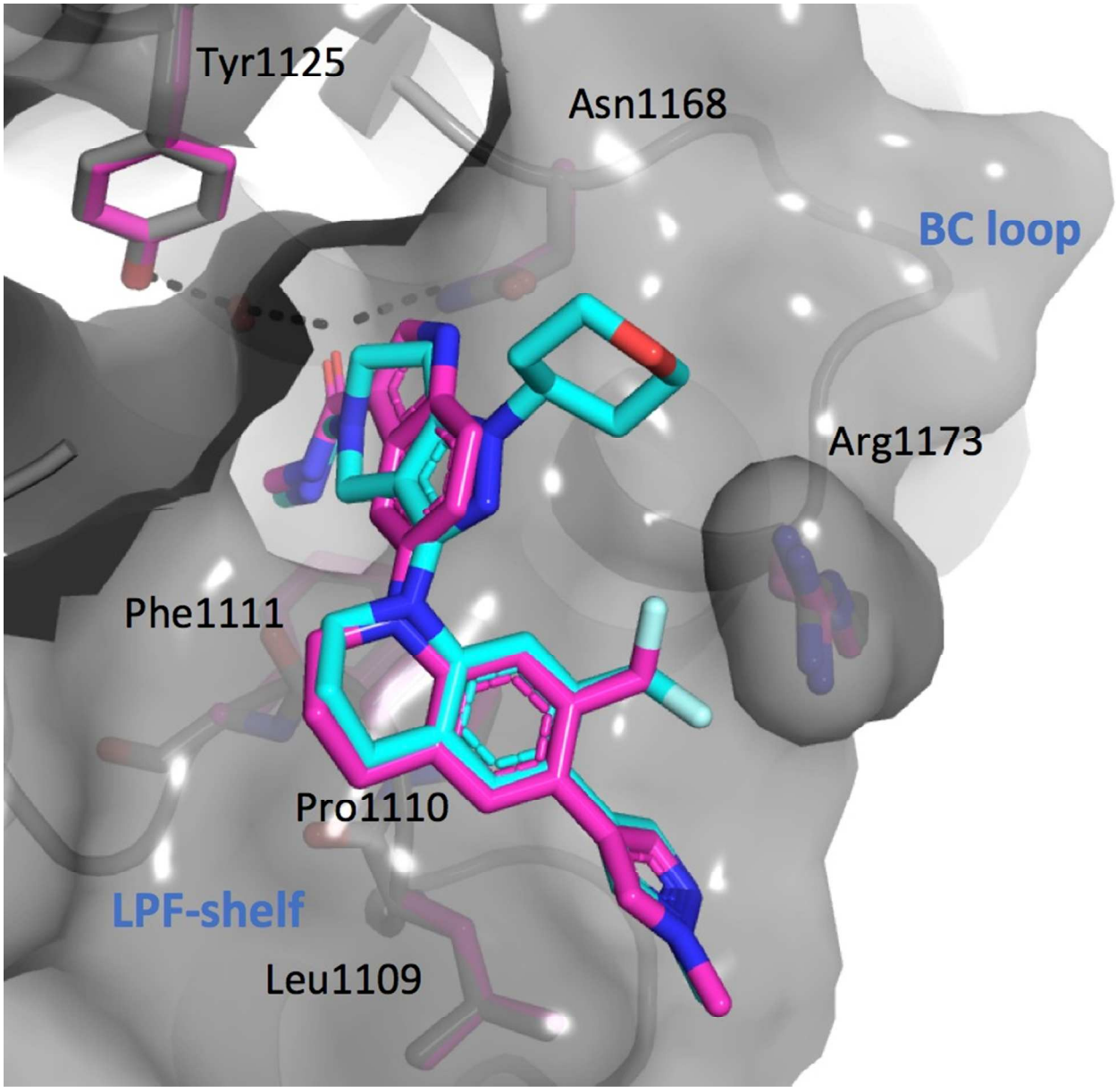

Figure 7b. Overlay of co-crystal structures of CBP BrD-bound indole hybrid **16** (magenta; PDB-ID 6AY3) and **3** (cyan; PDB-ID 5W0E).

Improvement of potency and metabolic stability were the primary goals of optimization of the thiazolone series; clearance of **17** as measured by mouse, rat, and human liver microsome-predicted hepatic clearance assays (LM Cl_{hep} M / R / H) was undesirably high at 71, 39, and 17 mL/min/kg, respectively (Figure 8). Initially, SAR of the Asn binder was examined using de novo design and ideas inspired by frequently appearing scaffolds in the HTS that had previously been overlooked because of lower LE. While other pharmacophores did not yield enhanced affinity, introduction of the benzimidazolone Asn binder resulted in a CBP IC_{50} of 20 nM (**26**, Figure 8). Expansion into the BC loop with morpholine **27** provided a good balance of biochemical potency and selectivity over BRD4(1), while imparting modest in vitro stability gains. Furthermore, **27** had excellent potency in a cellular assay of MYC expresssion[48,60] with an EC_{50} of 12 nM.

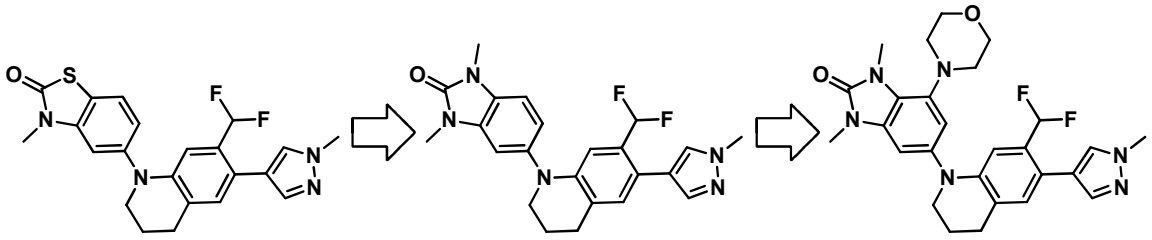

17
CBP IC_{50} = 69 nM
BRD4(1) IC_{50} = 18,000 nM
Fold Selectivity = 260
LM Cl_{hep} M / R / H = 71 / 39 / 17

26
CBP IC_{50} = 20 nM
BRD4(1) IC_{50} = 4,100 nM
Fold Selectivity = 210
LM Cl_{hep} M / R / H = 61 / 38 / 16
MYC EC_{50} = 1,000 nM

27
CBP IC_{50} = 3.6 nM
BRD4(1) IC_{50} = 1,100 nM
Fold Selectivity = 310
LM Cl_{hep} M / R / H = 48 / 23 / 15
MYC EC_{50} = 12 nM

Figure 8. Optimization of the thiazolone-THQ hybrid.

Efforts to optimize the indole series also centered on improvement of potency and metabolic stability. While indole hybrid **16** had moderate in vitro clearance (LM Cl_{hep} M / R / H = 47 / 20 / 13 mL/min/kg), efforts to improve potency by growing into the BC loop by

substitution at C7 of the indole resulted in decreased metabolic stability. To address these limitations, a nitrogen walk around the indole skeleton was performed leading to the identification of azaindole **28** that demonstrated improved CBP potency and metabolic stability (Figure 9). Azaindole **28** proved to be a suitable starting point for expansion into the critical BC loop, and isopropyl substitution at C7 provided a good balance of biochemical potency (CBP IC_{50} = 2.2 nM), and in vitro clearance (LM Cl_{hep} M / R / H = 50 / 25 / 13 mL/min/kg). Furthermore, **29** displayed an impressive improvement in potency in the MYC assay relative to hybrids **16** and **28** (EC_{50} = 53, 360, and 2,200 nM, respectively). Compound **29** was tested in an in vivo pharmacokinetics (PK) experiment, exhibiting low clearance (18.2 mL/min/kg) and moderate bioavailability (52%) when dosed to mice.

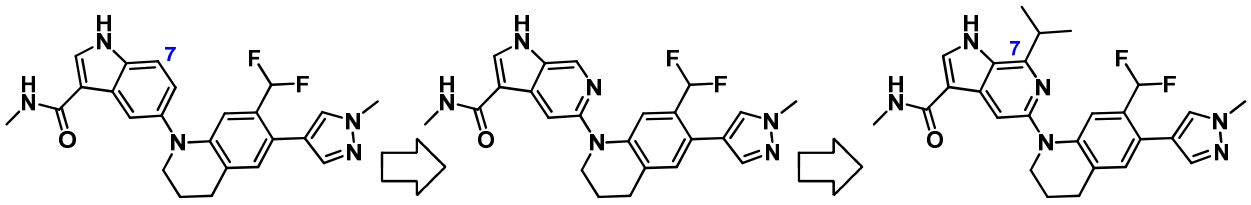

16
CBP IC_{50} = 9.5 nM
BRD4(1) IC_{50} = 12,000 nM
Fold Selectivity = 1,300
LM Cl_{hep} M / R / H = 47 / 20 / 13
MYC EC_{50} = 2,200 nM

28
CBP IC_{50} = 5.0 nM
BRD4(1) IC_{50} = 3,900 nM
Fold Selectivity = 780
LM Cl_{hep} M / R / H = 39 / 17 / 6.9
MYC EC_{50} = 360 nM

29
CBP IC_{50} = 2.2 nM
BRD4(1) IC_{50} = 2,300 nM
Fold Selectivity = 1,050
LM Cl_{hep} M / R / H = 50 / 25 / 13
MYC EC_{50} = 53 nM

Mouse PK Parameters
Cl_T = 18.2 mL/min/kg
V_{ss} = 1.9 L/kg
$T_{1/2\,(IV)}$ = 1.3 h
F = 52%

Figure 9. Optimization of the indole-THQ hybrid.

To probe the broader bromodomain selectivity of optimized THQ hybrids, **27** and **29** were submitted to the DiscoveRx BROMOscan® selectivity panel, which assesses binding in a competitive fashion by quantitating the reduction in capture of DNA-tagged bromodomain on

ligand-coated beads in the presence of compound.[61] Benzimidazolone **27** proved to have exquisite selectivity over other bromodomains. Out of 39 bromodomain-containing constructs surveyed, only 4 had any activity other than CBP and P300, with BRD9 being the most potent off target (K_d = 3,600 nM). Other off target hits were BRD7, TRIM24(BrD), and BRD3(2), with potencies of K_d = 5,100, 7,600, and 8,700 nM, respectively. Azaindole **29** also displayed exceptional selectivity in the BROMOscan selectivity panel, and no activity was detected in any potential bromodomain off-targets (K_d > 10,000 nM).

Chemistry

The target compounds were synthesized as depicted in Schemes 1–15. In all cases, aryl bromide coupling partners were obtained from either commercial sources or accessed through diverse synthetic sequences of varying complexity. Buchwald coupling of intermediate **31** was used to install the requisite tetrahydroquinoline, and conditions utilizing Pd-PEPPSI-IPent catalyst were found to be suitable for accessing most Buchwald adducts.

Scheme 1. Preparation of Compound **5**.0

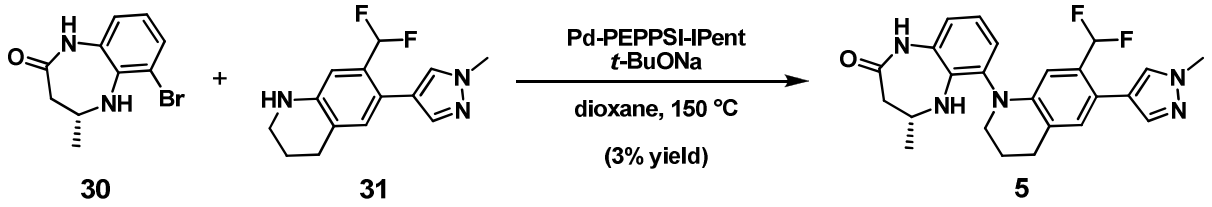

30 31 5

Scheme 2. Preparation of Compound **16**.

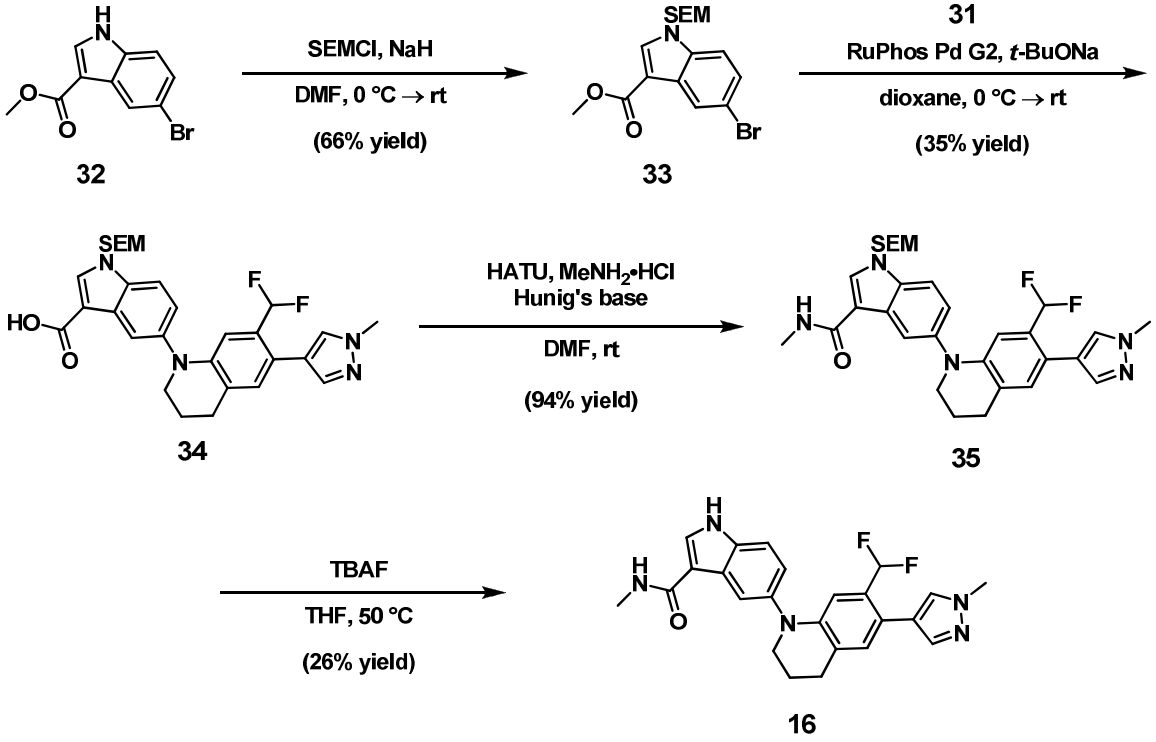

Scheme 3. Preparation of Compound **17**.

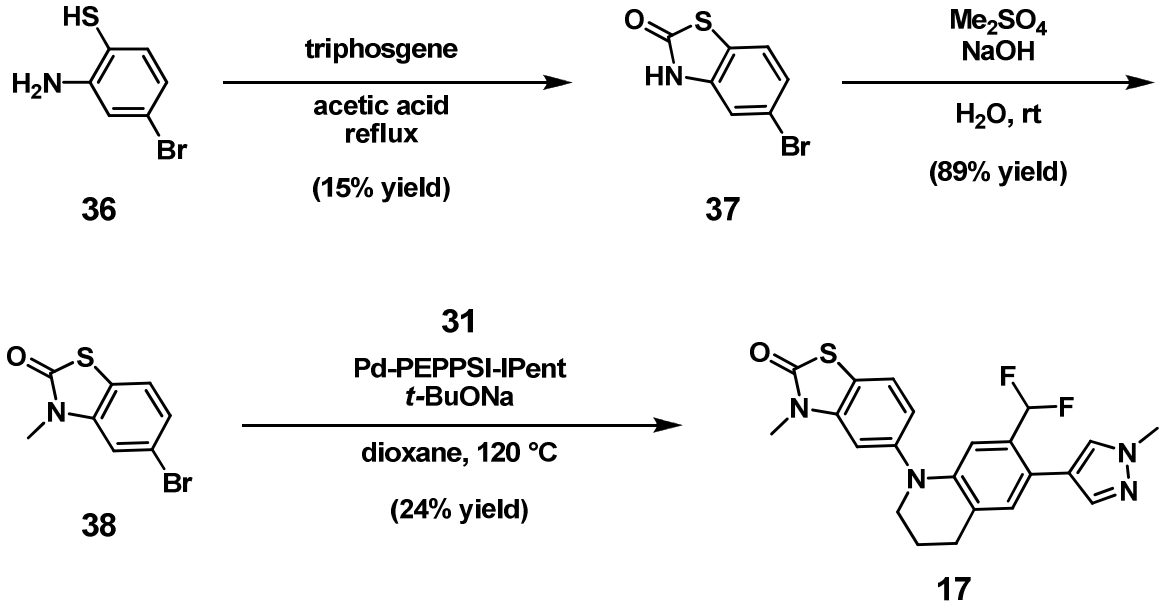

Scheme 4. Preparation of Compound **18**.

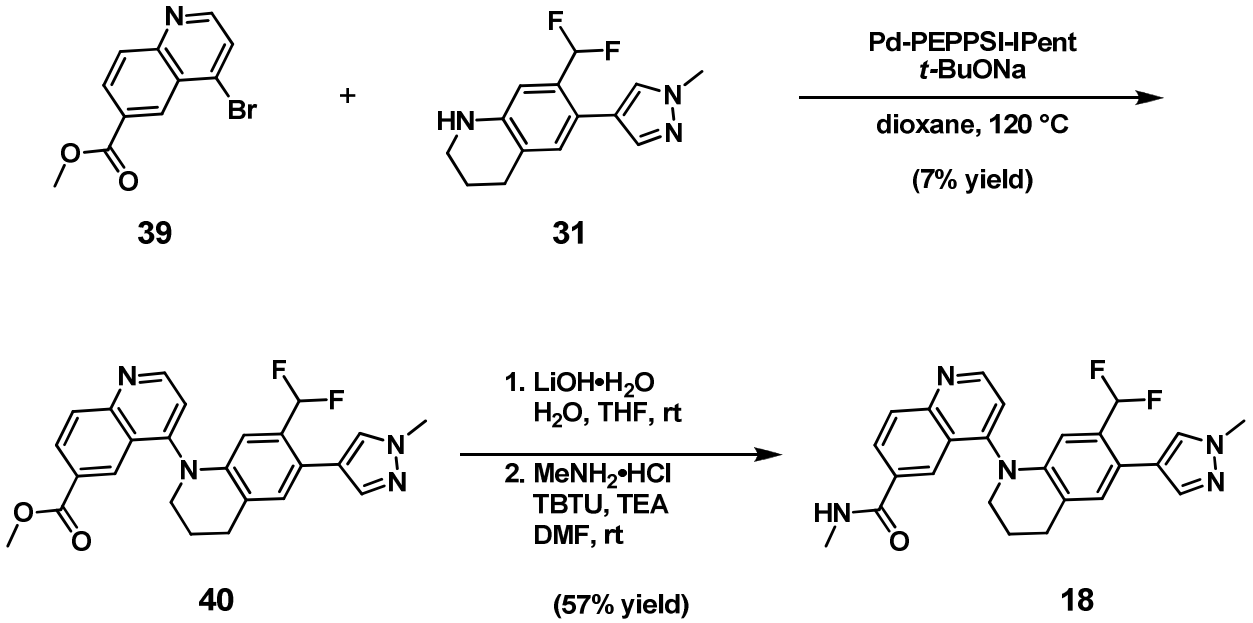

Scheme 5. Preparation of Compound **19**.

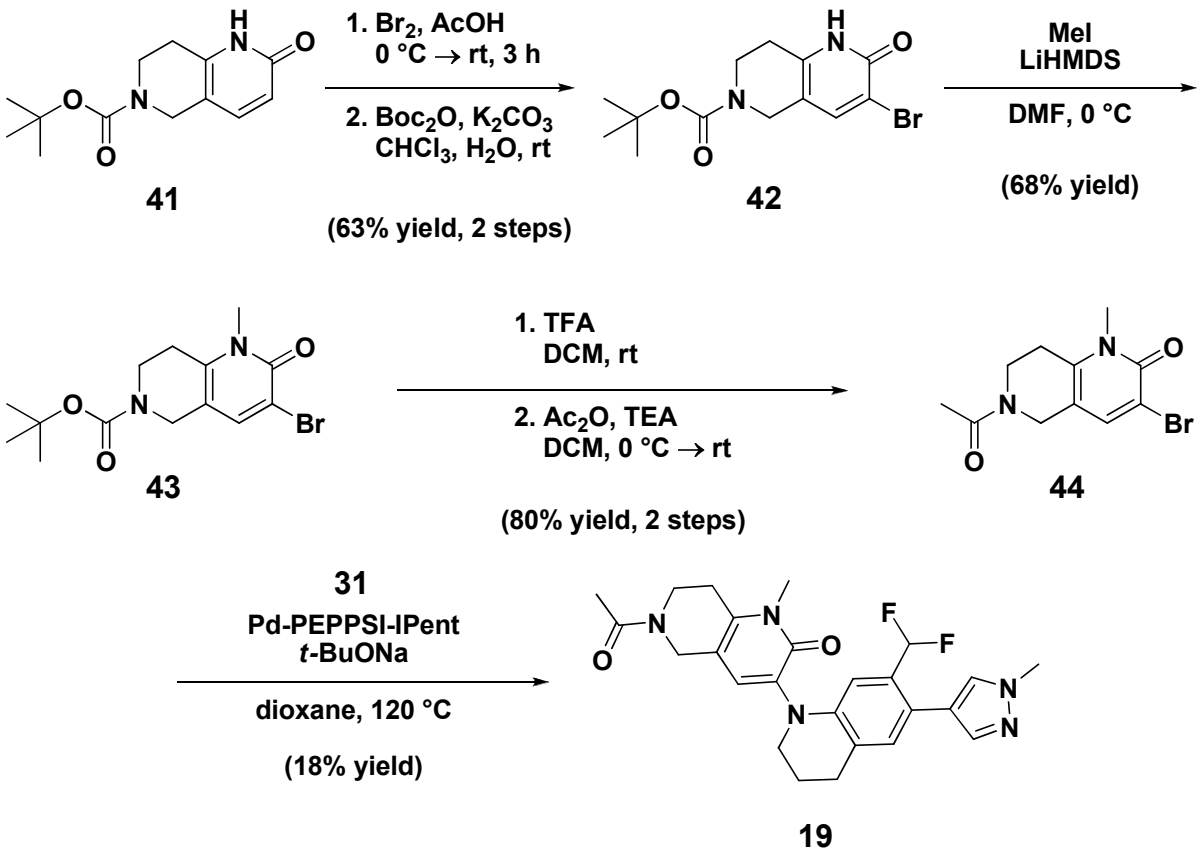

Scheme 6. Preparation of Compound **20**.

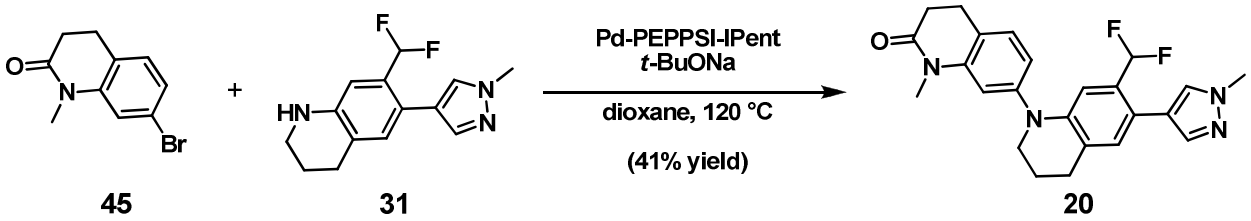

Scheme 7. Preparation of Compound **21**.

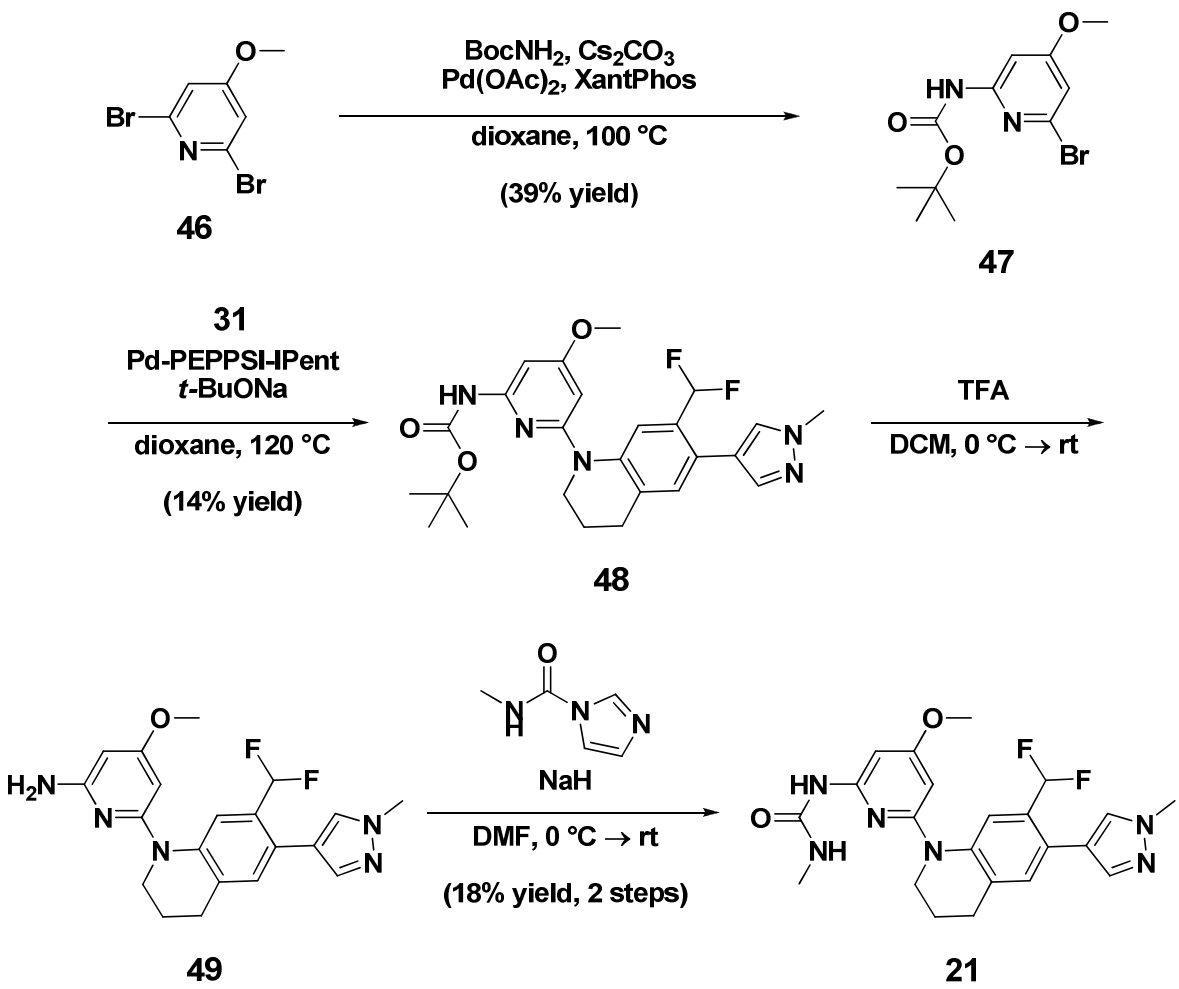

Scheme 8. Preparation of Compound **22**.

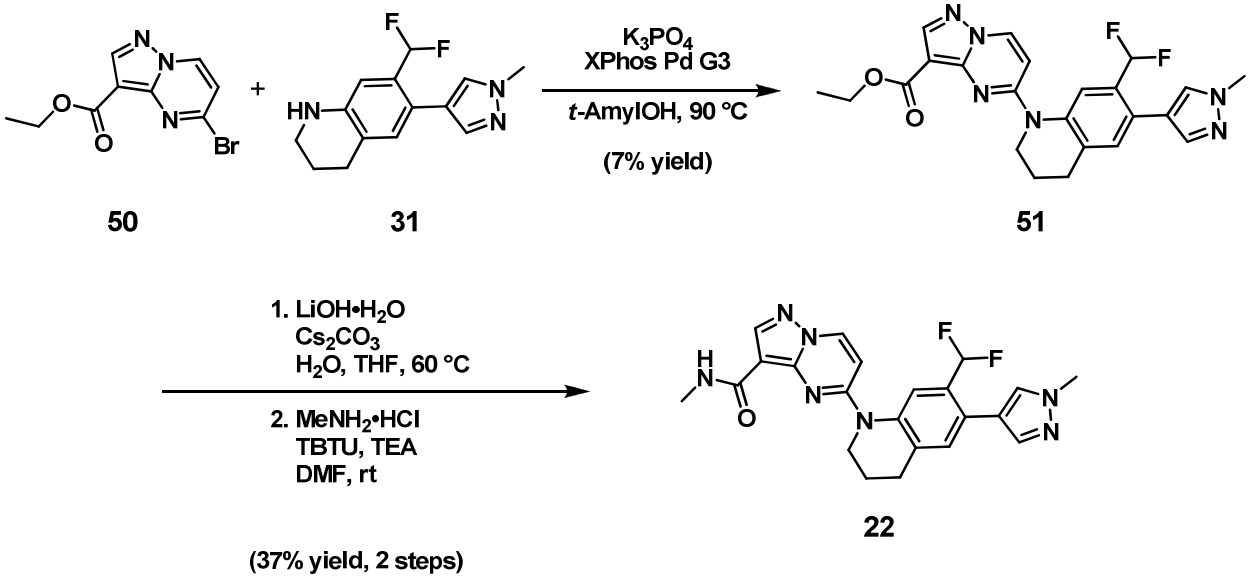

Scheme 9. Preparation of Compound **23**.

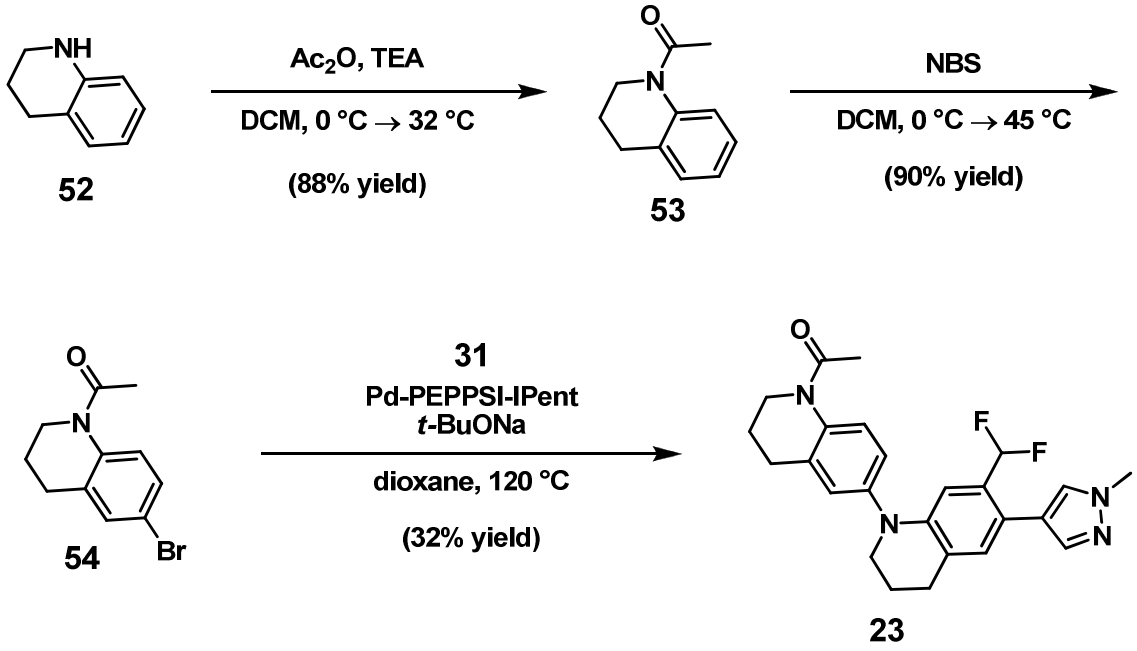

Scheme 10. Preparation of Compound **24**.

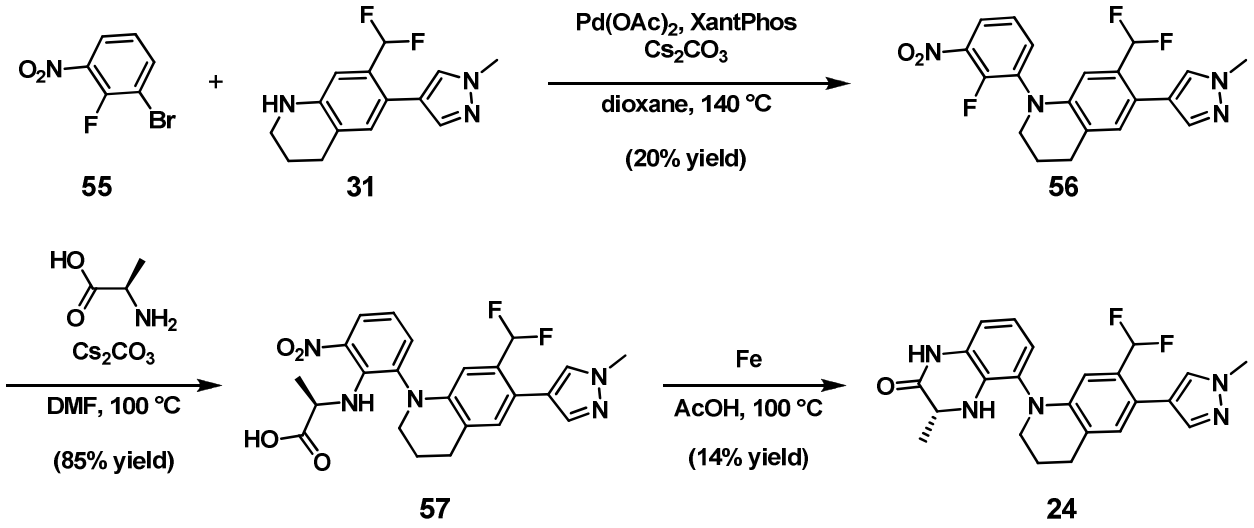

Scheme 11. Preparation of Compound **25**.

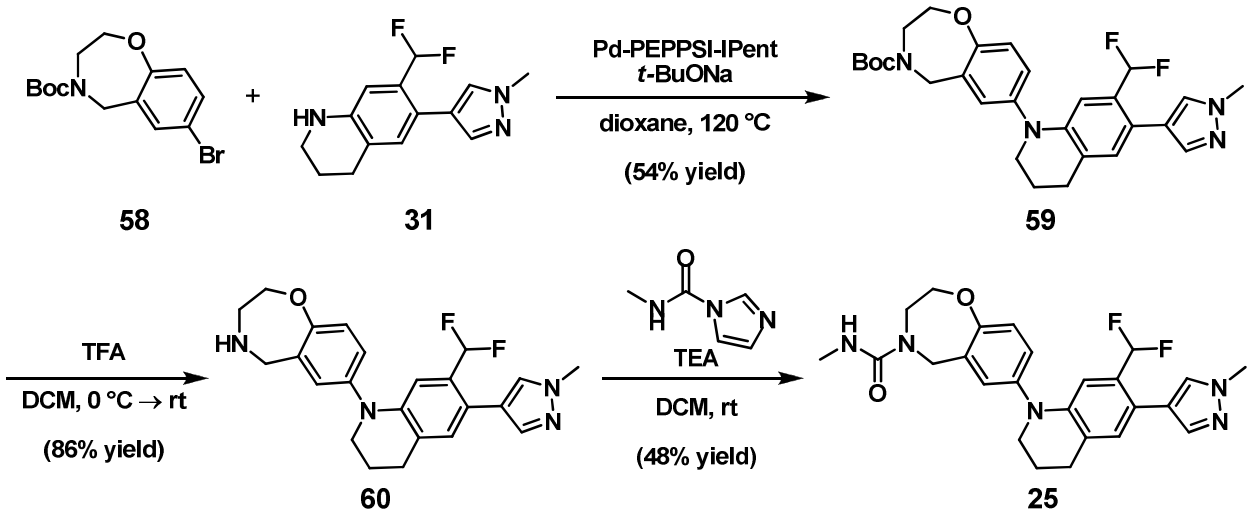

Scheme 12. Preparation of Compound **26**.

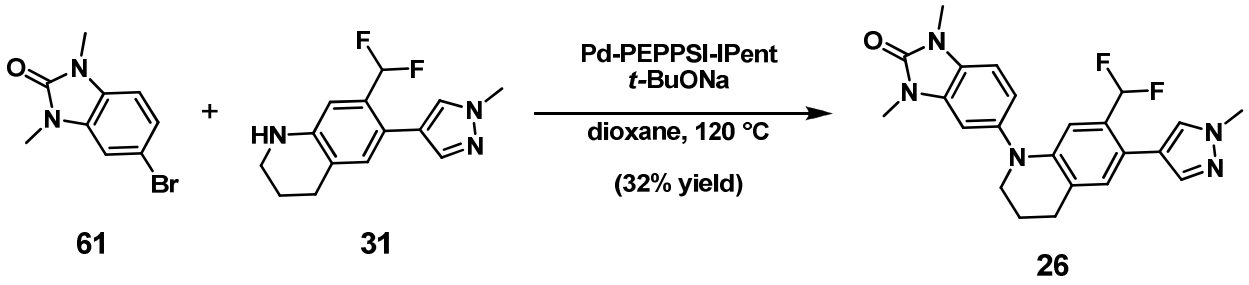

61 31 26

Scheme 13. Preparation of Compound **27**.

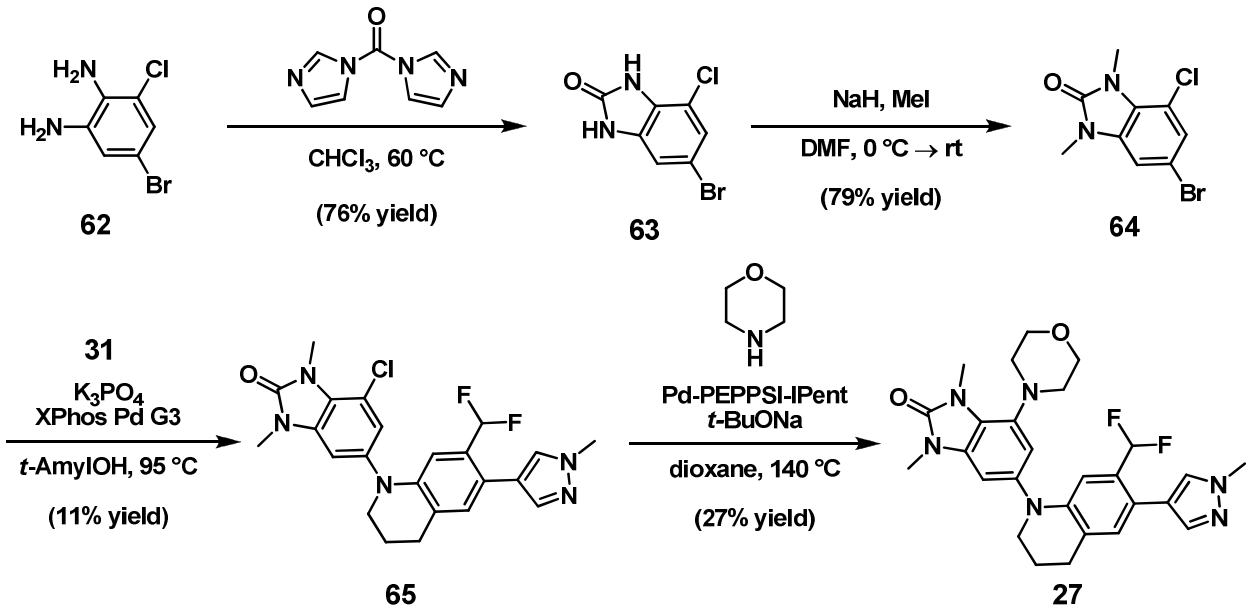

62 63 64 65 27

Scheme 14. Preparation of Compound **28**.

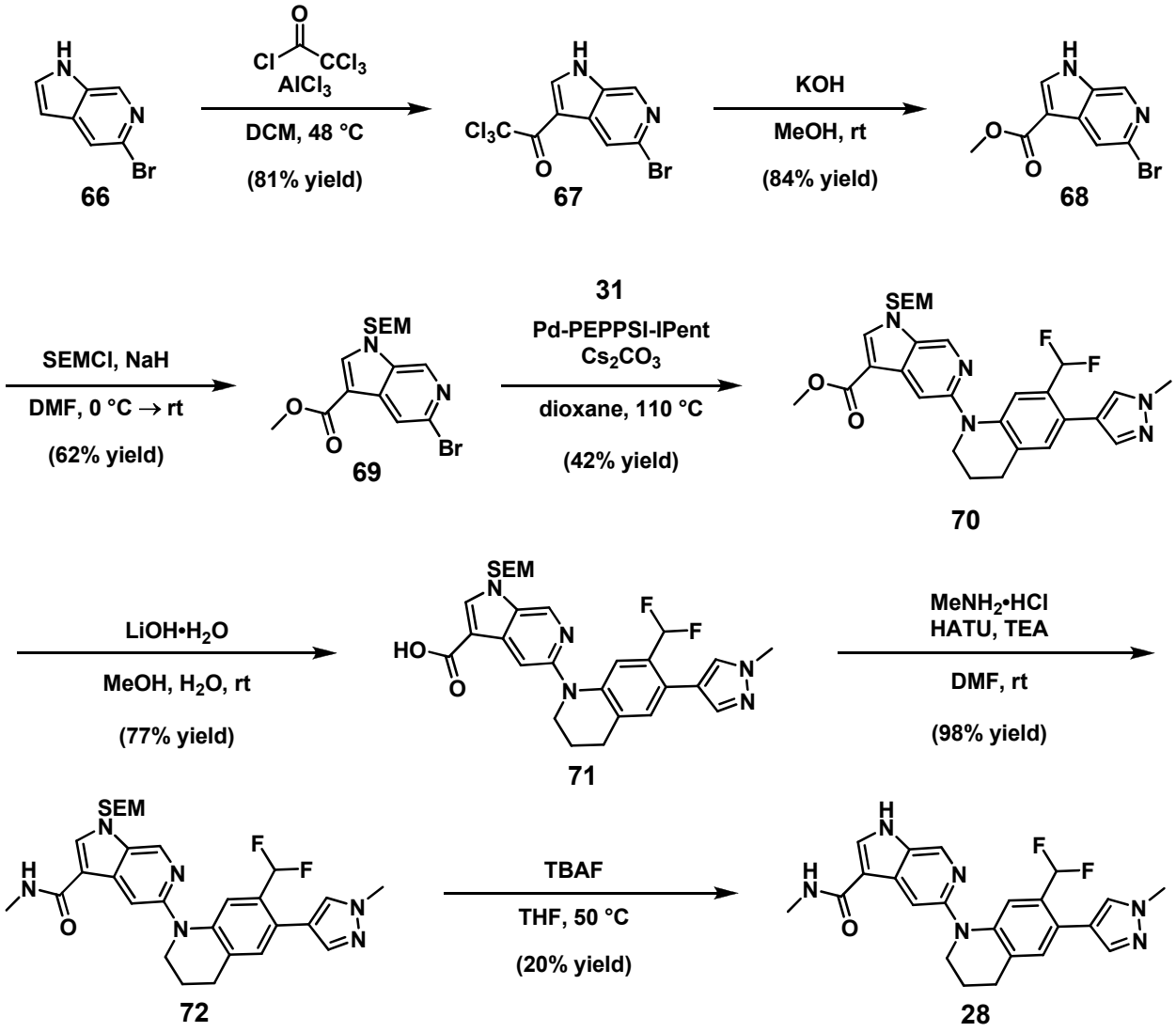

Scheme 15. Preparation of Compound **29**.

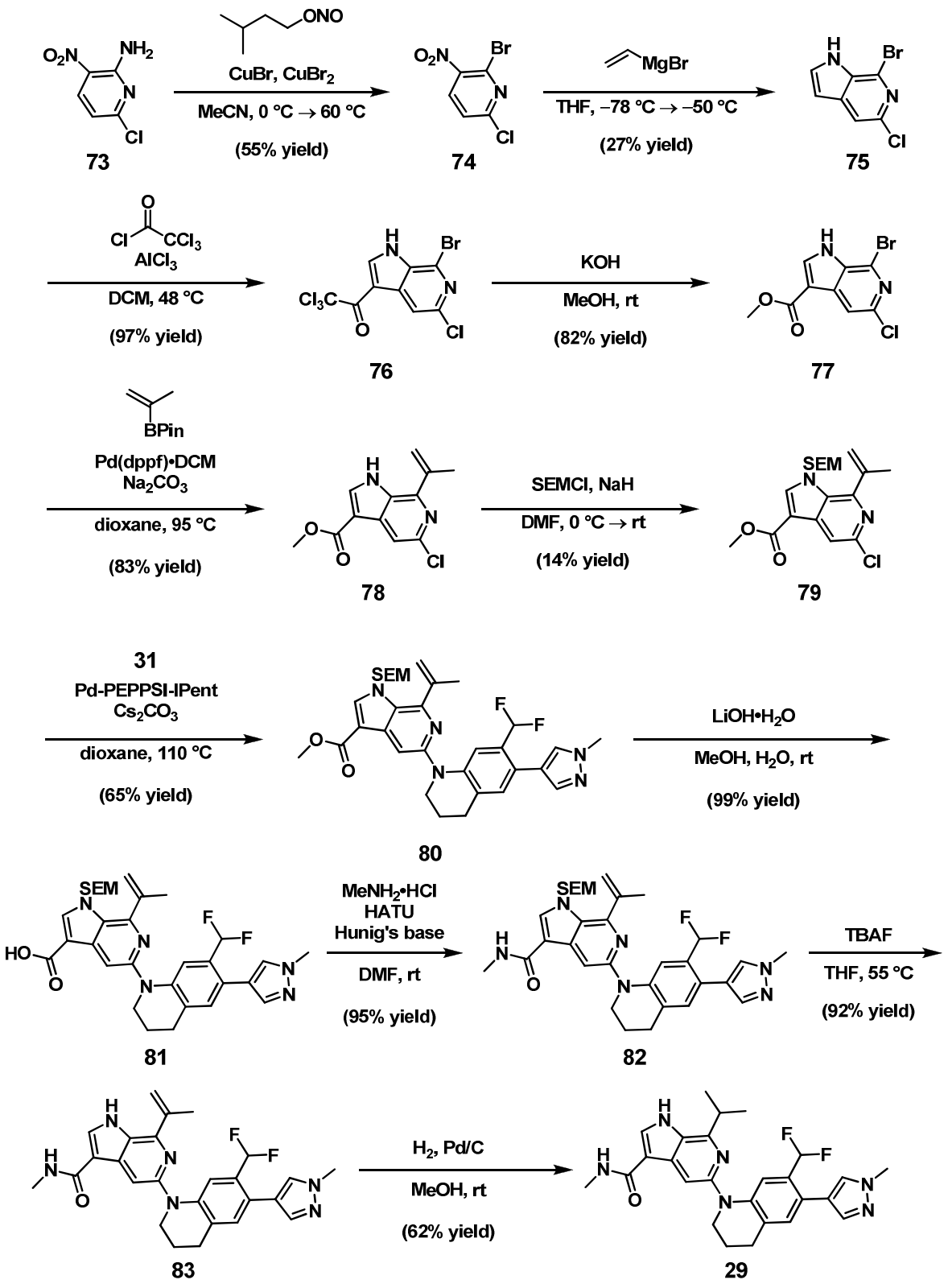
CuBr, CuBr2
MeCN, 0 °C → 60 °C
(55% yield)
MgBr
THF, –78 °C → –50 °C
(27% yield)
AlCl3
DCM, 48 °C
(97% yield)
KOH
MeOH, rt
(82% yield)
Pd(dppf)•DCM
Na2CO3
dioxane, 95 °C
(83% yield)
SEMCl, NaH
DMF, 0 °C → rt
(14% yield)
31
Pd-PEPPSI-IPent
Cs2CO3
dioxane, 110 °C
(65% yield)
LiOH•H2O
MeOH, H2O, rt
(99% yield)
MeNH2•HCl
HATU
Hunig's base
DMF, rt
(95% yield)
TBAF
THF, 55 °C
(92% yield)
H2, Pd/C
MeOH, rt
(62% yield)
73
74
75
76
77
78
79
80
81
82
83
29

Conclusion

This work demonstrates that a variety of unique Asn binders can be hybridized with the THQ-CF_2H-pyrazole LPF fragment to create potent, selective, and structurally diverse CBP probes. Structure-based drug design (SBDD) provided a robust foundation for rapid optimization of novel cores in the hybridization process, as evidenced by the development of the THQ-benzimidazolone and THQ-indole series; 43 hybrids were synthesized in the case of the thiazolone/imidazolone series, while optimization of the indole series required the synthesis of 29 analogues. Generally in SBDD, larger structural modifications are associated with greater risk of potency loss. The novelty in this work is that half of the inhibitor was replaced with a completely new scaffold while potency was maintained; furthermore, the fragment necessary for ligand recognition, the Asn binder, underwent significant alteration. While this was a highly structurally enabled project, in many cases, crystal structures were not necessary and hybrids could be effectively designed simply with computationally docked structures. Rarely is SBDD executed in such a predictable manner.

Whereas previously disclosed bromodomain inhibitors were developed by first identifying an Asn-binding starting point and then building into the LPF shelf, our THQ-hybridization strategy provides a complimentary and unique strategy to efficiently perform hit-to-lead optimization. While an Asn-binding element was still necessary to maintain activity, these findings illustrate that both CBP bromodomain potency and selectivity over other bromodomains can be controlled via favorable interactions with the LPF shelf and adjacent residues. Optimization of the LPF shelf/ligand interaction provides a robust potency and

selectivity handle for the development of CBP inhibitors that can be used to probe the biology of this epigenetic target. Furthermore, we anticipate that this novel hybridization strategy will have a broader application for the discovery of inhibitors of the medicinally-relevant bromodomain family beyond CBP and P300.

Experimental Procedures

General Methods. All solvents and reagents were used as obtained. NMR analysis performed in a deuterated solvent with a Varian Avance 300-MHz or Bruker Avance 400- or 500-MHz NMR spectrometers, referenced to trimethylsilane (TMS). Chemical shifts are expressed as δ units using TMS as the external standard (in NMR description, s = singlet, d = doublet, t = triplet, q = quartet, m = multiplet, and br = broad peak). All coupling constants (*J*) are reported in Hertz. Mass spectra were measured with a Finnigan SSQ710C spectrometer using an ESI source coupled to a Waters 600MS high performance liquid chromatography (HPLC) system operating in reverse-phase mode with an X-bridge Phenyl column of dimensions 150 mm by 2.6 mm, with 5 μm sized particles. Preparatory-scale silica gel chromatography was performed using medium-pressure liquid chromatography (MPLC) on a CombiFlash Companion (Teledyne ISCO) with RediSep normal phase silica gel (35−60 μm) columns and UV detection at 254 nm. Reverse-phase high performance liquid chromatography (HPLC) was used to purify compounds as needed by elution from a Phenomenex Gemini-NX C18 column (30 × 50 mm, 5 micron) as stationary phase using mobile phase indicated, and operating at a 60 mL/min flow rate on a Interchim PuriFlash SFC UV-directed prep instrument. Super critical fluid (SFC) chromatography was used to purify compounds as needed by elution from a Phenomenex

Gemini-NX C18 column (30 × 50 mm, 5 micron) as stationary phase using mobile phase indicated, and operating at a 100 mL/min flow rate on a Thar 100 SFC UV-directed prep instrument. Chemical purities were >95% for all final compounds as assessed by LC/MS analysis. The following analytical method was used to determine chemical purity of final compounds: HPLC-Agilent 1200, water with 0.05% TFA, acetonitrile with 0.05% TFA (buffer B), Agilent SB-C18, 1.8 μM, 2.1 x 30 mm, 25 ºC, 3–95% buffer B in 8.5 min, 95% in 2.5 min, 400 μL/min, 220 nm and 254 nm, equipped with Agilent quadrupole 6140, ESI positive, 90–1300 amu.

Synthesis and characterization of (4*R*)-6-[7-(difluoromethyl)-6-(1-methylpyrazol-4-yl)-3,4-dihydro-2*H*-quinolin-1-yl]-4-methyl-1,3,4,5-tetrahydro-1,5-benzodiazepin-2-one (5).

(*R*)-6-bromo-4-methyl-4,5-dihydro-1*H*-benzo[*b*][1,4]diazepin-2(3*H*)-one **(30)**[48] and 1-methyl-7-(difluoromethyl)-6-(1-methylpyrazol-4-yl)-1,2,3,4-tetrahydroquinoline **(31)**[53] were synthesized as previously described. To a solution of (*R*)-6-bromo-4-methyl-4,5-dihydro-1*H*-benzo[*b*][1,4]diazepin-2(3*H*)-one (**30**, 100 mg, 0.392 mmol, 1.0 equiv) in 1,4-dioxane (2 mL) was added 7-(difluoromethyl)-6-(1-methylpyrazol-4-yl)-1,2,3,4-tetrahydroquinoline (**31,** 125 mg, 0.475 mmol, 1.2 equiv), *t*-BuONa (190 mg, 1.98 mmol, 4.2 equiv) and dichloro[1,3-bis(2,6-di-3-pentylphenyl)imidazol-2-ylidene](3-chloropyridyl)palladium(II) (32 mg, 0.040 mmol, 10 mol%). The mixture was heated to 120 °C for 16 h under nitrogen atmosphere. After cooling to room temperature, the mixture was filtered and the filtrate was concentrated in vacuo. The crude residue was diluted with water (10 mL) and the mixture was extracted with EtOAc (10 mL × 3). The combined organic layers were washed with sat. aq. $NaHCO_3$ (10 mL x 3), dried over

anhydrous Na_2SO_4 and concentrated in vacuo. The crude residue was purified by reverse phase chromatography (acetonitrile 10–40% / 0.2% formic acid in water) to give (4*R*)-6-[7-(difluoromethyl)-6-(1-methylpyrazol-4-yl)-3,4-dihydro-2*H*-quinolin-1-yl]-4-methyl-1,3,4,5-tetrahydro-1,5-benzodiazepin-2-one (**5,** 6 mg, 3%) as a white solid. ^{1}H NMR (400 MHz, $CDCl_3$): δ 7.71 (s, 1H), 7.53 (s, 1H), 7.40 (s, 1H), 7.07 (s, 1H), 6.98–6.95 (m, 1H), 6.87–6.82 (m, 2H), 6.54 (s, 1H), 6.46 (t, *J* = 55.6 Hz, 1H), 4.38–4.30 (m, 1H), 4.00–3.94 (m, 4H), 3.59–3.56 (m, 1H), 3.46–3.36 (m, 1H), 3.05–2.97 (m, 1H), 2.95–2.85 (m, 1H), 2.79–2.60 (m, 1H), 2.58–2.44 (m, 1H), 2.15–2.08 (m, 2H), 1.27–1.17 (m, 3H). LCMS (*m/z*) $[M+H]^+$ 438.

Synthesis and characterization of 5-(7-(difluoromethyl)-6-(1-methyl-1*H*-pyrazol-4-yl)-3,4-dihydroquinolin-1(2*H*)-yl)-*N*-methyl-1*H*-indole-3-carboxamide (16)

Step 1, methyl 5-bromo-1-((2-(trimethylsilyl)ethoxy)methyl)-1H-indole-3-carboxylate (**33**): To a solution of methyl 5-bromo-1*H*-indole-3-carboxylate (**32**, 800 mg, 3.15 mmol, 1.0 equiv) in DMF (3 mL) at 0 °C was added NaH (60% dispersion in mineral oil, 139 mg, 3.48 mmol, 1.1 equiv) portionwise. The mixture was stirred at room temperature for 0.5 h. (2-(Chloromethoxy)ethyl)trimethylsilane (0.61 mL, 3.47 mmol, 1.1 equiv) was added dropwise and the mixture stirred at room temperature for an additional 3 h. The mixture was quenched with water (20 mL) and extracted with EtOAc (20 mL x 3). The combined organic layers were washed with brine (20 mL), dried over anhydrous Na_2SO_4, filtered and concentrated in vacuo. The crude residue was purified by silica gel chromatography (petroleum ether / EtOAc = 10 : 1) to give methyl 5-bromo-1-((2-(trimethylsilyl)ethoxy)methyl)-1*H*-indole-3-carboxylate (**33**, 800 mg, 66%) as a colorless oil. ^{1}H NMR (400 MHz, $CDCl_3$): δ 8.33 (s, 1H), 7.87 (s, 1H), 7.43–7.38

(m, 2H), 5.48 (s, 2H), 3.94 (s, 3H), 3.47 (t, J = 8.0 Hz, 2H), 0.89 (t, J = 8.0 Hz, 2H), –0.03 (s, 9H).

Step 2, 5-(7-(difluoromethyl)-6-(1-methyl-1H-pyrazol-4-yl)-3,4-dihydroquinolin-1(2H)-yl)-1-((2-(trimethylsilyl)ethoxy)methyl)-1H-indole-3-carboxylic acid (**34**): To a solution of methyl 5-bromo-1-((2-(trimethylsilyl)ethoxy)methyl)-1*H*-indole-3-carboxylate (**33**, 200 mg, 0.520 mmol, 1.0 equiv) and 7-(difluoromethyl)-6-(1-methyl-1*H*-pyrazol-4-yl)-1,2,3,4-tetrahydroquinoline (**31**, 164 mg, 0.623 mmol, 1.2 equiv) in 1,4-dioxane (4 mL) was added chloro(2-dicyclohexylphosphino-2',6'-di-*i*-propoxy-1,1'-biphenyl)(2'-amino-1,1'-biphenyl-2-yl)palladium(II) (39 mg, 0.050 mmol, 10 mol%), 2-dicyclohexylphosphino-2',6'-di-*i*-propoxy-1,1'-biphenyl (23 mg, 0.050 mmol, 10 mol%) and *t*-BuONa (150 mg, 1.56 mmol, 3 equiv). The mixture was heated to 120 °C for 12 h under a nitrogen atmosphere. After cooling the reaction to room temperature, DCM (40 mL) was added and washed with water (30 mL x 2). The organic layer was dried over anhydrous Na_2SO_4, filtered and concentrated in vacuo. The crude residue was purified by Prep-TLC (DCM / MeOH = 10 : 1) to give 5-(7-(difluoromethyl)-6-(1-methyl-1*H*-pyrazol-4-yl)-3,4-dihydroquinolin-1(2*H*)-yl)-1-((2-(trimethylsilyl)ethoxy)methyl)-1*H*-indole-3-carboxylic acid (**34**, 100 mg, 35%) as a white solid. LCMS (*m/z*) $[M+H]^+$ 553.

Step 3, 5-(7-(difluoromethyl)-6-(1-methyl-1H-pyrazol-4-yl)-3,4-dihydroquinolin-1(2H)-yl)-N-methyl-1-((2-(trimethylsilyl)ethoxy)methyl)-1H-indole-3-carboxamide (**35**): To a solution of 5-(7-(difluoromethyl)-6-(1-methyl-1*H*-pyrazol-4-yl)-3,4-dihydroquinolin-1(2*H*)-yl)-1-((2-(trimethylsilyl)ethoxy)methyl)-1*H*-indole-3-carboxylic acid (**34**, 140 mg, 0.247 mmol, 1.0 equiv) and *N,N*-diisopropylethylamine (0.13 mL, 0.76 mmol, 3.0 equiv) in DMF (3 mL) was added *O*-(7-azabenzotriazol-1-yl)-*N,N,N',N'*-tetramethyluronium hexafluorophosphate (116 mg, 0.305 mmol, 1.2 equiv) and methylamine hydrochloride (21 mg, 0.31 mmol, 1.2 equiv). The reaction

was stirred at room temperature for 2 h. EtOAc (50 mL) was added and washed with water (50 mL x 3) and brine (50 mL). The organic layer was dried over anhydrous Na_2SO_4, filtered and concentrated in vacuo to give 5-(7-(difluoromethyl)-6-(1-methyl-1*H*-pyrazol-4-yl)-3,4-dihydroquinolin-1(2*H*)-yl)-*N*-methyl-1-((2-(trimethylsilyl)ethoxy)methyl)-1*H*-indole-3-carboxamide (**35**, 135 mg, 94%) as a white solid that required no further purification. LCMS (*m/z*) $[M+H]^+$ 566.

Step 4, 5-(7-(difluoromethyl)-6-(1-methyl-1H-pyrazol-4-yl)-3,4-dihydroquinolin-1(2H)-yl)-N-methyl-1H-indole-3-carboxamide (**16**): To a solution of 5-(7-(difluoromethyl)-6-(1-methyl-1*H*-pyrazol-4-yl)-3,4-dihydroquinolin-1(2*H*)-yl)-*N*-methyl-1-((2-(trimethylsilyl)ethoxy)methyl)-1*H*-indole-3-carboxamide (**35**, 135 mg, 0.24 mmol) in THF (2 mL) was added TBAF (4.0 mL, 4.0 mmol, 1 M in THF, 17 equiv). The mixture was heated to 50 °C for 40 h under a nitrogen atmosphere. After cooling to room temperature, the mixture was filtered and concentrated in vacuo. EtOAc (40 mL) was added and washed with water (30 mL x 2), brine (30 mL). The organic layer was dried over anhydrous Na_2SO_4, filtered and concentrated in vacuo. The crude residue was purified by reverse phase chromatography (acetonitrile 28–58% / 0.05% NH_4OH in water) to give 5-(7-(difluoromethyl)-6-(1-methyl-1*H*-pyrazol-4-yl)-3,4-dihydroquinolin-1(2*H*)-yl)-*N*-methyl-1*H*-indole-3-carboxamide (**16**, 28 mg, 26%) as a white solid. ^{1}H NMR (400 MHz, DMSO-d_6): δ 11.61 (s, 1H), 8.02 (d, J = 1.2 Hz, 1H), 8.00 (d, J = 2.8 Hz, 1H), 7.87 (d, J = 4.4 Hz, 1H), 7.72 (s, 1H), 7.50 (d, J = 8.4 Hz, 1H), 7.47 (s, 1H), 7.07 (s, 1H), 7.05–7.03 (m, 1H), 6.68 (t, J = 55.2 Hz, 1H), 6.49 (s, 1H), 3.85 (s, 3H), 3.65–3.55 (m, 2H), 2.91–2.86 (m, 2H), 2.75 (d, J = 4.4 Hz, 3H), 2.11–1.98 (m, 2H). LCMS (*m/z*) $[M+H]^+$ 436.

Synthesis and characterization of 5-[7-(difluoromethyl)-6-(1-methylpyrazol-4-yl)-3,4-dihydro-2*H*-quinolin-1-yl]-3-methyl-1,3-benzothiazol-2-one (17)

Step 1, 5-bromo-3H-1,3-benzothiazol-2-one (**37**): To a solution of 2-amino-4-bromobenzenethiol (**36**, 544 mg, 2.67 mmol, 1.00 equiv) in acetic acid (26.7 mL) was added triphosgene (530 mg, 1.79 mmol, 0.67 equiv). The mixture was heated at reflux for 18 h. After cooling to room temperature, the solution was partially concentrated under reduced pressure, water was added, and the resulting precipitate was removed via filtration, and washed with aqueous NaOH (1.0 M). The filtrate was acidified with aq. HCl (2 N) to pH 2, and placed in a refrigerator for 12 h. The resulting precipitate was filtered, washed with water, and dried under reduced pressure to give 5-bromo-3*H*-1,3-benzothiazol-2-one (**37**, 94 mg, 15%) as a while powder that required no further purification. ^{1}H NMR (400 MHz, DMSO-d_6): δ 12.07 (s, 1H), 7.55 (d, J = 8.4 Hz, 1H), 7.30 (d, J = 8.0 Hz, 1H), 7.24 (s, 1H).

Step 2, 5-bromo-3-methyl-1,3-benzothiazol-2-one (**38**): To a solution of 5-bromo-3*H*-1,3-benzothiazol-2-one (**37**, 94.4 mg, 0.410 mmol, 1.0 equiv) in water (2.1 mL) was added NaOH (16.4 mg, 0.410 mmol, 1.0 equiv) and then dimethyl sulfate (62.1 mg, 0.492 mmol, 1.2 equiv). After stirring at room temperature for 3 h, the resulting precipitate was filtered, washed with water, and dried under reduced pressure to give 5-bromo-3-methyl-1,3-benzothiazol-2-one (**38**, 89.3 mg, 89%) as a white powder that required no further purification. ^{1}H NMR (400 MHz, $CDCl_3$): δ 7.32–7.29 (m, 2H), 7.20 (dd, J = 1.5, 0.6 Hz, 1H), 3.45 (s, 3H).

Step 3, 5-[7-(difluoromethyl)-6-(1-methylpyrazol-4-yl)-3,4-dihydro-2H-quinolin-1-yl]-3-methyl-1,3-benzothiazol-2-one (**17**): To a vial was added 7-(difluoromethyl)-6-(1-methylpyrazol-4-yl)-1,2,3,4-tetrahydroquinoline (**31**, 25.0 mg, 0.0950 mmol, 1.0 equiv), 5-bromo-3-methyl-1,3-benzothiazol-2-one (**38**, 27.8 mg, 0.114 mmol, 1.2 equiv), dichloro[1,3-

bis(2,6-di-3-pentylphenyl)imidazol-2-ylidene](3-chloropyridyl)palladium(II) (11.9 mg, 0.0142 mmol, 15 mol%), *t*-BuONa (18.2 mg, 0.190 mmol, 2.0 equiv) and 1,4-dioxane (0.20 mL). The mixture was sparged with an argon balloon, and then heated to 120 °C for 16 h under an argon atmosphere. After cooling the reaction to room temperature, DCM (3 mL) was added and the reaction was filtered through celite and concentrated under reduced pressure. The crude residue was purified by reverse phase preparative HPLC (acetonitrile 30–70% / 0.1 % ammonium hydroxide in water) to give 5-[7-(difluoromethyl)-6-(1-methylpyrazol-4-yl)-3,4-dihydro-2*H*-quinolin-1-yl]-3-methyl-1,3-benzothiazol-2-one (**17**, 9.6 mg, 24%) as a white solid. ^{1}H NMR (400 MHz, DMSO-d_6): δ 7.76 (d, J = 0.8 Hz, 1H), 7.66 (d, J = 8.4 Hz, 1H), 7.51 (d, J = 0.8 Hz, 1H), 7.26 (d, J = 2.1 Hz, 1H), 7.18–7.14 (m, 1H), 7.11 (dd, J = 8.4, 2.1 Hz, 1H), 6.87–6.77 (m, 2H), 3.87 (s, 3H), 3.70–3.63 (m, 2H), 3.38 (s, 3H), 2.86 (t, J = 6.4 Hz, 2H), 2.06–1.96 (m, 2H). LCMS (*m/z*) $[M+H]^+$ 427.

Synthesis and characterization of 4-[7-(difluoromethyl)-6-(1-methylpyrazol-4-yl)-3,4-dihydro-2*H*-quinolin-1-yl]-*N*-methyl-quinoline-6-carboxamide (18)

Step 1, methyl 4-[7-(difluoromethyl)-6-(1-methylpyrazol-4-yl)-3,4-dihydro-2H-quinolin-1-yl]quinoline-6-carboxylate (**40**): To a vial was added 7-(difluoromethyl)-6-(1-methylpyrazol-4-yl)-1,2,3,4-tetrahydroquinoline (**31**, 200 mg, 0.760 mmol, 1.0 equiv), methyl 4-bromoquinoline-6-carboxylate (**39**, 243 mg, 0.912 mmol, 1.2 equiv), dichloro[1,3-bis(2,6-di-3-pentylphenyl)imidazol-2-ylidene](3-chloropyridyl)palladium(II) (95.2 mg, 0.114 mmol, 15 mol%), *t*-BuONa (146 mg, 1.52 mmol, 2.0 equiv) and 1,4-dioxane (1.52 mL). The mixture was sparged with an argon balloon, and then heated to 120 °C for 16 h under an argon atmosphere. After cooling the reaction to room temperature, DCM (4 mL) was added and the reaction was

filtered through celite and concentrated under reduced pressure. The residue was purified by silica gel chromatography (1% TEA in Heptanes to 100% EtOAc gradient) to afford methyl 4-[7-(difluoromethyl)-6-(1-methylpyrazol-4-yl)-3,4-dihydro-2*H*-quinolin-1-yl]quinoline-6-carboxylate (**40**, 23.6 mg, 7%) as a yellow solid. ^{1}H NMR (400 MHz, $CDCl_3$): δ 8.92 (d, *J* = 4.9 Hz, 1H), 8.76 (dd, *J* = 2.0, 0.6 Hz, 1H), 8.31 (dd, *J* = 8.8, 1.9 Hz, 1H), 8.18 (dd, *J* = 8.8, 0.6 Hz, 1H), 7.57 (d, *J* = 0.8 Hz, 1H), 7.45 (d, *J* = 0.7 Hz, 1H), 7.31–7.27 (m, 1H), 7.18 (t, *J* = 1.1 Hz, 1H), 6.88 (s, 1H), 6.58–6.30 (m, 1H), 3.96 (s, 3H), 3.96 (s, 3H), 3.80 (dd, *J* = 6.7, 4.2 Hz, 2H), 3.03 (t, *J* = 6.6 Hz, 2H), 2.18–2.08 (m, 2H).

Step 2, 4-[7-(difluoromethyl)-6-(1-methylpyrazol-4-yl)-3,4-dihydro-2H-quinolin-1-yl]-N-methyl-quinoline-6-carboxamide (**18**): To a solution of methyl 4-[7-(difluoromethyl)-6-(1-methylpyrazol-4-yl)-3,4-dihydro-2H-quinolin-1-yl]quinoline-6-carboxylate (**40**, 23.4 mg, 0.0522 mmol, 1.0 equiv) in THF (0.5 mL) and water (0.5 mL) was added lithium hydroxide monohydrate (2.6 mg, 0.063 mmol, 1.2 equiv). The mixture was stirred at the room temperature for 1 h. After completion of the reaction, the reaction mixture was concentrated under reduced pressure. The resulting residue was dissolved in DMF (1.0 mL), and TEA (21.1 mg, 0.209 mmol, 4.0 equiv), methylamine hydrochloride (10.6 mg, 0.157 mmol, 3.0 equiv), and TBTU (34.2 mg, 0.104 mmol, 2.0 equiv) were added. The mixture was stirred at room temperature for 14 h, and then concentrated under reduced pressure. The crude residue was purified by reverse phase preparative HPLC (acetonitrile 5–50% / 0.1 % formic acid in water) to give 4-[7-(difluoromethyl)-6-(1-methylpyrazol-4-yl)-3,4-dihydro-2*H*-quinolin-1-yl]-*N*-methyl-quinoline-6-carboxamide (**18**, 13.7 mg, 57%, 2 steps) as a yellow solid. ^{1}H NMR (400 MHz, DMSO-d_6): δ 8.96 (d, *J* = 4.8 Hz, 1H), 8.69 (q, *J* = 4.5 Hz, 1H), 8.46 (dd, *J* = 2.0, 0.6 Hz, 1H), 8.19 (dd, *J* = 8.8, 1.9 Hz, 1H), 8.13 (dd, *J* = 8.8, 0.6 Hz, 1H), 7.78 (d, *J* = 0.8 Hz, 1H), 7.53 (d, *J* = 0.8 Hz,

1H), 7.45 (d, *J* = 4.8 Hz, 1H), 7.26 (s, 1H), 6.87–6.50 (m, 2H), 3.87 (s, 3H), 3.73 (t, *J* = 5.4 Hz, 2H), 3.00 (t, *J* = 6.5 Hz, 2H), 2.80 (d, *J* = 4.5 Hz, 3H), 2.19–1.90 (m, 2H). LCMS (*m/z*) $[M+H]^+$ 448.

Synthesis and characterization of 6-acetyl-3-[7-(difluoromethyl)-6-(1-methylpyrazol-4-yl)-3,4-dihydro-2*H*-quinolin-1-yl]-1-methyl-7,8-dihydro-5*H*-1,6-naphthyridin-2-one (19)

Step 1, tert-butyl 3-bromo-2-oxo-1,5,7,8-tetrahydro-1,6-naphthyridine-6-carboxylate (**42**): To a solution of *tert*-butyl 2-oxo-1,5,7,8-tetrahydro-1,6-naphthyridine-6-carboxylate (**41**, 275 mg, 1.10 mmol, 1.0 equiv) in acetic acid (2.2 mL) at 0 ^oC was added bromine (67.7 μL, 1.32 mmol, 1.2 equiv) portionwise. The mixture was stirred at room temperature for 3 h, then concentrated under reduced pressure. The resulting residue was dissolved in chloroform (4 mL) and water (2.0 mL). To the solution was added Boc_2O (312 mg, 1.43 mmol, 1.3 equiv) and K_2CO_3 (304 mg, 2.20 mmol, 2.0 equiv). The mixture was stirred for 14 h at room temperature. The resulting precipitate was filtered, washed with diethyl ether, and dried under reduced pressure to give the first batch of **42**. The mother liquor was poured into a separatory funnel, the organic layer was separated, dried over Na_2SO_4 and concentrated under reduced pressure. The resulting solid was washed with diethyl ether, and then dried under reduced pressure to give the second batch of *tert*-butyl 3-bromo-2-oxo-1,5,7,8-tetrahydro-1,6-naphthyridine-6-carboxylate (**42**, 228 mg total, 63%) that required no further purification. ^1H NMR (400 MHz, $CDCl_3$, 16 / 17 H): δ 7.59 (s, 1H), 4.32 (s, 2H), 3.67 (t, *J* = 5.8 Hz, 2H), 2.74 (t, *J* = 5.8 Hz, 2H), 1.48 (s, 9H).

Step 2, tert-butyl 3-bromo-1-methyl-2-oxo-7,8-dihydro-5H-1,6-naphthyridine-6-carboxylate (**43**): To a solution of *tert*-butyl 3-bromo-2-oxo-1,5,7,8-tetrahydro-1,6-naphthyridine-6-carboxylate (**42**, 124 mg, 0.378 mmol, 1.0 equiv) in DMF (1.5 mL) at 0 °C was

added a solution of LiHMDS in hexane (1.0 M, 0.567 mL, 0.567 mmol, 1.5 equiv). After stirring for 15 min, iodomethane (47.1 μL, 0.756 mmol, 2.0 equiv) was added. After stirring for an additional 30 min, the reaction mixture was concentrated under reduced pressure. The residue was purified by silica gel chromatography (100% Heptanes to 100% EtOAc gradient) to afford *tert*-butyl 3-bromo-1-methyl-2-oxo-7,8-dihydro-5*H*-1,6-naphthyridine-6-carboxylate (**43**, 87.5 mg, 68%). ^{1}H NMR (400 MHz, DMSO-d_6): δ 7.50 (s, 1H), 4.31 (t, J = 1.6 Hz, 2H), 3.69 (t, J = 5.8 Hz, 2H), 3.57 (s, 3H), 2.69 (t, J = 1.7 Hz, 2H), 1.49 (s, 9H).

Step 3, 6-acetyl-3-bromo-1-methyl-7,8-dihydro-5H-1,6-naphthyridin-2-one (**44**): A mixture of *tert*-butyl 3-bromo-1-methyl-2-oxo-7,8-dihydro-5H-1,6-naphthyridine-6-carboxylate (**43**, 60.0 mg, 0.175 mmol, 1.0 equiv) and trifluoroacetic acid (0.5 mL) in DCM (4 mL) was stirred at room temperature for 2 h. The solvent was concentrated under reduced pressure and the crude product was re-dissolved in DCM (4 mL). The solution was cooled to 0 °C before TEA (0.12 mL, 0.87 mmol, 5.0 equiv) and acetic anhydride (33 μL, 0.35 mmol, 2.0 equiv) were added dropwise. The reaction mixture was stirred at room temperature for additional 3 h before it was quenched with water. The organic layer was dried over anhydrous Na_2SO_4, filtered and concentrated under reduced pressure. The crude residue was purified by silica gel chromatography (100% Heptanes to 10% MeOH in EtOAc gradient) to afford 6-acetyl-3-bromo-1-methyl-7,8-dihydro-5*H*-1,6-naphthyridin-2-one (**44**, 39.8 mg, 80%) as a white solid. ^{1}H NMR (400 MHz, $CDCl_3$): δ 7.52 (d, J = 4.6 Hz, 1H), 4.53–4.32 (m, 2H), 3.88–3.74 (m, 2H), 3.57 (d, J = 1.3 Hz, 3H), 2.82–2.64 (m, 2H), 2.17 (d, J = 9.4 Hz, 3H).

Step 4, 6-acetyl-3-[7-(difluoromethyl)-6-(1-methylpyrazol-4-yl)-3,4-dihydro-2H-quinolin-1-yl]-1-methyl-7,8-dihydro-5H-1,6-naphthyridin-2-one (**19**): To a vial was added 6-acetyl-3-[7-(difluoromethyl)-6-(1-methylpyrazol-4-yl)-3,4-dihydro-2*H*-quinolin-1-yl]-1-methyl-

7,8-dihydro-5*H*-1,6-naphthyridin-2-one (**44**, 12 mg, 0.042 mmol, 1.0 equiv), 7-(difluoromethyl)-6-(1-methylpyrazol-4-yl)-1,2,3,4-tetrahydroquinoline (**31**, 12 mg, 0.046 mmol, 1.1 equiv), dichloro[1,3-bis(2,6-di-3-pentylphenyl)imidazol-2-ylidene](3-chloropyridyl)palladium(II) (5.3 mg, 0.0063 mmol, 15 mol%), *t*-BuONa (8.1 mg, 0.084 mmol, 2.0 equiv) and 1,4-dioxane (0.2 mL). The mixture was sparged with an argon balloon, and then heated to 120 °C for 16 h under an argon atmosphere. After cooling the reaction to room temperature, DCM (2 mL) was added and the reaction was filtered through celite and concentrated under reduced pressure. The crude residue was purified by reverse phase preparative HPLC (acetonitrile 5–50% / 0.1 % NH_4OH in water) to afford 6-acetyl-3-[7-(difluoromethyl)-6-(1-methylpyrazol-4-yl)-3,4-dihydro-2*H*-quinolin-1-yl]-1-methyl-7,8-dihydro-5*H*-1,6-naphthyridin-2-one (**19**, 4.2 mg, 18%) as a light yellow solid. ^{1}H NMR (400 MHz, DMSO-d_6): δ 7.72 (s, 1H), 7.47 (t, J = 1.1 Hz, 1H), 7.40–7.36 (m, 1H), 7.05 (s, 1H), 6.89–6.57 (m, 1H), 6.42–6.39 (m, 1H), 4.42–4.39 (m, 2H), 3.86 (s, 3H), 3.73 (t, J = 5.9 Hz, 2H), 3.48–3.41 (m, 5H), 2.90–2.79 (m, 4H), 2.10–2.06 (m, 3H), 1.97 (t, J = 6.0 Hz, 2H). LCMS (*m/z*) $[M+H]^+$ 468.

Synthesis and characterization of 7-[7-(difluoromethyl)-6-(1-methylpyrazol-4-yl)-3,4-dihydro-2*H*-quinolin-1-yl]-1-methyl-3,4-dihydroquinolin-2-one (20)

To a vial was added 7-(difluoromethyl)-6-(1-methylpyrazol-4-yl)-1,2,3,4-tetrahydroquinoline (**31**, 50 mg, 0.19 mmol, 1.0 equiv), 7-bromo-1-methyl-3,4-dihydroquinolin-2(1H)-one (**45**, 55 mg, 0.23 mmol, 1.2 equiv), dichloro[1,3-bis(2,6-di-3-pentylphenyl)imidazol-2-ylidene](3-chloropyridyl)palladium(II) (24 mg, 0.028 mmol, 15 mol%), *t*-BuONa (37 mg, 0.38 mmol, 2.0 equiv) and 1,4-dioxane (0.4 mL). The mixture was sparged with an argon balloon, and then heated to 120 °C for 16 h under an argon atmosphere. After cooling the reaction to room

temperature, DCM (2 mL) was added and the reaction was filtered through celite and concentrated under reduced pressure. The crude residue was purified by reverse phase preparative HPLC (acetonitrile 30–70% / 0.1 % NH_4OH in water) to afford 7-[7-(difluoromethyl)-6-(1-methylpyrazol-4-yl)-3,4-dihydro-2*H*-quinolin-1-yl]-1-methyl-3,4-dihydroquinolin-2-one (**20**, 33 mg, 41%) as a white solid. ^{1}H NMR (400 MHz, DMSO-d_6): δ 7.75 (d, J = 0.8 Hz, 1H), 7.50 (d, J = 0.8 Hz, 1H), 7.24 (d, J = 8.0 Hz, 1H), 7.12 (s, 1H), 6.99 (d, J = 2.0 Hz, 1H), 6.93–6.60 (m, 3H), 3.86 (s, 3H), 3.68–3.59 (m, 2H), 3.21 (s, 3H), 2.91–2.80 (m, 4H), 2.57 (dd, J = 8.6, 6.1 Hz, 2H), 1.99 (p, J = 6.2 Hz, 2H). LCMS (*m/z*) $[M+H]^+$ 423.

Synthesis and characterization of 1-(6-(7-(difluoromethyl)-6-(1-methyl-1*H*-pyrazol-4-yl)-3,4-dihydroquinolin-1(2*H*)-yl)-4-methoxypyridin-2-yl)-3-methylurea (21)

Step 1, tert-butyl (6-bromo-4-methoxypyridin-2-yl)carbamate (**47**): To a solution of 2,6-dibromo-4-methoxypyridine (**46**, 2.00 g, 7.49 mmol, 1.0 equiv), *tert*-butyl carbamate (877 mg, 7.49 mmol, 1.0 equiv) and Cs_2CO_3 (4.80 g, 15.0 mmol, 2.0 equiv) in 1,4-dioxane (50 mL) were added palladium(II) acetate (168 mg, 0.75 mmol, 10 mol%) and 4,5-bis(diphenylphosphino)-9,9-dimethylxanthene (433 mg, 0.75 mmol, 10 mol%). The reaction mixture was heated to 100 °C for 16 h under a nitrogen atmosphere. After cooling the reaction to room temperature, water (100 mL) was added and extracted with EtOAc (50 mL x 3). The combined organic layers were washed with brine (50 mL x 2), dried over anhydrous Na_2SO_4, filtered and concentrated in vacuo. The crude residue was purified by silica gel column chromatography (petroleum ether/EtOAc = 9:1) to give *tert*-butyl (6-bromo-4-methoxypyridin-2-yl)carbamate (**47**, 900 mg, 39%) as a white solid. LCMS (*m/z*) $[M+H]^+$ 303.

Step 2, tert-butyl (6-(7-(difluoromethyl)-6-(1-methyl-1H-pyrazol-4-yl)-3,4-dihydroquinolin-1(2H)-yl)-4-methoxypyridin-2-yl)carbamate (**48**): To a solution of *tert*-butyl (6-bromo-4-methoxypyridin-2-yl)carbamate (**47**, 460 mg, 1.52 mmol, 1.0 equiv), 7-(difluoromethyl)-6-(1-methyl-1*H*-pyrazol-4-yl)-1,2,3,4-tetrahydroquinoline (**31**, 400 mg, 1.52 mmol, 1.0 equiv) and *t*-BuONa (436 mg, 4.54 mmol, 3.0 equiv) in 1,4-dioxane (15 mL) was added dichloro[1,3-bis(2,6-di-3-pentylphenyl)imidazol-2-ylidene](3-chloropyridyl)palladium(II) (120 mg, 0.15 mmol, 10 mol%). The reaction mixture was heated to 120 °C for 16 h under a nitrogen atmosphere. After cooling the reaction to room temperature, water (50 mL) was added and extracted with EtOAc (30 mL x 3). The combined organic layers were washed with brine (30 mL x 2), dried over anhydrous Na_2SO_4, filtered and concentrated in vacuo. The crude residue was purified by Prep-TLC (petroleum ether/EtOAc = 2:1) to give *tert*-butyl (6-(7-(difluoromethyl)-6-(1-methyl-1*H*-pyrazol-4-yl)-3,4-dihydroquinolin-1(2*H*)-yl)-4-methoxypyridin-2-yl)carbamate (**48**, 100 mg, 14%) as a white solid.

Step 3, 6-(7-(difluoromethyl)-6-(1-methyl-1H-pyrazol-4-yl)-3,4-dihydroquinolin-1(2H)-yl)-4-methoxypyridin-2-amine (**49**): To a solution of *tert*-butyl (6-(7-(difluoromethyl)-6-(1-methyl-1*H*-pyrazol-4-yl)-3,4-dihydroquinolin-1(2*H*)-yl)-4-methoxypyridin-2-yl)carbamate (**48**, 100 mg, 0.21 mmol, 1.0 equiv) in DCM (10 mL) at 0 ^{o}C was added trifluoroacetic acid (0.076 mL, 1.03 mmol, 4.9 equiv). The reaction mixture was stirred at room temperature for 5 h and concentrated in vacuo to give 6-(7-(difluoromethyl)-6-(1-methyl-1*H*-pyrazol-4-yl)-3,4-dihydroquinolin-1(2*H*)-yl)-4-methoxypyridin-2-amine (**49**) as yellow oil that required no further purification. LCMS (*m/z*) $[M+H]^+$ 386.

Step 4, 1-(6-(7-(difluoromethyl)-6-(1-methyl-1H-pyrazol-4-yl)-3,4-dihydroquinolin-1(2H)-yl)-4-methoxypyridin-2-yl)-3-methylurea (**21**): To a solution of 6-(7-(difluoromethyl)-6-

(1-methyl-1*H*-pyrazol-4-yl)-3,4-dihydroquinolin-1(2*H*)-yl)-4-methoxypyridin-2-amine (**49**, 40 mg, 0.10 mmol, 1.0 equiv) in anhydrous DMF (2 mL) at 0 ^{o}C was added NaH (60% dispersion in mineral oil, 20 mg, 0.50 mmol, 5.0 equiv). After stirring at 0 ^{o}C for 10 min, *N*-methyl-1*H*-imidazole-1-carboxamide (36 mg, 0.29 mmol, 2.9 equiv) was added. The reaction solution was stirred at room temperature for an additional 2 h. The reaction mixture was poured into water (50 mL) and extracted with EtOAc (30 mL x 3). The combined organic layers were washed with brine (30 mL x 2), dried over anhydrous Na_2SO_4, filtered and concentrated in vacuo. The crude residue was purified by reverse phase chromatography (acetonitrile 40–70% / 0.2% formic acid in water) to give 1-(6-(7-(difluoromethyl)-6-(1-methyl-1*H*-pyrazol-4-yl)-3,4-dihydroquinolin-1(2*H*)-yl)-4-methoxypyridin-2-yl)-3-methylurea (**21**, 8.0 mg, 18% over 2 steps) as a white solid. ^{1}H NMR (400 MHz, $CDCl_3$): δ 8.88 (s, 1H), 7.69 (s, 1H), 7.60 (s, 1H), 7.49 (s, 1H), 7.18 (s, 1H),7.06 (s, 1H), 6.58 (t, *J* = 55.2 Hz, 1H), 6.17 (s, 1H), 5.75 (s, 1H), 3.99 (s, 3H), 3.81–3.76 (m, 2H), 3.79 (s, 3H), 2.82–2.80 (m, 2H), 2.70 (d, *J* = 4.0 Hz, 3H), 2.06 (t, *J* = 6.0 Hz, 2H). LCMS (*m/z*) $[M+H]^+$ 443.

Synthesis and characterization of 5-[7-(difluoromethyl)-6-(1-methylpyrazol-4-yl)-3,4-dihydro-2H-quinolin-1-yl]-N-methyl-pyrazolo[1,5-a]pyrimidine-3-carboxamide (22)

Step 1, ethyl 5-[7-(difluoromethyl)-6-(1-methylpyrazol-4-yl)-3,4-dihydro-2H-quinolin-1-yl]pyrazolo[1,5-a]pyrimidine-3-carboxylate (**51**): To a solution of ethyl 5-bromopyrazolo[1,5-a]pyrimidine-3-carboxylate (**50**, 185 mg, 0.684 mmol, 1.2 equiv), 7-(difluoromethyl)-6-(1-methyl-1*H*-pyrazol-4-yl)-1,2,3,4-tetrahydroquinoline (**31**, 150 mg, 0.570 mmol, 1.0 equiv) and K_3PO_4 (249 mg, 1.14 mmol, 2.0 equiv) in *t*-amyl alcohol (4 mL) was added (2-dicyclohexylphosphino-2′,4′,6′-triisopropyl-1,1′-biphenyl)[2-(2′-amino-1,1′-

biphenyl)]palladium(II) methanesulfonate (50.8 mg, 0.0570 mmol, 10 mol%). The reaction mixture was heated to 90 °C for 16 h under a nitrogen atmosphere. After cooling the reaction to room temperature, DCM (2 mL) was added and the reaction was filtered through celite and concentrated under reduced pressure. The crude residue was purified by preparative SFC (carbon dioxide 5–50% / 0.1 % NH_4OH in methanol) to afford ethyl 5-[7-(difluoromethyl)-6-(1-methylpyrazol-4-yl)-3,4-dihydro-2H-quinolin-1-yl]pyrazolo[1,5-a]pyrimidine-3-carboxylate (**51**, 18.5 mg, 7%) as a white solid. ^{1}H NMR (400 MHz, DMSO-d_6): δ 8.81 (d, J = 7.9 Hz, 1H), 8.32 (s, 1H), 7.91 (d, J = 0.8 Hz, 1H), 7.76 (s, 1H), 7.65 (d, J = 0.8 Hz, 1H), 7.41 (s, 1H), 7.14–6.83 (m, 2H), 4.23 (q, J = 7.1 Hz, 2H), 4.06 (t, J = 6.4 Hz, 2H), 3.91 (s, 3H), 2.83 (t, J = 6.5 Hz, 2H), 2.00 (p, J = 6.5 Hz, 2H), 1.28 (t, J = 7.1 Hz, 3H).

Step 2, 5-[7-(difluoromethyl)-6-(1-methylpyrazol-4-yl)-3,4-dihydro-2H-quinolin-1-yl]-N-methyl-pyrazolo[1,5-a]pyrimidine-3-carboxamide (**22**): To a solution of ethyl 5-[7-(difluoromethyl)-6-(1-methylpyrazol-4-yl)-3,4-dihydro-2H-quinolin-1-yl]pyrazolo[1,5-a]pyrimidine-3-carboxylate (**51**, 18.5 mg, 0.0405 mmol, 1.0 equiv) in THF (0.5 mL) and water (0.5 mL) was added lithium hydroxide monohydrate (17.0 mg, 0.405 mmol, 10 equiv) and Cs_2CO_3 (20 mg, 0.0614 mmol, 1.5 equiv). The mixture was stirred at 60 °C for 3 d. After completion of the reaction, the reaction mixture was concentrated under reduced pressure. The crude residue was purified by reverse phase preparative HPLC (acetonitrile 20–60% / 0.1 % NH_4OH in water). The resulting carboxylic acid (9.9 mg, 0.0233 mmol, 1.0 equiv) was dissolved in DMF (1.0 mL), and TEA (13 μL, 0.093 mmol, 4.0 equiv), methylamine hydrochloride (4.7 mg, 0.070 mmol, 3.0 equiv), and TBTU (22.5 mg, 0.070 mmol, 3.0 equiv) were added. The mixture was stirred at room temperature for 14 h, and then concentrated under reduced pressure. The crude residue was purified by reverse phase preparative HPLC (acetonitrile 5–50% / 0.1 %

NH_4OH in water) to give 5-[7-(difluoromethyl)-6-(1-methylpyrazol-4-yl)-3,4-dihydro-2H-quinolin-1-yl]-N-methyl-pyrazolo[1,5-a]pyrimidine-3-carboxamide (**22**, 6.5 mg, 37%, 2 steps) as a yellow solid. ^{1}H NMR (400 MHz, DMSO-d_6, 20 / 21 H): δ 8.88 (d, J = 7.8 Hz, 1H), 8.26 (s, 1H), 7.93 (d, J = 0.8 Hz, 1H), 7.85 (s, 1H), 7.55 (d, J = 4.8 Hz, 1H), 7.43 (s, 1H), 7.22–6.80 (m, 2H), 4.01 (t, J = 6.4 Hz, 2H), 3.91 (s, 3H), 2.80 (dd, J = 10.5, 5.6 Hz, 5H), 2.01 (t, J = 6.3 Hz, 2H). LCMS (*m/z*) $[M+H]^+$ 438.

Synthesis and characterization of 1-[6-[7-(difluoromethyl)-6-(1-methylpyrazol-4-yl)-3,4-dihydro-2H-quinolin-1-yl]-3,4-dihydro-2H-quinolin-1-yl]ethanone (23)

Step 1, 1-(3,4-dihydro-2H-quinolin-1-yl)ethanone (**53**): To a solution of 1,2,3,4-tetrahydroquinoline (**52**, 2.00 g, 15.0 mmol, 1.0 equiv) in DCM (30 mL) at 0 °C was added TEA (3.14 mL, 22.5 mmol, 1.5 equiv), and acetic anhydride (1.70 mL, 18.0 mmol, 1.2 equiv). The mixture was heated to 32 °C for 2 h, and then allowed to cool to room temperature. Water (50 mL) was added and the mixture was extracted with DCM (50 mL x 2). The combined organic layers were washed with brine (30 mL), dried over anhydrous Na_2SO_4 and then concentrated in under reduced pressure. The residue was purified by silica gel chromatography (100% Heptanes to 50% EtOAc in Heptanes gradient) to afford 1-(3,4-dihydro-2*H*-quinolin-1-yl)ethanone (**53**, 2.32 g, 88%) as a pale yellow oil. ^{1}H NMR (400 MHz, DMSO-d_6): δ 7.26–7.05 (m, 4H), 3.81 (t, J = 6.6 Hz, 2H), 2.73 (t, J = 6.7 Hz, 2H), 2.24 (s, 3H), 1.97 (p, J = 6.6 Hz, 2H).

Step 2, 1-(6-bromo-3,4-dihydro-2H-quinolin-1-yl)ethanone (**54**): To a solution of 1-(3,4-dihydro-2*H*-quinolin-1-yl)ethanone (**53**, 400 mg, 2.0 mmol, 1.0 equiv) in DCM (10 mL) at 0 ^{o}C was added *N*-bromosuccinimide (400 mg, 2.2 mmol, 1.1 equiv) portionwise. The mixture was

stirred at room temperature for 2 h, then heated at 45 ^{o}C for 14 h. After cooling to room temperature, the reaction was concentrated under reduced pressure. The residue was purified by silica gel chromatography (100% Heptanes to 60% EtOAc in Heptanes gradient) to afford 1-(6-bromo-3,4-dihydro-2*H*-quinolin-1-yl)ethanone (**54**, 0.542 g, 90%) as a yellow oil. ^{1}H NMR (400 MHz, $CDCl_3$): δ 7.40–7.03 (m, 3H), 3.76 (t, *J* = 6.5 Hz, 2H), 2.71 (t, *J* = 6.6 Hz, 2H), 2.22 (s, 3H), 2.04–1.86 (m, 2H).

Step 3, 1-[6-[7-(difluoromethyl)-6-(1-methylpyrazol-4-yl)-3,4-dihydro-2H-quinolin-1-yl]-3,4-dihydro-2H-quinolin-1-yl]ethanone (**23**): To a vial was added 7-(difluoromethyl)-6-(1-methylpyrazol-4-yl)-1,2,3,4-tetrahydroquinoline (**31**, 70.0 mg, 0.266 mmol, 1.0 equiv), 1-(6-bromo-3,4-dihydro-2*H*-quinolin-1-yl)ethanone (**54**, 243 mg, 0.912 mmol, 3.4 equiv), dichloro[1,3-bis(2,6-di-3-pentylphenyl)imidazol-2-ylidene](3-chloropyridyl)palladium(II) (33.3 mg, 0.0399 mmol, 15 mol%), *t*-BuONa (51.1 mg, 0.532 mmol, 2.0 equiv) and 1,4-dioxane (0.53 mL). The mixture was sparged with an argon balloon, and then heated to 120 °C for 16 h under an argon atmosphere. After cooling the reaction to room temperature, DCM (3 mL) was added and the reaction was filtered through celite and concentrated under reduced pressure. The crude residue was purified by reverse phase chromatography (acetonitrile 30–70% / 0.1 % ammonium hydroxide in water) to give 1-[6-[7-(difluoromethyl)-6-(1-methylpyrazol-4-yl)-3,4-dihydro-2H-quinolin-1-yl]-3,4-dihydro-2H-quinolin-1-yl]ethanone (**23**, 40.5 mg, 32%) as a white solid. ^{1}H NMR (400 MHz, DMSO-d_6, 330 K): δ 7.72 (s, 1H), 7.53 (s, 1H), 7.48 (d, *J* = 0.8 Hz, 1H), 7.13–7.02 (m, 3H), 6.87–6.60 (m, 2H), 3.86 (s, 3H), 3.73–3.67 (m, 2H), 3.62–3.55 (m, 2H), 2.83 (t, *J* = 6.5 Hz, 2H), 2.71 (t, *J* = 6.6 Hz, 2H), 2.18 (s, 3H), 2.03–1.95 (m, 2H), 1.93–1.84 (m, 2H). LCMS (*m/z*) $[M+H]^+$ 437.

Synthesis and characterization of (*R*)-5-(7-(difluoromethyl)-6-(1-methyl-1*H*-pyrazol-4-yl)-3,4-dihydroquinolin-1(2*H*)-yl)-3-methyl-3,4-dihydroquinoxalin-2(1*H*)-one (24)

Step 1, 7-(difluoromethyl)-1-(2-fluoro-3-nitrophenyl)-6-(1-methyl-1H-pyrazol-4-yl)-1,2,3,4-tetrahydroquinoline (**56**): To a solution of 1-bromo-2-fluoro-3-nitrobenzene (**55**, 300 mg, 1.36 mmol, 1.3 equiv) and 7-(difluoromethyl)-6-(1-methyl-1*H*-pyrazol-4-yl)-1,2,3,4-tetrahydroquinoline (**31**, 276 mg, 1.05 mmol, 1.0 equiv) in 1,4-dioxane (2 mL) was added Cs_2CO_3 (684 mg, 2.1 mmol, 2.0 equiv), palladium(II) acetate (24 mg, 0.10 mmol, 10 mol%) and 4,5-bis(diphenylphosphino)-9,9-dimethylxanthene (61 mg, 0.10 mmol, 10 mol%). The mixture was irradiated in a microwave at 140 °C for 1 h. The mixture was filtered and concentrated in vacuo. The crude residue was purified by Prep-TLC (petroleum ether/EtOAc = 1:1) to give 7-(difluoromethyl)-1-(2-fluoro-3-nitrophenyl)-6-(1-methyl-1*H*-pyrazol-4-yl)-1,2,3,4-tetrahydroquinoline (**56**, 110 mg, 20%) as a red solid. LCMS (*m/z*) $[M+H]^+$ 403.

Step 2, (R)-2-((2-(7-(difluoromethyl)-6-(1-methyl-1H-pyrazol-4-yl)-3,4-dihydroquinolin-1(2H)-yl)-6-nitrophenyl)amino)propanoic acid (**57**): To a solution of 7-(difluoromethyl)-1-(2-fluoro-3-nitrophenyl)-6-(1-methyl-1*H*-pyrazol-4-yl)-1,2,3,4-tetrahydroquinoline (**56**, 300 mg, 0.75 mmol, 1.0 equiv) in DMF (3 mL) was added (*R*)-2-aminopropanoic acid (100 mg, 1.12 mmol, 1.5 equiv) and Cs_2CO_3 (486 mg, 1.49 mmol, 2.0 equiv). The reaction mixture was heated to 100 ^oC for 4 h. After cooling to room temperature, EtOAc (30 mL) was added and washed with water (20 mL x 3). The combined aqueous layers were acidified with HCl (2 N) to pH 4 and then extracted with EtOAc (40 mL x 3). The combined organic layers were washed with brine (20 mL), dried over anhydrous Na_2SO_4 and concentrated in vacuo to give (*R*)-2-((2-(7-(difluoromethyl)-6-(1-methyl-1*H*-pyrazol-4-yl)-3,4-dihydroquinolin-1(2*H*)-yl)-6-

nitrophenyl)amino)propanoic acid (**57**, 300 mg, 85%) as a brown solid that required no further purification. LCMS (*m/z*) $[M+H]^+$ 472.

Step 3, (R)-5-(7-(difluoromethyl)-6-(1-methyl-1H-pyrazol-4-yl)-3,4-dihydroquinolin-1(2H)-yl)-3-methyl-3,4-dihydroquinoxalin-2(1H)-one (**24**): To a solution of (*R*)-2-((2-(7-(difluoromethyl)-6-(1-methyl-1*H*-pyrazol-4-yl)-3,4-dihydroquinolin-1(2*H*)-yl)-6-nitrophenyl)amino)propanoic acid (**57**, 300 mg, 0.64 mmol, 1.0 equiv) in AcOH (4 mL) was added Fe powder (178 mg, 3.18 mmol, 5.0 equiv). The reaction mixture was heated to 100 °C for 3 h under a nitrogen atmosphere. After cooling to room temperature, the mixture was filtered and concentrated in vacuo. The crude residue was purified by reverse phase chromatography (acetonitrile 36–56% / 0.2 % formic acid in water) to give (*R*)-5-(7-(difluoromethyl)-6-(1-methyl-1*H*-pyrazol-4-yl)-3,4-dihydroquinolin-1(2*H*)-yl)-3-methyl-3,4-dihydroquinoxalin-2(1*H*)-one (**24**, 39 mg, 14%) as a yellow solid. ^{1}H NMR (400 MHz, DMSO-d_6): δ 10.36 (s, 1H), 7.73 (s, 1H), 7.48 (s, 1H), 7.22–7.02 (m, 1H), 6.89–6.51 (m, 4H), 6.45–6.24 (m, 1H), 5.41 (d, J = 12.8 Hz, 1H), 3.91–3.66 (m, 1H), 3.86 (s, 3H), 3.50–3.36 (m, 2H), 2.89–2.85 (m, 2H), 2.33–1.94 (m, 2H), 1.28–1.07 (m, 3H). LCMS (*m/z*) $[M+H]^+$ 424.

Synthesis and characterization of 7-(7-(difluoromethyl)-6-(1-methyl-1*H*-pyrazol-4-yl)-3,4-dihydroquinolin-1(2*H*)-yl)-*N*-methyl-2,3-dihydrobenzo[*f*][1,4]oxazepine-4(5*H*)-carboxamide (25)

Step 1, tert-butyl 7-(7-(difluoromethyl)-6-(1-methyl-1H-pyrazol-4-yl)-3,4-dihydroquinolin-1(2H)-yl)-2,3-dihydrobenzo[f][1,4]oxazepine-4(5H)-carboxylate (**59**): To a solution of *tert*-butyl 7-bromo-3,5-dihydro-2*H*-1,4-benzoxazepine-4-carboxylate (**58**, 800 mg,

2.44 mmol, 1.0 equiv), 7-(difluoromethyl)-6-(1-methyl-1*H*-pyrazol-4-yl)-1,2,3,4-tetrahydroquinoline (**31**, 642 mg, 2.44 mmol, 1.0 equiv) and *t*-BuONa (586 mg, 6.09 mmol, 2.5 equiv) in 1,4-dioxane (6 mL) was added dichloro[1,3-bis(2,6-di-3-pentylphenyl)imidazol-2-ylidene](3-chloropyridyl)palladium(II) (193 mg, 0.24 mmol, 10 mol%). The reaction mixture was heated to 120 ^{o}C for 16 h under a nitrogen atmosphere. After cooling to room temperature, the mixture was filtered and concentrated in vacuo. The crude residue was purified by silica gel column chromatography (petroleum ether/EtOAc = 3:2) to give *tert*-butyl 7-(7-(difluoromethyl)-6-(1-methyl-1*H*-pyrazol-4-yl)-3,4-dihydroquinolin-1(2*H*)-yl)-2,3-dihydrobenzo[*f*][1,4]oxazepine-4(5*H*)-carboxylate (**59**, 670 mg, 54%) as a yellow solid. LCMS (*m/z*) $[M+H]^+$ 511.

Step 2, 7-(7-(difluoromethyl)-6-(1-methyl-1H-pyrazol-4-yl)-3,4-dihydroquinolin-1(2H)-yl)-2,3,4,5-tetrahydrobenzo[f][1,4]oxazepine (**60**): To a solution of *tert*-butyl 7-(7-(difluoromethyl)-6-(1-methyl-1*H*-pyrazol-4-yl)-3,4-dihydroquinolin-1(2*H*)-yl)-2,3-dihydrobenzo[*f*][1,4]oxazepine-4(5*H*)-carboxylate (**59**, 870 mg, 1.7 mmol, 1.0 equiv) in DCM (5 mL) at 0 ^{o}C was added trifluoroacetic acid (1.26 mL, 17.0 mmol, 10 equiv) dropwise. The reaction mixture was stirred at room temperature for 1 h and concentrated in vacuo to give 7-(7-(difluoromethyl)-6-(1-methyl-1*H*-pyrazol-4-yl)-3,4-dihydroquinolin-1(2*H*)-yl)-2,3,4,5-tetrahydrobenzo[*f*][1,4]oxazepine (**60**, 600 mg, 86%) as a yellow solid that required no further purification. LCMS (*m/z*) $[M+H]^+$ 411.

Step 3, 7-(7-(difluoromethyl)-6-(1-methyl-1H-pyrazol-4-yl)-3,4-dihydroquinolin-1(2H)-yl)-N-methyl-2,3-dihydrobenzo[f][1,4]oxazepine-4(5H)-carboxamide (**25**): To a stirred solution of 7-(7-(difluoromethyl)-6-(1-methyl-1*H*-pyrazol-4-yl)-3,4-dihydroquinolin-1(2*H*)-yl)-2,3,4,5-tetrahydrobenzo[*f*][1,4]oxazepine (**60**, 150 mg, 0.37 mmol, 1.0 equiv) and triethylamine (0.25

mL, 1.83 mmol, 5.0 equiv) in DCM (5 mL) was added *N*-methyl-1*H*-imidazole-1-carboxamide (92 mg, 0.74 mmol, 2.0 equiv). The reaction mixture was stirred at room temperature for 16 h and concentrated in vacuo. The crude residue was purified by reverse phase chromatography (acetonitrile 35–65% / 0.2% formic acid in water) to give 7-(7-(difluoromethyl)-6-(1-methyl-1*H*-pyrazol-4-yl)-3,4-dihydroquinolin-1(2*H*)-yl)-*N*-methyl-2,3-dihydrobenzo[*f*][1,4]oxazepine-4(5*H*)-carboxamide (**25,** 83 mg, 48%) as a white solid. ^{1}H NMR (400 MHz, DMSO-d_6): δ 7.74 (s, 1H), 7.49 (s, 1H), 7.31 (d, J = 2.2 Hz, 1H), 7.13–7.04 (m, 2H), 7.03–6.96 (m, 1H), 6.90–6.59 (m, 2H), 6.48–6.43 (m, 1H), 4.42 (s, 2H), 4.01–3.98 (m, 2H), 3.86 (s, 3H), 3.72–3.69 (m, 2H), 3.59–3.51 (m, 2H), 2.88–2.79 (m, 2H), 2.52 (s, 3H), 2.03–1.92 (m, 2H). LCMS (*m/z*) $[M+Na]^+$ 490.

Synthesis and characterization of 5-[7-(difluoromethyl)-6-(1-methylpyrazol-4-yl)-3,4-dihydro-2*H*-quinolin-1-yl]-1,3-dimethyl-benzimidazol-2-one (26)

To a vial was added 7-(difluoromethyl)-6-(1-methylpyrazol-4-yl)-1,2,3,4-tetrahydroquinoline (**31**, 40.0 mg, 0.152 mmol, 1.0 equiv), 5-bromo-1,3-dimethyl-benzimidazol-2-one (**61**, 44.0 mg, 0.182 mmol, 1.2 equiv), dichloro[1,3-bis(2,6-di-3-pentylphenyl)imidazol-2-ylidene](3-chloropyridyl)palladium(II) (19.0 mg, 0.0228 mmol, 15 mol%), *t*-BuONa (29.2 mg, 0.304 mmol, 2.0 equiv) and 1,4-dioxane (0.3 mL). The mixture was sparged with an argon balloon, and then heated to 120 °C for 16 h under an argon atmosphere. After cooling the reaction to room temperature, DCM (3 mL) was added and the reaction was filtered through celite and concentrated under reduced pressure. The crude residue was purified by reverse phase chromatography (acetonitrile 20–60% / 0.1 % ammonium hydroxide in water) to give 5-[7-

(difluoromethyl)-6-(1-methylpyrazol-4-yl)-3,4-dihydro-2*H*-quinolin-1-yl]-1,3-dimethyl-benzimidazol-2-one (**26**, 40.5 mg, 32%) as a white solid. ^{1}H NMR (400 MHz, DMSO-d_6, 20 / 23 H): δ 7.72 (d, J = 0.8 Hz, 1H), 7.47 (d, J = 0.8 Hz, 1H), 7.20 (d, J = 8.2 Hz, 1H), 7.14 (d, J = 2.0 Hz, 1H), 7.08 (d, J = 1.4 Hz, 1H), 6.98 (dd, J = 8.3, 2.0 Hz, 1H), 6.86–6.55 (m, 2H), 3.86 (s, 3H), 3.64–3.56 (m, 2H), 3.35 (s, 3H), 2.95–2.76 (m, 2H), 2.10–1.93 (m, 2H). LCMS (*m/z*) $[M+H]^+$ 424.

Synthesis and characterization of 6-(7-(difluoromethyl)-6-(1-methyl-1*H*-pyrazol-4-yl)-3,4-dihydroquinolin-1(2*H*)-yl)-1,3-dimethyl-4-morpholino-1*H*-benzo[*d*]imidazol-2(3*H*)-one (27)

Step 1, 6-bromo-4-chloro-1H-benzo[d]imidazol-2(3H)-one (**63**): To a solution of 5-bromo-3-chlorobenzene-1,2-diamine (**62**, 200 mg, 0.90 mmol, 1.0 equiv) in chloroform (3 mL) was added di(1*H*-imidazol-1-yl)methanone (220 mg, 1.35 mmol, 1.5 equiv). The mixture was heated to 60 ^{o}C for 12 h under a nitrogen atmosphere. After cooling the reaction to room temperature, the white precipitate was collected, washed with chloroform (3 mL x 2), and dried in vacuo to give 6-bromo-4-chloro-1*H*-benzo[*d*]imidazol-2(3*H*)-one (**63**, 170 mg, 76%) as a white solid. ^{1}H NMR (400 MHz, DMSO-d_6): δ 11.35 (s, 1H), 11.05 (s, 1H), 7.21 (d, J = 1.6 Hz, 1H), 7.04 (d, J = 1.6 Hz, 1H).

Step 2, 6-bromo-4-chloro-1,3-dimethyl-1H-benzo[d]imidazol-2(3H)-one (**64**): To a stirred solution of 6-bromo-4-chloro-1*H*-benzo[*d*]imidazol-2(3*H*)-one (**63**, 170 mg, 0.69 mmol, 1.0 equiv) in DMF (2 mL) at 0 °C was added NaH (60% dispersion in mineral oil, 69 mg, 1.72 mmol, 2.5 equiv) and the mixture was stirred for 15 min. Methyl iodide (0.13 mL, 2.06 mmol, 3.0 equiv) was added dropwise and the mixture stirred at room temperature for an additional 12

h. Water (30 mL) was added and extracted with EtOAc (30 mL x 3). The combined organic layers were dried over anhydrous Na_2SO_4, filtered and concentrated in vacuo. The crude residue was purified by silica gel chromatography (petroleum ether / EtOAc = 5: 1) to give title compound (**64**, 150 mg, 79%) as a white solid. LCMS M/Z (*m/z*) $[M+H]^+$ 275.

Step 3, 4-chloro-6-(7-(difluoromethyl)-6-(1-methyl-1H-pyrazol-4-yl)-3,4-dihydroquinolin-1(2H)-yl)-1,3-dimethyl-1H-benzo[d]imidazol-2(3H)-one (**65**): To a solution of 7-(difluoromethyl)-6-(1-methyl-1*H*-pyrazol-4-yl)-1,2,3,4-tetrahydroquinoline (**31**, 143 mg, 0.54 mmol, 1.0 equiv), 6-bromo-4-chloro-1,3-dimethyl-1*H*-benzo[*d*]imidazol-2(3*H*)-one (**64**, 150 mg, 0.54 mmol, 1.0 equiv) and K_3PO_4 (347 mg, 1.63 mmol, 3.0 equiv) in 2-methyl-2-butanol (5 mL) was added methanesulfonato(2-dicyclohexylphosphino-2',4',6'-tri-*i*-propyl-1,1'-biphenyl)(2'-amino-1,1'-biphenyl-2-yl)palladium(II) (46 mg, 0.054 mmol, 10 mol%). The mixture was heated to 95 ^oC for 12 h under an argon atmosphere. After cooling the reaction to room temperature, the mixture was filtered and concentrated in vacuo. The crude residue was purified by reverse phase chromatography (acetonitrile 35–65% / 0.2% formic acid in water) to give 4-chloro-6-(7-(difluoromethyl)-6-(1-methyl-1*H*-pyrazol-4-yl)-3,4-dihydroquinolin-1(2*H*)-yl)-1,3-dimethyl-1*H*-benzo[*d*]imidazol-2(3*H*)-one (**65**, 28 mg, 11%) as a yellow solid. ^1H NMR (400 MHz, $CDCl_3$): δ 7.55 (s, 1H), 7.42 (s, 1H), 7.07 (s, 1H), 6.94 (d, *J* = 1.6 Hz, 1H), 6.88 (s, 1H), 6.80 (d, *J* = 1.6 Hz, 1H), 6.49 (t, *J* = 55.6 Hz, 1H), 3.96 (s, 3H), 3.76 (s, 3H), 3.64–3.61 (m, 2H), 3.38 (s, 3H), 2.92–2.89 (m, 2H), 2.11–2.09 (m, 2H). LCMS (*m/z*) $[M+H]^+$ 458.

Step 4, 6-(7-(difluoromethyl)-6-(1-methyl-1H-pyrazol-4-yl)-3,4-dihydroquinolin-1(2H)-yl)-1,3-dimethyl-4-morpholino-1H-benzo[d]imidazol-2(3H)-one (**27**): To a solution of 4-chloro-6-(7-(difluoromethyl)-6-(1-methyl-1*H*-pyrazol-4-yl)-3,4-dihydroquinolin-1(2*H*)-yl)-1,3-dimethyl-1*H*-benzo[*d*]imidazol-2(3*H*)-one (**65**, 200 mg, 0.44 mmol, 1.0 equiv) in 1,4-dioxane (3

mL) was added morpholine (0.038 mL, 0.44 mmol, 1.0 equv), dichloro[1,3-bis(2,6-di-3-pentylphenyl)imidazol-2-ylidene](3-chloropyridyl)palladium(II) (76 mg, 0.10 mmol, 23 mol%) and *t*-BuONa (277 mg, 2.88 mmol, 6.5 equiv). The mixture was irradiated in a microwave at 140 °C for 0.5 h. EtOAc (30 mL) was added and washed with water (30 mL x 2), brine (30 mL). The organic layer was dried over anhydrous Na_2SO_4, filtered and concentrated in vacuo. The crude residue was purified by reverse phase chromatography (acetonitrile 42–72% / 0.2% formic acid in water) to give title compound 6-(7-(difluoromethyl)-6-(1-methyl-1*H*-pyrazol-4-yl)-3,4-dihydroquinolin-1(2*H*)-yl)-1,3-dimethyl-4-morpholino-1*H*-benzo[*d*]imidazol-2(3*H*)-one (**27**, 60 mg, 27%) as a white solid. ^{1}H NMR (400 MHz, DMSO-d_6): δ 7.73 (d, J = 0.8 Hz, 1H), 7.48 (d, J = 0.8 Hz, 1H), 7.09 (s, 1H), 6.92 (d, J = 1.9 Hz, 1H), 6.90–6.56 (m, 3H), 3.86 (s, 3H), 3.76 (s, 4H), 3.63 (s, 5H), 3.29 (s, 3H), 2.87 (dt, J = 12.3, 5.6 Hz, 6H), 2.10–1.94 (m, 2H). ^{13}C NMR (100 MHz, DMSO-d_6): δ 155.2, 144.5, 141.7, 138.2, 138.1, 132.5, 131.1, 128.8 (t, J = 21 Hz), 126.3, 120.9, 120.6 (t, J = 6.0 Hz), 119.0, 117.6, 114.2, 111.8, 110.3 (t, J = 7.0 Hz), 103.0, 66.6, 53.5, 51.6, 39.0, 29.7, 27.61, 27.56, 22.3. HRMS-ESI (*m/z*) $[M+H]^+$ calcd for $C_{27}H_{31}O_2N_6F_2$ = 509.2471; found, 509.2461.

Synthesis and characterization of 5-(7-(difluoromethyl)-6-(1-methyl-1*H*-pyrazol-4-yl)-3,4-dihydroquinolin-1(2*H*)-yl)-*N*-methyl-1*H*-pyrrolo[2,3-*c*]pyridine-3-carboxamide (28)

Step 1, 1-(5-bromo-1H-pyrrolo[2,3-c]pyridin-3-yl)-2,2,2-trichloroethanone (**67**): To a solution of 5-bromo-1*H*-pyrrolo[2,3-*c*]pyridine (**66**, 2.50 g, 12.7 mmol, 1.0 equiv) and aluminum chloride (12.69 g, 95.16 mmol, 7.5 equiv) in DCM (75 mL) at 48 °C was added trichloroacetyl chloride (1.48 mL, 13.3 mmol, 1.05 equiv) dropwise. The reaction mixture was heated to 48 °C

for 2 h. After cooling the reaction to room temperature, the mixture was quenched with ice-water (100 mL), and extracted with EtOAc (150 mL x 3). The combined organic layers were dried over anhydrous Na_2SO_4, filtered and concentrated in vacuo. The crude residue was purified by silica gel chromatography (petroleum ether / EtOAc = 1 : 1) to give 1-(5-bromo-1*H*-pyrrolo[2,3-*c*]pyridin-3-yl)-2,2,2-trichloroethanone (**67**, 3.5 g, 81%) as a brown solid. LCMS (*m/z*) $[M+H]^+$ 343.

Step 2, methyl 5-bromo-1H-pyrrolo[2,3-c]pyridine-3-carboxylate (**68**): To a solution of 1-(5-bromo-1*H*-pyrrolo[2,3-*c*]pyridin-3-yl)-2,2,2-trichloroethanone (**67**, 3.2 g, 9.35 mmol, 1.0 equiv) in MeOH (50 mL) was added potassium hydroxide (577 mg, 10.28 mmol, 1.1 equiv). The reaction was stirred at room temperature for 16 h and concentrated in vacuo. Water (50 mL) was added and extracted with EtOAc (50 mL x 3). The combined organic layers were dried over anhydrous Na_2SO_4, filtered and concentrated in vacuo to give methyl 5-bromo-1*H*-pyrrolo[2,3-*c*]pyridine-3-carboxylate (**68**, 2.0 g, 84%) as a brown solid that required no further purification. LCMS (*m/z*) $[M+H]^+$ 255.

Step 3, methyl 5-bromo-1-((2-(trimethylsilyl)ethoxy)methyl)-1H-pyrrolo[2,3-c]pyridine-3-carboxylate (**69**): To a solution of methyl 5-bromo-1*H*-pyrrolo[2,3-*c*]pyridine-3-carboxylate (**68**, 700 mg, 2.74 mmol, 1.0 equiv) in DMF (8 mL) at 0 °C was added NaH (60% dispersion in mineral oil, 154 mg, 3.84 mmol, 1.4 equiv) portionwise. The mixture was stirred at room temperature for 0.5 h. (2-(Chloromethoxy)ethyl)trimethylsilane (0.58 mL, 3.29 mmol, 1.2 equiv) was added dropwise and the mixture stirred at room temperature for an additional 1 h. The mixture was quenched with water (20 mL) and extracted with EtOAc (20 mL x 3). The combined organic layers were washed with brine (20 mL), dried over anhydrous Na_2SO_4, filtered and concentrated in vacuo. The crude residue was purified by silica gel chromatography

(petroleum ether / EtOAc = 20 : 1) to give methyl 5-bromo-1-((2-(trimethylsilyl)ethoxy)methyl)-1*H*-pyrrolo[2,3-*c*]pyridine-3-carboxylate (**69**, 650 mg, 62%) as a white solid.

Step 4, methyl 5-(7-(difluoromethyl)-6-(1-methyl-1H-pyrazol-4-yl)-3,4-dihydroquinolin-1(2H)-yl)-1-((2-(trimethylsilyl)ethoxy)methyl)-1H-pyrrolo[2,3-c]pyridine-3-carboxylate (**70**): To a solution of methyl 5-bromo-1-((2-(trimethylsilyl)ethoxy)methyl)-1*H*-pyrrolo[2,3-*c*]pyridine-3-carboxylate (**69**, 480 mg, 1.25 mmol, 1.0 equiv) in 1,4-dioxane (3 mL) was added 7-(difluoromethyl)-6-(1-methyl-1*H*-pyrazol-4-yl)-1,2,3,4-tetrahydroquinoline (**31**, 361 mg, 1.37 mmol, 1.1 equiv), dichloro[1,3-bis(2,6-di-3-pentylphenyl)imidazol-2-ylidene](3-chloropyridyl)palladium(II) (99 mg, 0.12 mmol, 10 mol%) and Cs_2CO_3 (1.01 g, 3.11 mmol, 2.5 equiv). The mixture was heated to 110 °C for 12 h under a nitrogen atmosphere. EtOAc (30 mL) was added and washed with water (30 mL x 2), brine (30 mL). The organic layer was dried over anhydrous Na_2SO_4, filtered and concentrated in vacuo. The crude residue was purified by silica gel chromatography (petroleum ether / EtOAc = 1 : 1) to give methyl 5-(7-(difluoromethyl)-6-(1-methyl-1*H*-pyrazol-4-yl)-3,4-dihydroquinolin-1(2*H*)-yl)-1-((2-(trimethylsilyl)ethoxy)methyl)-1*H*-pyrrolo[2,3-*c*]pyridine-3-carboxylate (**70**, 300 mg, 42%) as a yellow solid. LCMS (*m/z*) $[M+H]^+$ 568.

Step 5, 5-(7-(difluoromethyl)-6-(1-methyl-1H-pyrazol-4-yl)-3,4-dihydroquinolin-1(2H)-yl)-1-((2-(trimethylsilyl)ethoxy)methyl)-1H-pyrrolo[2,3-c]pyridine-3-carboxylic acid (**71**): To a solution of methyl 5-(7-(difluoromethyl)-6-(1-methyl-1*H*-pyrazol-4-yl)-3,4-dihydroquinolin-1(2*H*)-yl)-1-((2-(trimethylsilyl)ethoxy)methyl)-1*H*-pyrrolo[2,3-*c*]pyridine-3-carboxylate (**70**, 200 mg, 0.35 mmol, 1.0 equiv) in MeOH (5 mL) and water (1 mL) was added lithium hydroxide monohydrate (45 mg, 1.06 mmol, 3.0 equiv). The reaction was stirred at room temperature for 3 h and concentrated in vacuo. Water (5 mL) was added and the mixture was acidified with HCl (2

N) to pH 2 and then extracted with EtOAc (20 mL × 3). The combined organic layers were dried over anhydrous Na_2SO_4, filtered and concentrated in vacuo to give 5-(7-(difluoromethyl)-6-(1-methyl-1*H*-pyrazol-4-yl)-3,4-dihydroquinolin-1(2*H*)-yl)-1-((2-(trimethylsilyl)ethoxy)methyl)-1*H*-pyrrolo[2,3-*c*]pyridine-3-carboxylic acid (**71**, 150 mg, 77%) as a brown solid that required no further purification.

Step 6, 5-(7-(difluoromethyl)-6-(1-methyl-1H-pyrazol-4-yl)-3,4-dihydroquinolin-1(2H)-yl)-N-methyl-1-((2-(trimethylsilyl)ethoxy)methyl)-1H-pyrrolo[2,3-c]pyridine-3-carboxamide (**72**): To a solution of 5-(7-(difluoromethyl)-6-(1-methyl-1*H*-pyrazol-4-yl)-3,4-dihydroquinolin-1(2*H*)-yl)-1-((2-(trimethylsilyl)ethoxy)methyl)-1*H*-pyrrolo[2,3-*c*]pyridine-3-carboxylic acid (**71**, 100 mg, 0.18 mmol, 1.0 equiv) and triethylamine (0.049 mL, 0.35 mmol, 1.9 equiv) in DMF (8 mL) was added *O*-(7-azabenzotriazol-1-yl)-*N,N,N',N*'-tetramethyluronium hexafluorophosphate (80 mg, 0.21 mmol, 1.2 equiv) and methylamine hydrochloride (18 mg, 0.26 mmol, 1.4 equiv). The reaction was stirred at room temperature for 16 h. EtOAc (30 mL) was added and washed with water (30 mL x 3) and brine (30 mL). The organic layer was dried over anhydrous Na_2SO_4, filtered and concentrated in vacuo. The crude residue was purified by silica gel chromatography (DCM / MeOH = 9 : 1) to give 5-(7-(difluoromethyl)-6-(1-methyl-1*H*-pyrazol-4-yl)-3,4-dihydroquinolin-1(2*H*)-yl)-*N*-methyl-1-((2-(trimethylsilyl)ethoxy)methyl)-1*H*-pyrrolo[2,3-*c*]pyridine-3-carboxamide (**72**, 100 mg, 98%) as brown oil.

Step 7, 5-(7-(difluoromethyl)-6-(1-methyl-1H-pyrazol-4-yl)-3,4-dihydroquinolin-1(2H)-yl)-N-methyl-1H-pyrrolo[2,3-c]pyridine-3-carboxamide (**28**): A mixture of 5-(7-(difluoromethyl)-6-(1-methyl-1*H*-pyrazol-4-yl)-3,4-dihydroquinolin-1(2*H*)-yl)-*N*-methyl-1-((2-(trimethylsilyl)ethoxy)methyl)-1*H*-pyrrolo[2,3-*c*]pyridine-3-carboxamide (**72**, 100 mg, 0.18 mmol, 1.0 equiv) and tetrabutylammonium fluoride (1.0 M in THF, 6.0 mL, 6.0 mmol, 3.3

equiv) was heated to 50 °C for 2 d. After cooling the reaction to room temperature, the mixture was concentrated in vacuo. The crude residue was purified by reverse phase chromatography (acetonitrile 30–60% / 0.05% NH_4OH in water) to give 5-(7-(difluoromethyl)-6-(1-methyl-1*H*-pyrazol-4-yl)-3,4-dihydroquinolin-1(2*H*)-yl)-*N*-methyl-1*H*-pyrrolo[2,3-*c*]pyridine-3-carboxamide (**28**, 16 mg, 20%) as a white solid. ^{1}H NMR (400 MHz, $CDCl_3$): δ 10.32 (s, 1H), 8.61 (s, 1H), 7.75 (s, 1H), 7.69 (s, 1H), 7.56 (s, 1H), 7.44 (s, 1H), 7.32 (s, 1H) , 7.10 (s, 1H), 6.51 (t, *J* = 55.6 Hz, 1H), 5.87–5.86 (m, 1H), 3.96 (s, 3H), 3.88–3.85 (m, 2H), 2.99 (d, *J* = 4.4 Hz, 3H), 2.90–2.88 (m, 2H), 2.08–2.05 (m, 2H). LCMS (*m/z*) $[M+H]^+$ 437.

Synthesis and characterization of 5-(7-(difluoromethyl)-6-(1-methyl-1*H*-pyrazol-4-yl)-3,4-dihydroquinolin-1(2*H*)-yl)-7-isopropyl-*N*-methyl-1*H*-pyrrolo[2,3-*c*]pyridine-3-carboxamide (29)

Step 1, 2-bromo-6-chloro-3-nitropyridine (**74**): To a solution of 6-chloro-3-nitro-2-pyridinylamine (**73**, 20.0 g, 115 mmol, 1.0 equiv), copper(II) bromide (25.7 g, 115 mmol, 1.0 equiv) and copper(I) bromide (2.48 g, 17.3 mmol, 6.7 equiv) in MeCN (500 mL) at 0 °C was added isopentyl nitrite (20.17 mL, 149.8 mmol, 1.3 equiv). The reaction mixture was heated to 60 ^{o}C for 1 h under a nitrogen atmosphere. After cooling the reaction to room temperature, the mixture was concentrated in vacuo. The crude residue was purified by silica gel chromatography (petroleum ether / EtOAc = 5 : 1) to give 2-bromo-6-chloro-3-nitropyridine (**74**, 15 g, 55%) as a yellow solid. ^{1}H NMR (400 MHz, DMSO-d_6): δ 8.56 (d, *J* = 8.4 Hz, 1H), 7.89 (d, *J* = 8.4 Hz, 1H).

Step 2, 7-bromo-5-chloro-1H-pyrrolo[2,3-c]pyridine (**75**): To a solution of 2-bromo-6-chloro-3-nitropyridine (**74**, 10.0 g, 42.1 mmol, 1.0 equiv) in anhydrous THF (240 mL) at –78 °C was added vinylmagnesium bromide (1.0 M in THF, 329 mL, 329 mmol, 7.8 equiv). The reaction mixture was stirred at –50 ^{o}C for 1 h under a nitrogen atmosphere. The mixture was quenched with water (150 mL), and extracted with EtOAc (150 mL x 3). The combined organic layers were dried over anhydrous Na_2SO_4, filtered and concentrated in vacuo. The crude residue was purified by silica gel chromatography (petroleum ether / EtOAc = 1 : 1) to give 7-bromo-5-chloro-1*H*-pyrrolo[2,3-*c*]pyridine (**75**, 2.6 g, 27%) as a brown solid. ^{1}H NMR (400 MHz, DMSO-d_6): δ 12.13 (s, 1H), 7.76 (s, 1H), 7.69 (s, 1H), 6.64 (s, 1H).

Step 3, 1-(7-bromo-5-chloro-1H-pyrrolo[2,3-c]pyridin-3-yl)-2,2,2-trichloroethanone (**76**): To a solution of 7-bromo-5-chloro-1*H*-pyrrolo[2,3-*c*]pyridine (**75**, 1.9 g, 8.21 mmol, 1.0 equiv) and aluminum chloride (8.21 g, 61.6 mmol, 7.5 equiv) in DCM (60 mL) at 48 ^{o}C was added trichloroacetyl chloride (2.74 mL, 24.6 mmol, 3.0 equiv) dropwise. The reaction mixture was heated to 48 ^{o}C for 2 h. After cooling the reaction to room temperature, the mixture was quenched with ice-water (60 mL), and extracted with EtOAc (70 mL x 3). The combined organic layers were dried over anhydrous Na_2SO_4, filtered and concentrated in vacuo. The crude residue was purified by silica gel chromatography (petroleum ether / EtOAc = 1 : 3) to give 7-bromo-5-chloro-1*H*-pyrrolo[2,3-*c*]pyridine (**76**, 3.0 g, 97%) as a brown solid. LCMS (*m/z*) $[M+H]^+$ 377.

Step 4, methyl 7-bromo-5-chloro-1H-pyrrolo[2,3-c]pyridine-3-carboxylate (**77**): To a solution of 1-(7-bromo-5-chloro-1*H*-pyrrolo[2,3-*c*]pyridin-3-yl)-2,2,2-trichloroethanone (**76**, 3.2 g, 8.49 mmol, 1.0 equiv) in MeOH (50 mL) was added potassium hydroxide (524 mg, 9.34 mmol, 1.1 equiv). The reaction was stirred at room temperature for 16 h and concentrated in vacuo. Water (50 mL) was added and extracted with EtOAc (50 mL x 3). The combined organic

layers were dried over anhydrous Na_2SO_4, filtered and concentrated in vacuo to give methyl 7-bromo-5-chloro-1*H*-pyrrolo[2,3-*c*]pyridine-3-carboxylate (**77**, 2.0 g, 82%) as a brown solid that required no further purification. LCMS (*m/z*) $[M+H]^+$ 291.

Step 5, methyl 5-chloro-7-(prop-1-en-2-yl)-1H-pyrrolo[2,3-c]pyridine-3-carboxylate (**78**): To a solution of methyl 7-bromo-5-chloro-1*H*-pyrrolo[2,3-*c*]pyridine-3-carboxylate (**77**, 2.50 g, 8.64 mmol, 1.0 equiv) in 1,4-dioxane (10 mL) and water (1.5 mL) was added [1,1′-bis(diphenylphosphino)ferrocene]dichloropalladium(II) (632 mg, 0.860 mmol, 10 mol%), Na_2CO_3 (2.75 g, 25.9 mmol, 3.0 equiv) and 4,4,5,5-tetramethyl-2-(prop-1-en-2-yl)-1,3,2-dioxaborolane (1.74 g, 10.4 mmol, 1.2 equiv). The mixture was heated to 95 ^oC for 16 h under a nitrogen atmosphere. After cooling the reaction to room temperature, the mixture was filtered and concentrated in vacuo. The crude residue was purified by silica gel chromatography (petroleum ether / EtOAc = 5 : 1) to give methyl 5-chloro-7-(prop-1-en-2-yl)-1*H*-pyrrolo[2,3-*c*]pyridine-3-carboxylate (**78**, 1.8 g, 83%) as a brown solid. LCMS (*m/z*) $[M+H]^+$ 251.

Step 6, methyl 5-chloro-7-(prop-1-en-2-yl)-1-((2-(trimethylsilyl)ethoxy)methyl)-1H-pyrrolo[2,3-c]pyridine-3-carboxylate (**79**): To a solution of methyl 5-chloro-7-(prop-1-en-2-yl)-1*H*-pyrrolo[2,3-*c*]pyridine-3-carboxylate (**78**, 1.50 g, 5.98 mmol, 1.0 equiv) in DMF (15 mL) at 0 °C was added NaH (60% dispersion in mineral oil, 0.50 g, 12 mmol, 2.0 equiv) portionwise. The mixture was stirred at room temperature for 0.5 h. (2-(Chloromethoxy)ethyl)trimethylsilane (1.28 mL, 7.18 mmol, 1.2 equiv) was added dropwise and the mixture stirred at room temperature for an additional 4 h. The mixture was quenched with water (15 mL) and extracted with EtOAc (15 mL x 3). The combined organic layers were dried over anhydrous Na_2SO_4, filtered and concentrated in vacuo. The crude residue was purified by silica gel chromatography (petroleum ether / EtOAc = 7 : 1) to give methyl 5-chloro-7-(prop-1-en-2-yl)-1-((2-

(trimethylsilyl)ethoxy)methyl)-1*H*-pyrrolo[2,3-*c*]pyridine-3-carboxylate (**79**, 310 mg, 14%) as a yellow solid. LCMS (*m/z*) $[M+H]^+$ 381.

Step 7, methyl 5-(7-(difluoromethyl)-6-(1-methyl-1H-pyrazol-4-yl)-3,4-dihydroquinolin-1(2H)-yl)-7-(prop-1-en-2-yl)-1-((2-(trimethylsilyl)ethoxy)methyl)-1H-pyrrolo[2,3-c]pyridine-3-carboxylate (**80**): To a solution of methyl 5-chloro-7-(prop-1-en-2-yl)-1-((2-(trimethylsilyl)ethoxy)methyl)-1*H*-pyrrolo[2,3-*c*]pyridine-3-carboxylate (**79**, 300 mg, 0.79 mmol, 1.0 equiv) in 1,4-dioxane (8 mL) was added 7-(difluoromethyl)-6-(1-methyl-1*H*-pyrazol-4-yl)-1,2,3,4-tetrahydroquinoline (**31**, 207 mg, 0.79 mmol, 1.0 equiv), dichloro[1,3-bis(2,6-di-3-pentylphenyl)imidazol-2-ylidene](3-chloropyridyl)palladium(II) (63 mg, 0.08 mmol, 10 mol%) and Cs_2CO_3 (770 mg, 2.36 mmol, 3.0 equiv). The mixture was heated to 110 °C for 16 h under a nitrogen atmosphere. EtOAc (30 mL) was added and washed with water (30 mL x 2), brine (30 mL). The organic layer was dried over anhydrous Na_2SO_4, filtered and concentrated in vacuo. The crude residue was purified by silica gel chromatography (petroleum ether / EtOAc = 3 : 1) to give methyl 5-(7-(difluoromethyl)-6-(1-methyl-1*H*-pyrazol-4-yl)-3,4-dihydroquinolin-1(2*H*)-yl)-7-(prop-1-en-2-yl)-1-((2-(trimethylsilyl)ethoxy)methyl)-1*H*-pyrrolo[2,3-*c*]pyridine-3-carboxylate (**80**, 310 mg, 65%) as a yellow solid. LCMS LCMS (*m/z*) $[M+H]^+$ 608.

Step 8, 5-(7-(difluoromethyl)-6-(1-methyl-1H-pyrazol-4-yl)-3,4-dihydroquinolin-1(2H)-yl)-7-(prop-1-en-2-yl)-1-((2-(trimethylsilyl)ethoxy)methyl)-1H-pyrrolo[2,3-c]pyridine-3-carboxylic acid (**81**): To a solution of methyl 5-(7-(difluoromethyl)-6-(1-methyl-1*H*-pyrazol-4-yl)-3,4-dihydroquinolin-1(2*H*)-yl)-7-(prop-1-en-2-yl)-1-((2-(trimethylsilyl)ethoxy)methyl)-1*H*-pyrrolo[2,3-*c*]pyridine-3-carboxylate (**80**, 310 mg, 0.51 mmol, 1.0 equiv) in MeOH (10 mL) and water (2 mL) was added lithium hydroxide monohydrate (107 mg, 2.55 mmol, 5.0 equiv). The reaction was stirred at room temperature for 12 h under a nitrogen atmosphere and concentrated

in vacuo. Water (10 mL) was added and the mixture was acidified with HCl (2 N) to pH 4 and then extracted with EtOAc (30 mL × 3). The combined organic layers were dried over anhydrous Na_2SO_4, filtered and concentrated in vacuo to give 5-(7-(difluoromethyl)-6-(1-methyl-1*H*-pyrazol-4-yl)-3,4-dihydroquinolin-1(2*H*)-yl)-7-(prop-1-en-2-yl)-1-((2-(trimethylsilyl)ethoxy)methyl)-1*H*-pyrrolo[2,3-*c*]pyridine-3-carboxylic acid (**81**, 300 mg, 99%) as a white solid that required no further purification. LCMS (*m/z*) $[M+H]^+$ 594.

Step 9, 5-(7-(difluoromethyl)-6-(1-methyl-1H-pyrazol-4-yl)-3,4-dihydroquinolin-1(2H)-yl)-N-methyl-7-(prop-1-en-2-yl)-1-((2-(trimethylsilyl)ethoxy)methyl)-1H-pyrrolo[2,3-c]pyridine-3-carboxamide (**82**): To a solution of 5-(7-(difluoromethyl)-6-(1-methyl-1*H*-pyrazol-4-yl)-3,4-dihydroquinolin-1(2*H*)-yl)-7-(prop-1-en-2-yl)-1-((2-(trimethylsilyl)ethoxy)methyl)-1*H*-pyrrolo[2,3-*c*]pyridine-3-carboxylic acid (**81**, 300 mg, 0.51 mmol, 1.0 equiv) and *N,N*-diisopropylethylamine (0.18 mL, 1.04 mmol, 2.0 equiv) in DMF (10 mL) was added *O*-(7-azabenzotriazol-1-yl)-*N,N,N',N*'-tetramethyluronium hexafluorophosphate (298 mg, 0.78 mmol, 1.5 equiv) and methylamine hydrochloride (46 mg, 0.68 mmol, 1.3). The reaction was stirred at room temperature for 16 h. EtOAc (30 mL) was added and washed with water (10 mL x 2) and brine (10 mL). The organic layer was dried over anhydrous Na_2SO_4, filtered and concentrated in vacuo. The crude residue was purified by silica gel chromatography (petroleum ether / EtOAc = 6 : 1) to give 5-(7-(difluoromethyl)-6-(1-methyl-1*H*-pyrazol-4-yl)-3,4-dihydroquinolin-1(2*H*)-yl)-*N*-methyl-7-(prop-1-en-2-yl)-1-((2-(trimethylsilyl)ethoxy)methyl)-1*H*-pyrrolo[2,3-*c*]pyridine-3-carboxamide (**82**, 290 mg, 95%) as a white solid. LCMS (*m/z*) $[M+H]^+$ 607.

Step 10, 5-(7-(difluoromethyl)-6-(1-methyl-1H-pyrazol-4-yl)-3,4-dihydroquinolin-1(2H)-yl)-N-methyl-7-(prop-1-en-2-yl)-1H-pyrrolo[2,3-c]pyridine-3-carboxamide (**83**): A mixture of 5-(7-(difluoromethyl)-6-(1-methyl-1*H*-pyrazol-4-yl)-3,4-dihydroquinolin-1(2*H*)-yl)-*N*-methyl-7-

(prop-1-en-2-yl)-1-((2-(trimethylsilyl)ethoxy)methyl)-1*H*-pyrrolo[2,3-*c*]pyridine-3-carboxamide (**82**, 290 mg, 0.48 mmol, 1.0 equiv) and tetrabutylammonium fluoride (1.0 M in THF, 10 mL, 10 mmol, 21 equiv) was heated to 55 °C for 2 h under a nitrogen atmosphere. After cooling the reaction to room temperature, the mixture was concentrated in vacuo. The crude residue was dissolved in DCM (50 mL), washed with brine (300 mL x 4). The organic layer was dried over anhydrous Na_2SO_4, filtered and concentrated in vacuo to give 5-(7-(difluoromethyl)-6-(1-methyl-1*H*-pyrazol-4-yl)-3,4-dihydroquinolin-1(2*H*)-yl)-*N*-methyl-7-(prop-1-en-2-yl)-1*H*-pyrrolo[2,3-*c*]pyridine-3-carboxamide (**83**, 210 mg, 92%) as brown oil that required no further purification.

Step 11, 5-(7-(difluoromethyl)-6-(1-methyl-1H-pyrazol-4-yl)-3,4-dihydroquinolin-1(2H)-yl)-7-isopropyl-N-methyl-1H-pyrrolo[2,3-c]pyridine-3-carboxamide (**29**): To a solution of 5-(7-(difluoromethyl)-6-(1-methyl-1*H*-pyrazol-4-yl)-3,4-dihydroquinolin-1(2*H*)-yl)-*N*-methyl-7-(prop-1-en-2-yl)-1*H*-pyrrolo[2,3-*c*]pyridine-3-carboxamide (**83**, 100 mg, 0.21 mmol, 1.0 equiv) in MeOH (20 mL) was added 10% Pd/C (10 mg, 0.009 mmol,). The mixture was stirred at room temperature for 18 h under a hydrogen atmosphere (50 psi). The mixture was filtered and the filtrate was concentrated in vacuo. The crude residue was purified by reverse phase chromatography (acetonitrile 20–50% / 0.2% formic acid in water) to give 5-(7-(difluoromethyl)-6-(1-methyl-1*H*-pyrazol-4-yl)-3,4-dihydroquinolin-1(2*H*)-yl)-7-isopropyl-*N*-methyl-1*H*-pyrrolo[2,3-*c*]pyridine-3-carboxamide (**29**, 62 mg, 62%) as a white solid. ^{1}H NMR (400 MHz, DMSO-d_6): δ 11.94 (s, 1H), 8.11 (s, 1H), 7.90 (q, J = 4.5 Hz, 1H), 7.77 (d, J = 0.9 Hz, 1H), 7.65 (s, 1H), 7.52 (d, J = 0.8 Hz, 1H), 7.34 (s, 1H), 7.12 (d, J = 1.4 Hz, 1H), 6.76 (t, J = 55.2 Hz, 1H), 3.87 (s, 3H), 3.82–3.74 (m, 2H), 3.56–3.45 (m, 1H), 2.86 (t, J = 6.5 Hz, 2H), 2.76 (d, J = 4.5 Hz, 3H), 2.09–1.95 (m, 2H), 1.28 (d, J = 6.8 Hz, 6H). ^{13}C NMR (100 MHz, DMSO-d_6): δ 164.9, 150.9, 149.8, 142.9, 138.3, 134.1, 131.4, 130.8, 129.8, 128.5, 128.31, 128.28, 128.1, 127.7, 121.5

(t, J = 6.0 Hz), 119.1, 114.3 (t, J = 234 Hz), 113.1, (t, J= 6.0 Hz), 49.3, 39.0, 31.1, 27.6, 25.9, 22.6, 21.9. HRMS-ESI (m/z) $[M+H]^+$ calcd for $C_{26}H_{29}ON_6F_2$ = 479.2365; found, 479.2362.

Modeling methods. The figures of crystal structures were created using PyMol: All figure were made using PyMOL Molecular Graphics System, Version 1.8 Schrödinger, LLC.

Expression and purification of bromodomain proteins. The expression and purification of bromodomain proteins for binding assays was carried out as previously described.[48,62]

Expression and purification of bromodomain proteins for crystallography. CBP bromodomain was expressed in E. coli as N-terminal His6-FLAG-tagged fusion with a thrombin protease site for removal of the affinity tags. Proteins were purified by sequential Ni affinity and size-exclusion chromatography steps. Affinity tags were removed after the Ni affinity step by dialysis against a thrombin-containing buffer. Additional ion-exchange steps were included as necessary to achieve homogeneous preparations, and the identity of the protein was verified by mass spectrometry.

Time-Resolved Fluorescence Resonance Energy Transfer assays. Compound potencies were evaluated in a panel of biochemical-bromodomain-binding assays. Binding of biotinylated small-molecule ligands to recombinant His-tagged bromodomains was assessed by time-resolved fluorescence resonance energy transfer (TR-FRET). Test compounds that compete with the biotinylated ligand for bromodomain binding reduce the TR-FRET signal. All biochemical assay protocols were carried out as previously described.[47,55] Normalized TR-FRET inhibition data were plotted as a function of compound concentration, and the resulting curves were fit to a 4-parameter Hill equation to determine the IC_{50} values (constraining upper and/or lower boundaries

where necessary). If compound inhibition did not reach 50%, then IC_{50} values were reported as greater than the highest concentration tested (50 μM for HTS IC_{50} determinations and 10 μM for compound optimization). IC_{50} values are reported as the geometric mean of between 2 to 8 replicates. In all cases, replicate values fall within 60% of the geometric mean.

Cellular assay protocol. To determine the inhibition of *MYC* expression, MV-4-11 cells (ATCC) were plated at 10,000 cells per well in 96-well plates in RPMI1640 media supplemented with 10% fetal bovine serum and 2 mM L-glutamine. Test compounds diluted in DMSO were transferred to the cell plates, keeping final DMSO concentration consistent at 0.1%, and incubated for 4 h at 37 ˚C. Lysis and analysis for *MYC* expression were carried out using QuantiGene 2.0 reagents (Affymetrix/eBioscience, probe set cat # SA-50182) and following the vendor's instructions. Luminescence was read using an EnVision plate reader (PerkinElmer) and EC_{50}s generated using a 4-parameter non-linear regression fit.

In vitro metabolic stability experiments. Experiments were carried out as previously described.[54]

In vivo PK of 29. Six CD-1 mice were obtained from Charles River Laboratory (Hollister, California, USA). All animals were female, 6−9 weeks old at the time of study and weighed between 20 to 35 g. Animals (n = 3 per dosing route) were dosed with **29** 1 mg/kg i.v. (in propyl ethylene glycol 400 (35% v/v), dimethyl sulfoxide (10% v/v) and water (55% v/v)) or 5 mg/kg p.o. (suspended in 0.5% w/v methylcellulose, 0.2% w/v Tween 80). Food and water were available ad libitum to all animals. Serial blood samples (15 μL) were collected by tail nick at 0.033, 0.083, 0.25, 0.5, 1, 3, 8, and 24 h after the intravenous administration and 0.083, 0.25, 0.5, 1, 3, 8, and 24 h after the oral administration. All blood samples were diluted with 60 μL water

containing 1.7 mg/mL K_2EDTA and kept at −80 °C until analysis. All animal studies were carried out in accordance with the Guide for the Care and Use of Laboratory Animals as adopted and were approved by the Institution's Animal Care and Use Committee.

Concentrations of **29** were determined by a non-validated LC-MS/MS assay. The diluted blood samples were prepared for analysis by placing a 15 µL aliquot into a 96-well plate followed by the addition of 150 µL of acetonitrile containing an internal standard mixture (labetalol, Indomethacin, and Loperamide at ~1 µg/mL). The samples were vortexed and centrifuged at 4000 rpm for 20 minutes at 4 °C; 100 µL of the supernatant was diluted with 150 µL water and 1 µL of the solution was injected onto an analytical column. A Nexera UPLC System (Shimadzu) coupled with an QTrap 6500 mass spectrometer (AB Sciex, Foster City, CA) was used for sample analysis. The mobile phases were 0.1% of formic acid in water (A) and 0.1% formic acid in acetonitrile (B). The gradient was as follows: starting at 10% B and increased to 90% B until 0.6 minute, maintained it at 90% for 0.2 minutes, then from 90% B to 10% B for 0.01 minute, maintained at 10% B for 0.2 minute. The total flow rate was 0.6 ml/min and samples were injected onto a Kinetex F5 (50 × 2.1 mm, 2.6 µm) analytical column with a total run time of 1 minute. Data was acquired using multiple reactions monitoring (MRM) in positive ion electrospray mode with an operating source temperature of 550 °C. The MRM transition was m/z 479.4 → 439.1 for 29 and 477.1 → 266.2 for loperamide. The lower and upper limits of quantitation of the assay for 29 were 0.001 and 69.6 µM, respectively.

Associated Content

Supporting Information

The Supporting Information is available free of charge on the ACS Publications website at DOI: XXX.

Full experimental details and characterization for reported compounds, BROMOscan data for **27** and **29**, and crystallography methods for **3**-CBP, **6**-CBP, **16**-CBP, and **17**-CBP are provided in the Supporting Information.

Molecular formula strings (CSV)

Accession Codes

PDB codes for the structures of the CBP bromodomain in complex with **3**, **6**, **16**, and **17** are 5W0E, 6AXQ, 6AY3, and 6AY5, respectively. Authors will release the atomic coordinates and experimental data upon article publication.

Author Information

Corresponding Author

*Phone: +1-650-467-4426. E-mail: bronner.sarah@gene.com.

Acknowledgements

The authors thank Mengling Wong, Michael Hayes, and Amber Guillen for compound purification. Baiwei Lin, Deven Wang, and Yutao Jiang are acknowledged for analytical support. Grady Howes, Jan Seerveld, Hao Zheng, and Gigi Yuen for help with compound management and logistics are also recognized. This research used resources of the Advanced Photon Source, a U.S. Department of Energy (DOE) Office of Science User Facility operated for the DOE Office of Science by Argonne National Laboratory under Contract No. DE-AC02-06CH11357. We

would like to acknowledge the beamline scientists at APS for assistance in data collection and processing

Abbreviations Used

Arg, arginine; Asn, asparagine; Asp, aspartic acid; BC, helices B and C; BrD, bromodomain; BRD4(1), bromodomain 1 of the bromodomain-containing protein 4; BRD9, bromodomain-containing protein 9; BRET, bioluminescence resonance energy transfer; BRPF, bromodomain and plant homeodomain finger containing; CX (X = 5, 7), carbon X (X = 5, 7); CBP, cyclic adenosine monophosphate response element binding portion binding protein; CECR2, cat eye syndrome chromosome region, candidate 2; CF_2H, difluoromethyl; Cl_{hep}, predicted hepatic clearance; CREBP, cyclic adenosine monophosphate response element binding portion binding protein; DMSO, dimethylsulfoxide; DNA, deoxyribonucleic acid; EC_{50}, half maximal effective concentration; g, gram; GNE, Genentech; HAT, histone acetyl transferase; IC_{50}, half maximal inhibitory concentration; i.v., intravenous; H, human; HTS, high throughput screen; K_2EDTA, dipotassium ethylenediaminetetraacetic acid; KAc, acetylated lysine; kg, kilogram; LC-MS/MS, liquid chromatography- mass spectrometry and tandem mass spectrometry; LE, ligand efficiency; Leu, leucine; LM, liver microsomes; LPF, leucine, proline, and phenylalanine; M, mouse; MRM, multiple reactions monitoring; p.o., per os; P300, adenoviral E1A binding protein; Phe, phenylalanine; PK, pharmacokinetic; Pro, proline; PTM, post-translational modification; R, rat; rpm, revolutions per minute; SAR, structure activity relationship; SBDD, structure-based drug discovery; THQ, tetrahydroquinoline; TR-FRET, time-resolved fluorescence energy transfer; TRIM24, tripartite motif-containing 24; v/v, volume per volume; w/v, weight per volumn; ZA, helices Z and A.

References

(1) Carey, N. *The Epigenetics Revolution: How Modern Biology is Rewriting Our Understanding of Genetics, Disease, and Inheritance,* Columbia University Press: New York, 2012.

(2) Carey, N. *Epigenetics for Drug Discovery,* Royal Society of Chemistry: United Kingdom, 2015.

(3) Kanherkar, R. R.; Bhatia-Dey, N.; Csoka, A. B. Epigenetics Across the Human Lifespan. *Front. Cell Dev. Biol.* **2014**, *2*, 49.

(4) Dawson, M. A.; Kouzarides, T. Cancer Epigenetics: From Mechanism to Therapy. *Cell* **2012**, *150*, 12−27.

(5) Campbell, R. M.; Tummino, P. J. Cancer Epigenetics Drug Discovery and Development: the Challenge of Hitting the Mark. *J. Clin. Invest.* **2014**, *124*, 64−69.

(6) Mau, T.; Yung, R. Potential of Epigenetic Therapies in Non-Cancerous Conditions. *Front. Genet.* **2014**, *5*, 438.

(7) Kelly, T. K.; De Carvalho, D. D.; Jones, P. A. Epigenetic Modifications as Therapeutic Targets. *Nat. Biotechnol.* **2010**, *28*, 1069−1078.

(8) Kwa, F. A. A.; Thrimawithana, T. R. Epigenetic Modifications as Potential Therapeutic Targets in Age-Related Macular Degeneration and Diabetic Retinopathy. *Drug Discovery Today* **2014**, *19*, 1387−1393.

(9) Arrowsmith, C. H.; Bountra, C.; Fish, P. V.; Lee, K.; Schapira, M. Epigenetic Protein Families: a New Frontier for Drug Discovery. *Nat. Rev. Drug Discovery* **2012**, *11*, 384−400.

(10) Gnyszka, A.; Jastrzebski, Z.; Flis, S. DNA Methyltransferase Inhibitors and Their Emerging Role in Epigenetic Therapy of Cancer. *Anticancer Res.* **2013**, *33*, 2989−2996.

(11) Szyf, M. The Implications of DNA Methylation for Toxicology: Toward Toxicomethylomics, the Toxicology of DNA Methylation. *Toxicol. Sci.* **2011**, *120*, 235−255.

(12) Cedar, H.; Bergman, Y. Linking DNA Methylation and Histone Modification: Patterns and Paradigms. *Nat. Rev. Genet.* **2009**, *10*, 295−304.

(13) Verdone, L.; Caserta, M.; Di Mauro, E. Role of Histone Acetylation in the Control of Gene Expression. *Biochem. Cell Biol.* **2005**, *83*, 344−353.

(14) Shahbazian, M. D.; Grunstein, M. Functions of Site-Specific Histone Acetylation and Deacetylation. *Annu. Rev. Biochem.* **2007**, *76*, 75−100.

(15) Grunstein, M. Histone Acetylation in Chromatin Structure and Transcription. *Nature* **1997**, *389*, 349−352.

(16) Jenuwein, T.; Allis, C. D. Translating the Histone Code. *Science* **2001**, *293*, 1074−1080.

(17) Strahl, B. D.; Allis, C. D. The Language of Covalent Histone Modifications. *Nature* **2000**, *403*, 41−45.

(18) Dawson, M. A.; Kouzarides, T.; Huntly, B. J. P. Targeting Epigenetic Readers in Cancer. *N. Engl. J. Med.* **2012**, *367*, 647−657.

(19) Filippakopoulos, P.; Knapp, S. Targeting Bromodomains: Epigenetic Readers of Lysine Acetylation. *Nat. Rev. Drug Discovery* **2014**, *13*, 337−356.

(20) Romero, F. A.; Taylor, A. M.; Crawford, T. D.; Tsui, V.; Côté, A; Magnuson, S. Disrupting Acetyl-Lysine Recognition: Progress in the Development of Bromodomain Inhibitors. *J. Med. Chem.* **2016**, *59*, 1271−1298.

(21) Sanchez, R.; Meslamani, J.; Zhou, M.-M. The Bromodomain: From Epigenome Reader to Druggable Target. *Biochim. Biophys. Acta* **2014**, *1839*, 676−685.

(22) Gallenkamp, D.; Gelato, K. A.; Haendler, B.; Weinmann, H. Bromodomains and Their Pharmacological Inhibitors. *ChemMedChem* **2014**, *9*, 438−464.

(23) Dekker, F. J.; Haisma, H. J. Histone Acetyl Transferases as Emerging Drug Targets. *Drug Discovery Today* **2009**, *14*, 942–948.

(24) Bannister, A. J.; Kouzarides, T. The CBP Co-Activator is a Histone Acetyltransferase. *Nature* **1996**, *384*, 641−643.

(25) Dancy, B. M.; Cole, P. A. Protein Lysine Acetylation by p300/CBP. *Chem. Rev.* **2015**, *115*, 2419−2452.

(26) Delvecchio, M.; Gaucher, J.; Aguilar-Gurrieri, C.; Ortega, E.; Panne, D. Structure of the P300 Catalytic Core and Implications for Chromatin Targeting and HAT Regulation. *Nat. Struct. Mol. Biol.* **2013**, *20*, 1040−1046.

(27) Panagopoulos, I.; Fioretos, T.; Isaksson, M.; Samuelsson, U.; Billstrom, R.; Strombeck, B.; Mitelman, F.; Johansson, B. Fusion of the *MORF* and *CBP* Genes in Acute Myeloid Leukemia with the t(10;16)(q22;p13). *Hum. Mol. Genet.* **2001**, *10*, 395−404.

(28) Dutta, R.; Tiu, B.; Sakamoto, K. M. CBP/P300 Acetyltransferase Activity in Hematologic Malignancies. *Mol. Gen. Metab.* **2016**, *119*, 37–43.

(29) Ianculescu, I.; Wu, D.-Y.; Siegmund, K. D.; Stallcup, M. R. Selective Roles for cAMP Response Element-Binding Protein Binding Protein and P300 Protein as Coregulators for

Androgen-Regulated Gene Expression in Advanced Prostate Cancer Cells. *J. Biol. Chem*. **2012**, *287*, 4000−4013.

(30) Iyer, N. G.; Özdag, H.; Caldas, C. P300/CBP and Cancer. *Oncogene* **2004**, *23*, 4225−4231.

(31) Fujisawa, T.; Filippakopoulos, P. Functions of Bromodomain-Containing Proteins and Their Roles in Homeostasis and Cancer. *Nat. Rev. Mol. Cell Biol.* **2017**, *18*, 246–262.

(32) Jin, L.; Garcia, J.; Chan, E.; la Cruz, de, C.; Segal, E.; Merchant, M.; Kharbanda, S.; Haverty, P. M.; Modrusan, Z.; Ly, J.; Choo, E. F.; Kaufman, S.; Beresini, M. H.; Romero, F. A.; Magnuson, S.; Gascoigne, K. E. Therapeutic Targeting of the CBP/P300 Bromodomain for the Treatment of Castration Resistant Prostate Cancer. *Cancer Res.* **2017**, *77*, 5564−5575.

(33) Faiola, F.; Liu, X.; Lo, S.; Pan, S.; Zhang, K.; Lymar, E.; Farina, A.; Martinez, E. Dual Regulation of C-Myc by P300 via Acetylation-Dependent Control of Myc Protein Turnover and Coactivation of Myc-Induced Transcription. *Mol. Cell. Biol.* **2005**, *25*, 10220−10234.

(34) Conery, A. R.; Centore, R. C.; Neiss, A.; Keller, P. J.; Joshi, S.; Spillane, K. L.; Sandy, P.; Hatton, C.; Pardo, E.; Zawadzke, L.; Bommi-Reddy, A.; Gascoigne, K. E.; Bryant, B. M.; Mertz, J. A.; Sims, R. J. Bromodomain Inhibition of the Transcriptional Coactivators CBP/EP300 as a Therapeutic Strategy to Target the IRF4 Network in Multiple Myeloma. *eLife* **2016**, *5*, e10483.

(35) Liu, Y.; Wang, L.; Predina, J.; Han, R.; Beier, U. H.; Wang, L.-C. S.; Kapoor, V.; Bhatti, T. R.; Akimova, T.; Singhal, S.; Brindle, P. K.; Cole, P. A.; Albelda, S. M.; Hancock, W.

W. Inhibition of P300 Impairs Foxp3+ T Regulatory Cell Function and Promotes Antitumor Immunity. *Nat. Med.* **2013**, *19*, 1173−1177.

(36) Ghosh, S.; Taylor, A.; Chin, M.; Huang, H.-R.; Conery, A. R.; Mertz, J. A.; Salmeron, A.; Dakle, P. J.; Mele, D.; Côté, A.; Jayaram, H.; Setser, J. W.; Poy, F.; Hatzivassiliou, G.; DeAlmeida-Nagata, D.; Sandy, P.; Hatton, C.; Romero, F. A.; Chiang, E.; Reimer, T.; Crawford, T.; Pardo, E.; Watson, V. G.; Tsui, V.; Cochran, A. G.; Zawadzke, L.; Harmange, J.-C.; Audia, J. E.; Bryant, B. M.; Cummings, R. T.; Magnuson, S. R.; Grogan, J. L.; Bellon, S. F.; Albrecht, B. K.; Sims, R. J., III; Lora, J. M. Regulatory T Cell Modulation by CBP/EP300 Bromodomain Inhibition. *J. Biol. Chem.* **2016**, *291*, 13014–13027.

(37) Sachchidanand; Resnick-Silverman, L.; Yan, S.; Mutjabi, S.; Liu, W.-j.; Zeng, L.; Manfredi, J. J.; Zhou, M.-M. Target Structure-Based Discovery of Small Molecules that Block Human p53 and CREB Binding Protein Association. *Chem. Biol.* **2006**, *13*, 81–90.

(38) Borah, J. C.; Mujtaba, S.; Karakikes, I.; Zeng, L.; Muller, M.; Patel, J.; Moshkina, N.; Morohashi, K.; Zhang, W.; Gerona-Navorro, G.; Hajjar, R. J.; Zhou, M.-M. *Chem. Biol.* **2011**, *18*, 531–541.

(39) Ito, T.; Umehara, T.; Sasaki, K.; Nakamura, Y.; Nishino, N.; Terada, T.; Shirouzu, M.; Padmanabhan, B.; Yokoyama, S.; Ito, A.; Yoshida, M. Real-Time Imaging of Histone Deacetylase and Bromodomain Inhibitors. *Chem. Biol.* **2011**, *18*, 495–507.

(40) Hewings, D. S.; Wang, M.; Philpott, M.; Fedorov, O.; Uttarkar, S.; Filippakopoulos, P.; Picaud, S.; Vuppusetty, C.; Marsden, B.; Knapp, S.; Conway, S. J.; Heightman, T. D. 3,5-Dimethylisoxazoles Act as Acetyl-Lysine-Mimetic Bromodomain Ligands. *J. Med. Chem.* **2011**, *54*, 6761–6770.

(41) *I-CBP112: A CREBBP/EP-300-Selective Chemical Probe*; SGC, 2015; http://www.thesgc.org/chemical-probes/I-CBP112 (accessed December 11, 2015).

(42) Hewings, D. S.; Fedorov, O.; Filippakopoulos, P.; Martin, S.; Picaud, S.; Tumber, A.; Wells, C.; Olcina, M. M.; Freeman, K.; Gill, A.; Ritchie, A. J.; Sheppard, D. W.; Russell, A. J.; Hammond, E. M.; Knapp, S.; Brennan, P. E.; Conway, S. J. Optimization of 3,5-Dimethylisoxazole Derivatives as Potent Bromodomain Ligands. *J. Med. Chem.* **2013**, *56*, 3217–3227.

(43) Hay, D. A.; Fedorov, O.; Martin, S.; Singleton, D. C.; Tallant, C.; Wells, C.; Picaud, S.; Philpott, M.; Monteiro, O. P.; Conway, S. J.; Tumber, A.; Yapp, C.; Filippakopoulos, P.; Bunnage, M. E.; Knapp, S.; Schofield, C. J.; Brennan, P. E. Discovery and Optimization of Small-Molecule Ligands for the CBP/P300 Bromodomains. *J. Am. Chem. Soc.* **2014**, *136*, 9308–9319.

(44) Rooney, T. P. C.; Filippakopoulos, P.; Fedorov, O.; Picaud, S.; Cortopassi, W. A.; Hay, D. A.; Martin, S.; Tumber, A.; Rogers, C. M.; Philpott, M.; Wang, M.; Thompson, A. L.; Heightman, T. D.; Pryde, D. C.; Cook, A.; Paton, R. S.; Müller, S.; Knapp, S.; Brennan, P. E.; Conway, S. J. A Series of Potent CREBBP Bromodomain Ligands Reveals an Induced-Fit Pocket Stabilized by a Cation-π Interaction. *Angew. Chem. Int. Ed.* **2014**, *53*, 6126–6130.

(45) Picaud, S.; Fedorov, O.; Thanasopoulou, A.; Leonards, K.; Jones, K.; Meier, J.; Olzscha, H.; Monteiro, O.; Martin, S.; Philpott, M.; Tumber, A.; Filippakopoulos, P.; Yapp, C.; Wells, C.; Che, K. H.; Bannister, A.; Robson, S.; Kumar, U.; Parr, N.; Lee, K.; Lugo, D.; Jeffrey, P.; Taylor, S.; Vecellio, M. L.; Bountra, C.; Brennan, P. E.; O'Mahony, A.; Velichko, S.; Müller, S.; Hay, D.; Daniels, D. L.; Urh, M.; La Thangue, N. B.;

Kouzarides, T.; Prinjha, R.; Schwaller, J.; Knapp, S. Generation of a Selective Small Molecule Inhibitor of the CBP/P300 Bromodomain for Leukemia Therapy. *Cancer Res.* **2015**, *75*, 5106–5119.

(46) Hammitzsch, A.; Tallant, C.; Fedorov, O.; O'Mahony, A.; Brennan, P. E.; Hay, D. A.; Martinez, F. O.; Al-Mossawi, M. H.; de Wit, J.; Vecellio, M.; Wells, C.; Wordsworth, P.; Müller, S.; Knapp, S.; Bowness, P. CBP30, a Selective CBP/P300 Bromodomain Inhibitor, Suppresses Human Th17 Responses. *Proc. Natl. Acad. Sci. U.S.A.* **2015**, *112*, 10768–10773.

(47) a) Xu, M.; Unzue, A.; Dong, J.; Spiliotopoulos, D.; Nevado, C.; Caflisch, A. Discovery of CREBB Bromodomain Inhibitors by High-Throughput Docking and Hit Optimization Guided by Molecular Dynamics. *J. Med. Chem.* **2016**, *59,* 1340−1349. b) Unzue, A.; Xu, M.; Dong, J.; Wiedmer, L.; Spiliotopoulos, D.; Caflisch, A.; Nevado, C. Fragment-Based Design of Selective Nano-molar Ligands of the CREBBP Bromodomain. *J. Med. Chem.* **2016**, *59,* 1350−1356.

(48) Taylor, A. M.; Côté, A.; Hewitt, M. C.; Pastor, R.; Leblanc, Y.; Nasveschuk, C. G.; Romero, F. A.; Crawford, T. D.; Cantone, N.; Jayaram, H.; Setser, J.; Murray, J.; Beresini, M. H.; de Leon Boenig, G.; Chen, Z.; Conery, A. R.; Cummings, R. T.; Dakin, L. A.; Flynn, E. M.; Huang, O. W.; Kaufman, S.; Keller, P. J.; Kiefer, J. R.; Lai, T.; Li, Y.; Liao, J.; Liu, W.; Lu, H.; Pardo, E.; Tsui, V.; Wang, J.; Wang, Y.; Xu, Z.; Yan, F.; Yu, D.; Zawadzke, L.; Zhu, X.; Zhu, X.; Sims, R. J., III; Cochran, A. G.; Bellon, S.; Audia, J. E.; Magnuson, S.; Albrecht, B. K. Fragment-Based Discovery of a Selective and Cell-Active Benzodiazepinone CBP/EP300 Bromodomain Inhibitor (CPI-637). *ACS Med. Chem. Lett.* **2016**, *7*, 531–536.

(49) Popp, T. A.; Tallant, C.; Rogers, C.; Fedorov, O.; Brennan, P. E.; Müller, S.; Knapp, S.; Bracher, F. Development of Selective CBP/P300 Benzoxazepine Bromodomain Inhibitors. *J. Med. Chem.* **2016**, *59*, 8889–8912.

(50) Denny, R. A.; Flick, A. C.; Coe, J. W.; Langille, J.; Basak, A.; Liu, S.; Stock, I. A.; Sahasrabudhe, P.; Bonin, P. D.; Hay, D. A.; Brennan, P. E.; Pletcher, M. T.; Jones, L. H.; Chekler, E. L. P. Structure-Based Design of Highly Selective Inhibitors of the CREB Binding Protein Bromodomain. *J. Med. Chem.* **2017**, *60*, 5349–5363.

(51) Spiliotopoulos, D.; Zhu, J.; Wamhoff, E.-C.; Deerain, N.; Marchand, J.-R.; Aretz, J.; Rademacher, C.; Caflisch, A. Virtual Screen to NMR (VS2NMR): Discovery of Fragment Hits for the CBP Bromodomain. *Bioorg. Med. Chem. Lett.* **2017**, *27*, 2472–2478.

(52) Hügle, M.; Lucas, X.; Ostrovskyi, D.; Regenass, P.; Gerhardt, S.; Einsle, O.; Hau, M.; Jung, M.; Breit, B.; Günther, S.; Wohlwend, D. Beyond the BET Family: Targeting CBP/p300 with 4-Acyl Pyrroles. *Angew. Chem. Int. Ed.* **2017**, *56*, 12476–12480.

(53) Romero, F. A.; Murray, J.; Lai, K. W.; Tsiu, V.; Albrecht, B. K.; Beresini, M. H.; de Leon Boenig, G.; Bronner, S. M.; Chan, E. W.; Chen, K.; Chen, Z.; Choo, E. F.; Clark, K.; Crawford, T. D.; Cyr, P.; De Almeida Nagata, D.; Gascoigne, K. E.; Grogan, J.; Hatzivassiliou, G.; Hunsaker, T. L.; Kaufman, S.; Li, Y.; Liao, J.; Liu, W.; Ly, J.; Maher, J.; Merchant, M.; Ran, Y.; Taylor, A. M.; Wai, J.; Wang, F.; Wei, X.; Yu, D.; Zhu, B.-Y.; Zhu, X.; Magnuson, S. GNE-781, A Highly Advanced Potent and Selective Bromodomain Inhibitor of CBP/P300. *J. Med. Chem.* [Online early access] DOI:10.1021/acs.jmedchem.7b00796.

(54) Crawford, T. D.; Romero, F. A.; Lai, K. W.; Tsui, V.; Taylor, A. M.; de Leon Boenig, G.; Noland, C. L.; Murray, J.; Ly, J.; Choo, E. F.; Hunsaker, T. L.; Chan, E. W.; Merchant, M.; Kharbanda, S.; Gascoigne, K. E.; Kaufman, S.; Beresini, M. H.; Liao, J.; Liu, W.; Chen, K. X.; Chen, Z.; Conery, A. R.; Côté, A.; Jayaram, H.; Jiang, Y.; Kiefer, J. R.; Kleinheinz, T.; Li, Y.; Maher, J.; Pardo, E.; Poy, F.; Spillane, K. L.; Wang, F.; Wang, J.; Wei, X.; Xu, Z.; Xu, Z.; Yen, I.; Zawadzke, L.; Zhu, X.; Bellon, S.; Cummings, R.; Cochran, A. G.; Albrecht, B. K.; Magnuson, S. Discovery of a Potent and Selective in Vivo Probe (GNE-272) for the Bromodomains of CBP/EP300. *J. Med. Chem.* **2016**, *59*, 10549–10563.

(55) Zhou, P.; Zou, J.; Tian, F.; Shang, Z. Fluorine Bonding – How Does It Work In Protein–Ligand Interactions? *J. Chem. Inf. Model.* **2017**, *49*, 2344–2355.

(56) Details regarding the computational docking protocol are provided in the Supporting Information.

(57) Bennett, J.; Fedorov, O.; Tallant, C.; Monteiro, O.; Meier, J.; Gamble, V.; Savitsky, P.; Nunez-Alonso, G. A.; Haendler, B.; Rogers, C.; Brennan, P. E.; Müller, S.; Knapp, S. Discovery of a Chemical Tool Inhibitor Targeting the Bromodomains of TRIM24 and BRPF. *J. Med. Chem.* **2016**, *59*, 1642–1647.

(58) CBP HTRF IC_{50} of published CBP inhibitors reported here as measured by Genentech assays.

(59) For a similar approach for the development of BET inhibitors, see: Sharp, P. P.; Garnier, J.-M.; Huang, D. C. S.; Burns, C. J. Evaluation of Functional Groups as Acetyl-Lysine Mimetics for BET Bromodomain Inhibition. *Med. Chem. Commun.* **2014**, *5*, 1834–1842.

(60) We found that high potencies in the biochemical assays were required in order for

reasonable potencies to be detected in the MYC assay. Less biochemically potent inhibitors displayed a large cell-shift.

(61) BROMOscan® recombinant protein binding assay, DiscoveRx Inc., www.discoverx.com.

(62) Crawford, T. D.; Tsui, V.; Flynn, E. M.; Wang, S.; Taylor, A. M.; Côté, A.; Audia, J. E.; Beresini, M. H.; Burdick, D. J.; Cummings, R. T.; Dakin, L. A.; Duplessis, M.; Good, A. C.; Hewitt, M. C.; Huang, H.-R.; Jayaram, H.; Kiefer, J. R.; Jiang, Y.; Murray, J. M.; Nasveschuk, C. G.; Pardo, E.; Poy, F.; Romero, F. A.; Tang, Y.; Wang, J.; Xu, Z.; Zawadzke, L. E.; Zhu, X.; Albrecht, B. K.; Magnuson, S. R.; Bellon, S. F.; Cochran, A. G. Diving Into the Water: Inducible Binding Conformations for BRD4, TAF1(2), BRD9, and CECR2 Bromodomains. *J. Med. Chem.* **2016**, *59*, 5391–5402.

Graphical Abstract

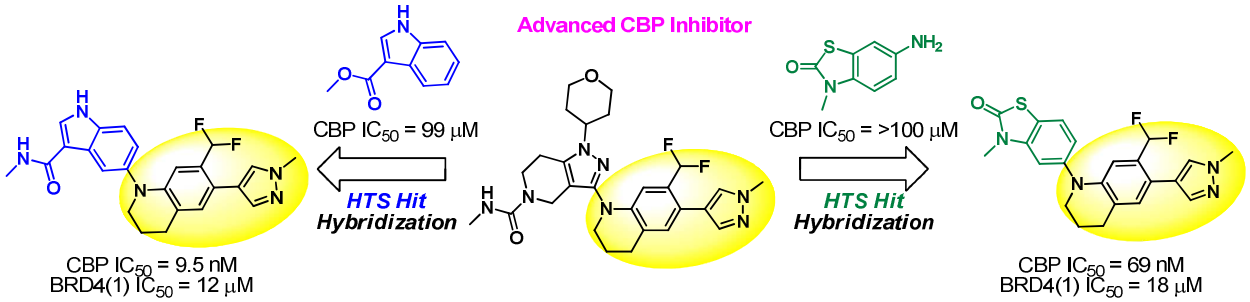

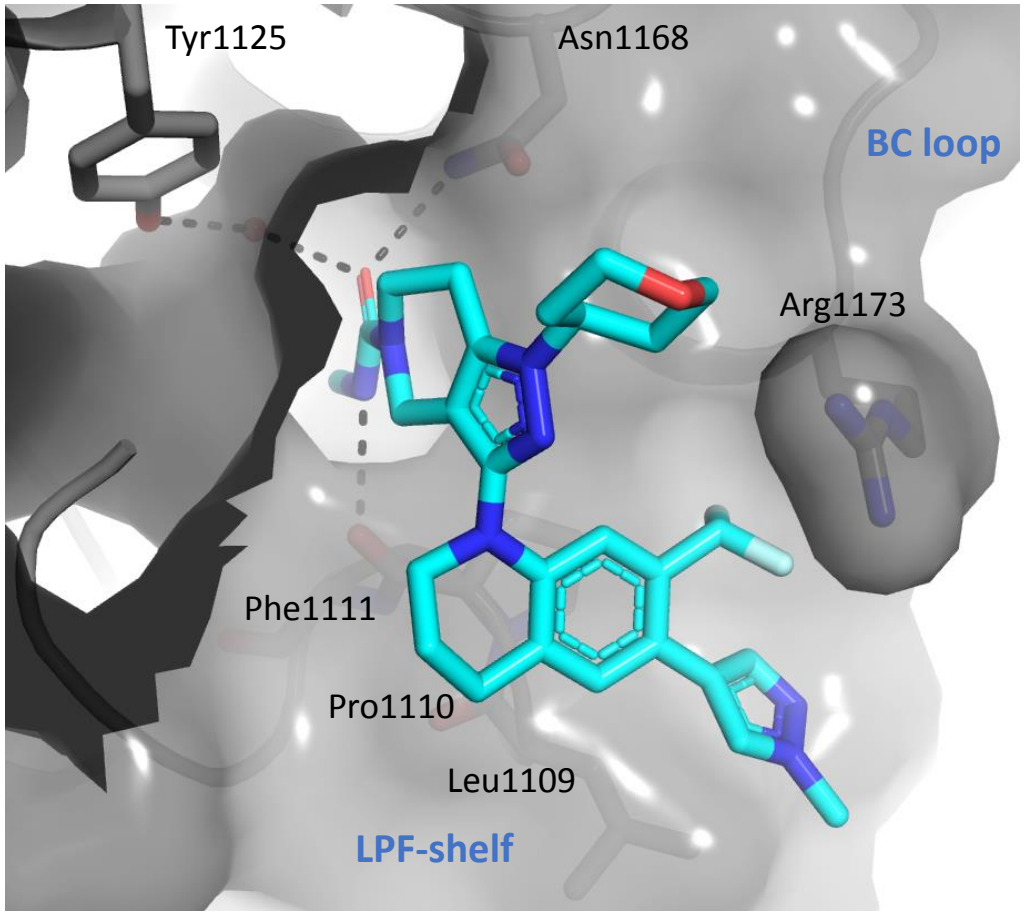

Figure 2. Co-crystal structure of CBP-bound **3** (PDB-ID 5W0E).

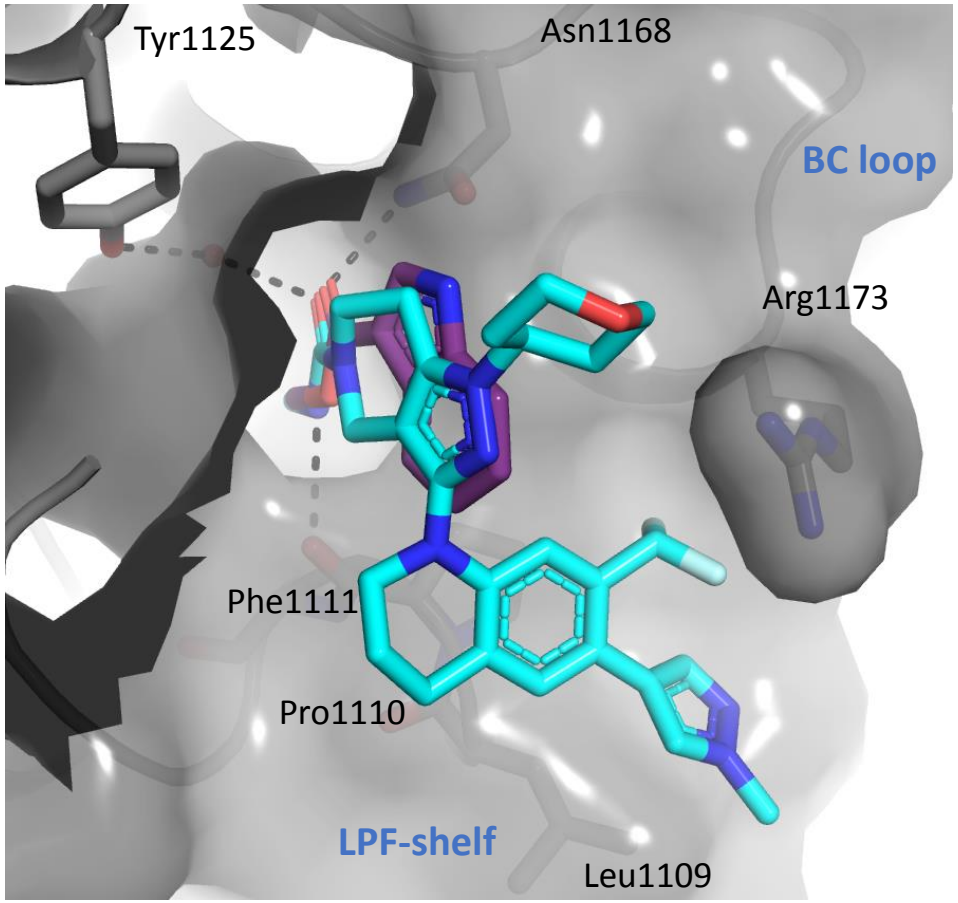

Figure 4a. Co-crystal structure of HTS hit **6** (purple, G00381004) overlaid with **3** (blue, G'8781).

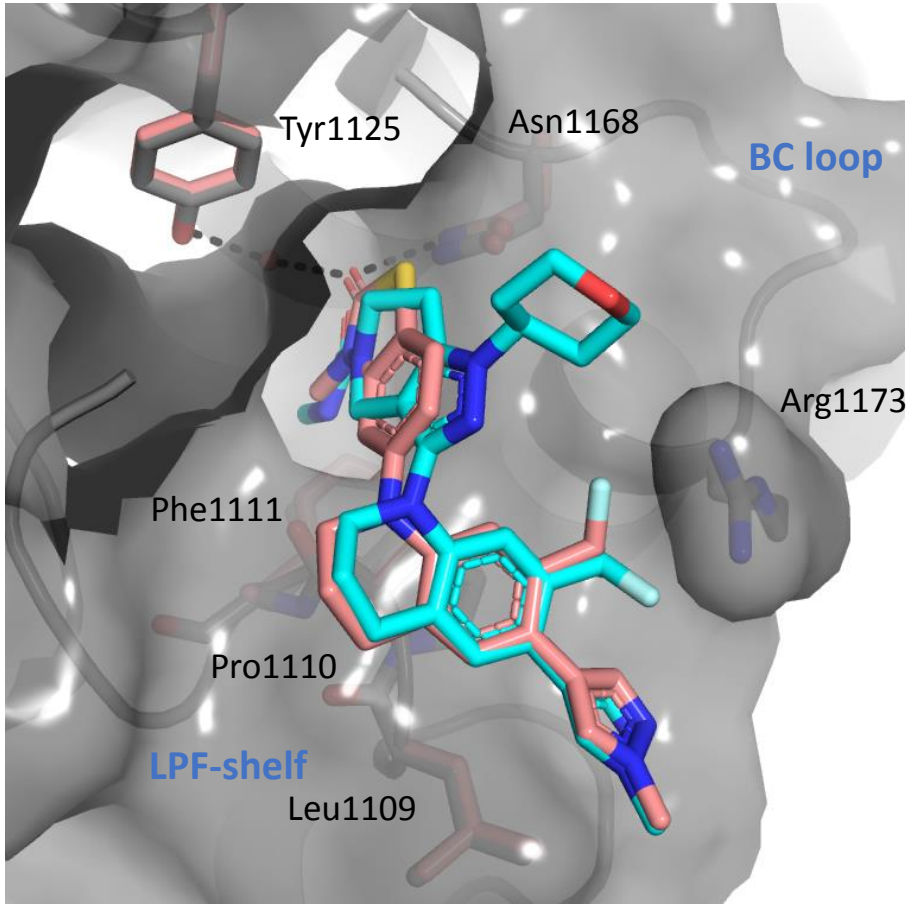

Figure 7a. Crystal structure of hybrid **17** (pink) overlaid with **3** (blue).

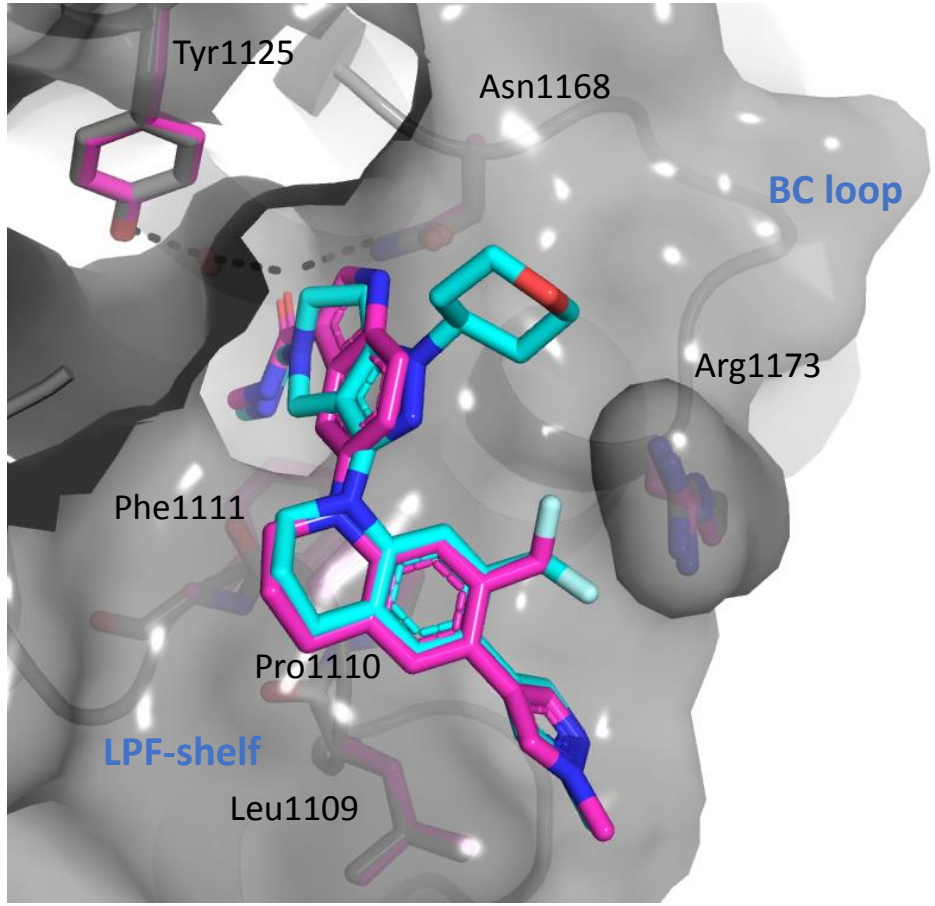

Figure 7b. Crystal structure of hybrid **16** (magenta) overlaid with **3** (blue).

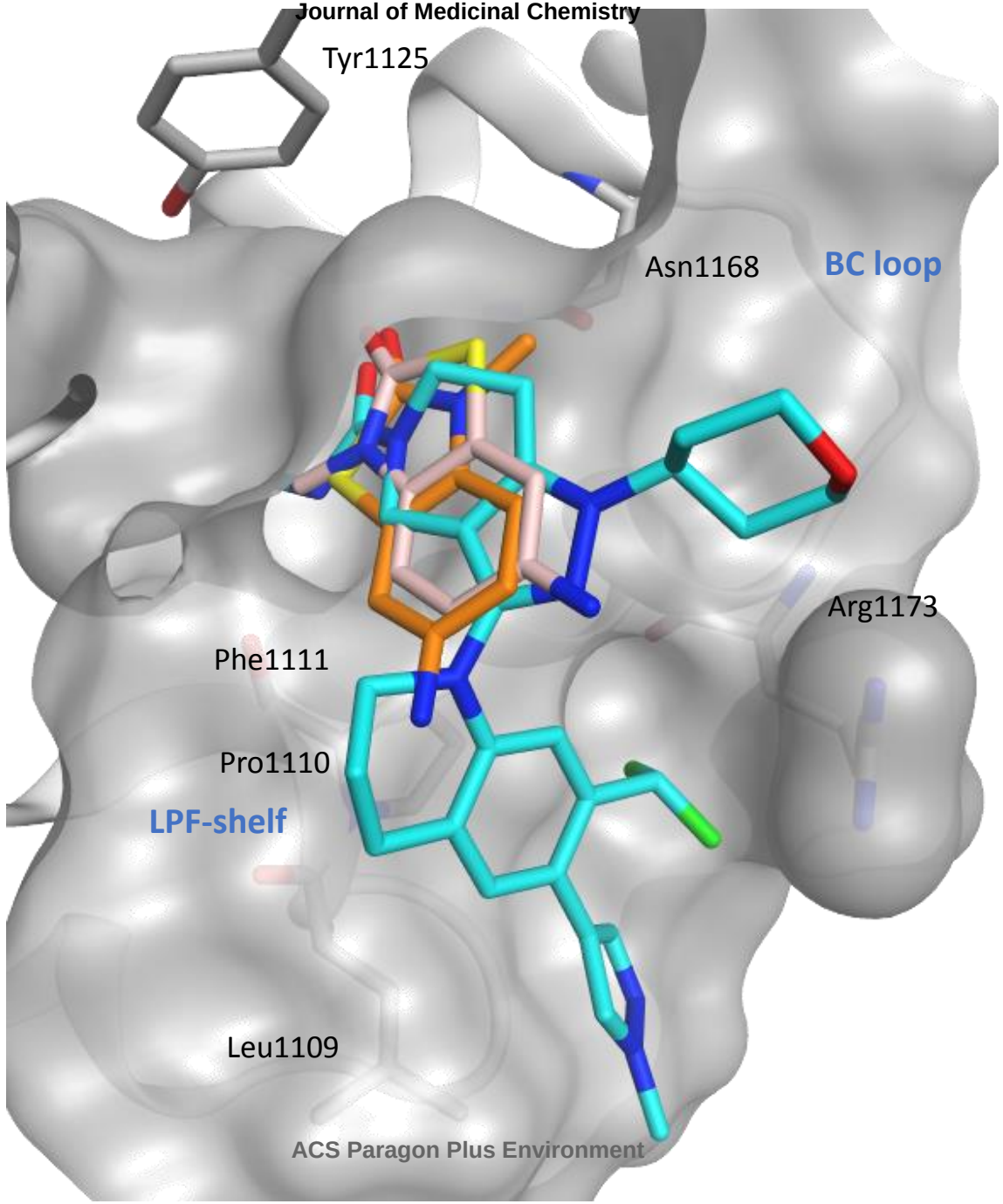

Figure 4b. Docked structures of HTS hit **7** (orange and pink) overlaid with co-crystal structure of **3** (cyan; PDB-ID 5W0E).

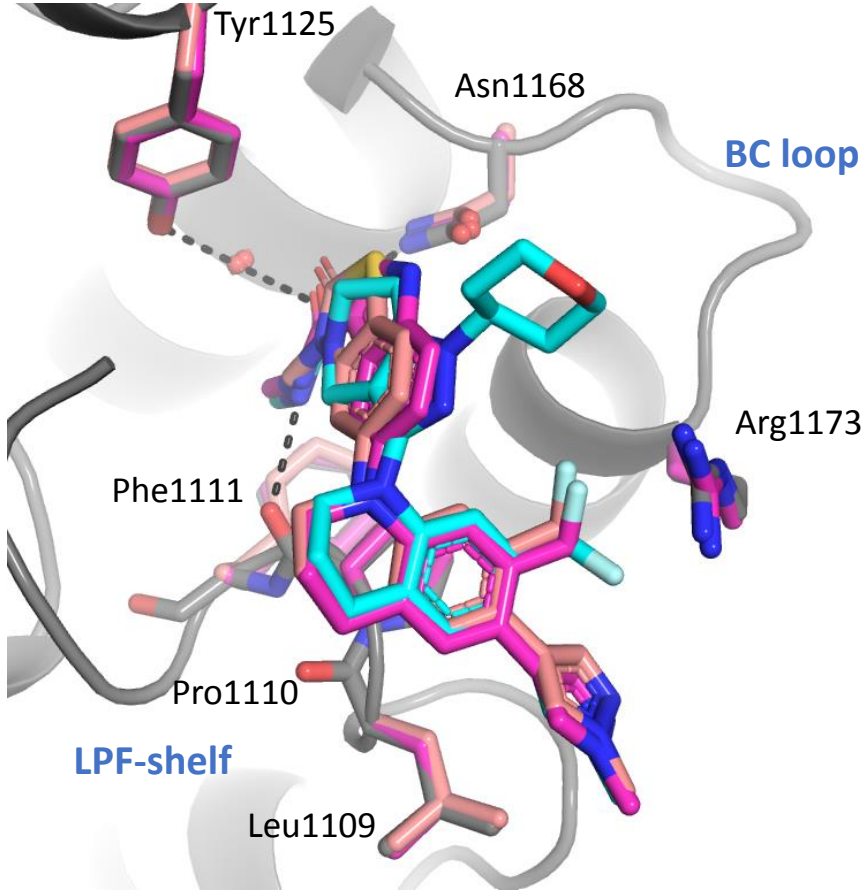
Tyr1125
Asn1168
BC loop
Arg1173
Phe1111
Pro1110
LPF-shelf
Leu1109

Figure 6.

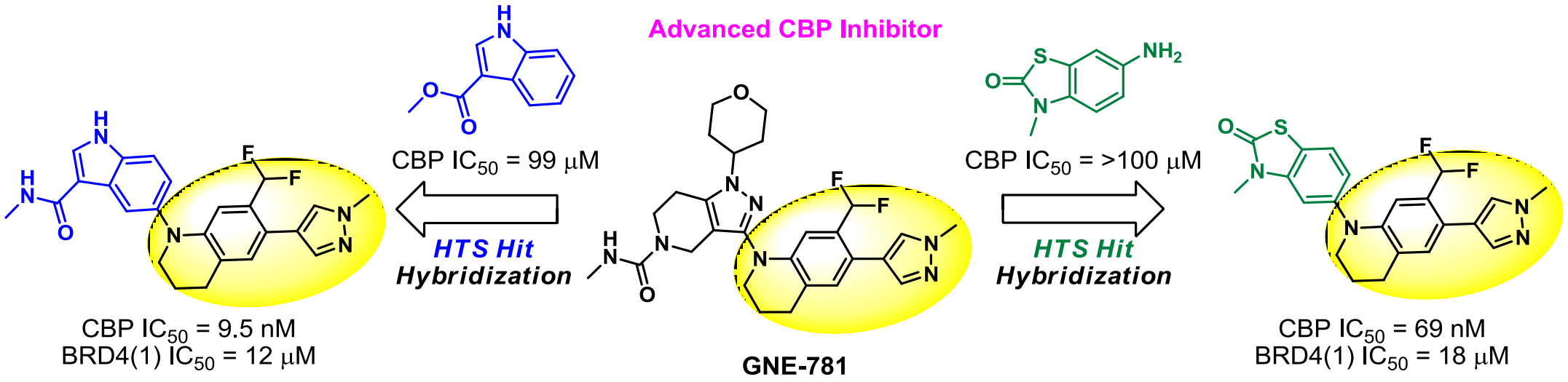

Rapid Development of Chemically Diverse, Potent, and Selective CBP Inhibitors

Rapid Development of Chemically Diverse, Potent, and Selective CBP Inhibitors